THE EFFECTS OF CHANGES IN CLIMATE AND OTHER

ENVIRONMENTAL FACTORS ON PERMAFROST EVOLUTION

By

Elchin Jafarov

RECOMMENDED:

Advisory Committee Chair

Chair, Department of Geology and Geophysics

APPROVED:

Dean, College of Natural Science and Mathematics

Dean of the Graduate School

29 April 2013

Date

THE EFFECTS OF CHANGES IN CLIMATE AND OTHER ENVIRONMENTAL FACTORS ON PERMAFROST EVOLUTION

A

THESIS

Presented to the Faculty

of the University of Alaska Fairbanks

in Partial Fulfillment of the Requirements

for the Degree of

DOCTOR OF PHILOSOPHY

By

Elchin Jafarov, B.S., M.S.

Fairbanks, Alaska

May 2013

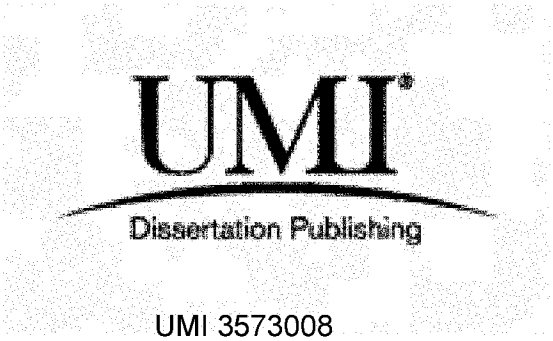

ProQuest LLC
789 East Eisenhower Parkway
P.O. Box 1346
Ann Arbor, MI 48106-1346

Abstract

Permafrost is a product of a past colder climate. It underlies most of the terrestrial Arctic, where it influences landscape hydrology, biogeochemical environments and human activity. The current thermal regime of permafrost is mediated by different environmental factors, including snow, topography, vegetation and soil texture. The dependence of permafrost on these factors greatly complicates the modeling of permafrost thermodynamics. Accurate modeling of permafrost is critical for evaluating potential impacts of climate change on permafrost stability. The objectives of this study were to a) improve modeling of ground temperature during snow season; b) analyze the effects of post-fire environmental changes on permafrost thermal stability; and c) predict 21st century ground temperature dynamics in Alaska with high spatial resolution. To achieve the proposed objectives, near-surface air and ground temperatures were measured at permafrost observation stations across Alaska. Measured ground temperatures were used to evaluate simulated ground temperatures, which were generated with the Geophysical Institute Permafrost Laboratory (GIPL) numerical transient model. The GIPL model takes into account climate, snow, soil texture, soil moisture, and the freeze/thaw effect. To better model ground temperatures within the soil column, it was necessary to improve the parameterization of snow layer thermal properties in the model. To improve ground temperature simulations during snow season, daily snow thermal properties were estimated using an inverse approach. Modeling bias was improved by including ground temperatures simulated using estimated daily snow thermal conductivities. To address the effects of fire disturbance on permafrost thermal stability, we applied the GIPL model to lowland and upland boreal forest permafrost environments. The results indicate that permafrost vulnerability depends on pre-fire organic soil layer thickness and wetness, the amount of organic matter burned during the fire, and post-fire soil organic layer recovery rates. High spatial resolution permafrost maps are necessary for evaluating the potential impacts of permafrost thawing on Arctic ecosystems, engineering facilities, infrastructure, and the remobilization of soil carbon. Simulated ground temperatures in Alaska during the 21st century indicate widespread permafrost degradation in the discontinuous permafrost zone. High ground temperature warming trends are projected for most of the continuous permafrost zone north of the Brooks Range.

Table of Contents

List of Figures

List of Tables

Page

Acknowledgements

I owe my deepest gratitude to my advisor, Dr. Vladimir Romanovsky, for providing me with the highest level of supervision. Without his valuable feedback, guidance and support this thesis would not have been possible. Dr. Vladimir Romanovsky created an atmosphere of colleagueship and friendship in which his expert guidance and assistance in any aspect of my research was truly indispensable. I would like to thank present and past members of my graduate committee: Dr. Paul Layer, Dr. John Walsh, Dr. Sergei Marchenko and Dr. David Verbyla for their critical review of my thesis, commitment of time and willingness to help me in this work.

I am thankful to Dr. Paul Layer, for rediscovering the geological statistics for me. I enjoyed attending his lectures and learning new statistical methods. I greatly appreciate Dr. John Walsh, who motivated me to write the manuscript on reconstruction of snow thermal properties. I would also like to deeply thank my friend and college Dr. Dmitry Nicolsky for his support and help during my Ph.D. study. He had an enormous contribution on the second chapter of this thesis, without his help and input this thesis would not be complete. I would like to thank Dr. Sergei Marchenko for introducing me to the GIPL permafrost model. With his support and invaluable advice a substantial part of this thesis was completed. Dr. Dmitry Nicolsky and Dr. Sergei Marchenko both helped me tremendously in acquiring, interpreting and validating computations, as well as publishing the results of our study. I am also thankful to Dr. David McGuire who helped me tremendously by sharing his experience, knowledge and advise on the third chapter of this thesis. He also supported my trips to conferences and workshops through his grants. I am also thankful to Dr. Helene Genet who helped me with the Terrestrial Ecological Model and with the manuscript preparation.

Special thanks to Dr. Sergei Avdonin, who gave me a chance to rediscover the beauty of mathematics over again. I am thankful to Dr. Edward Bueler for his inspirational course on numerical analysis. My special appreciation is expressed to my friend and college Dr. Santosh Panda for his friendship and invaluable help with my thesis submission.

My special appreciation is expressed to Igor and Anna. Being a graduate student, I could always rely on their advice whether it was on research or in life. I am particularly thankful to Jenya and Ramil for helping me to start my graduate journey. I am thankful to

all my friends whom I met in Fairbanks: Artem, Lila, Bahram, Vasil, Jake, Victor, Valeriy, Michel, Roman and many others.

I would like to thank my colleagues Guido Grosse, Alexandr Kholodov, Ronald Daanen, Bill Cable, Reginald Muskett, Prajna Regmi and Andrew (Cody) Beedlow for their advice, assurance and help along the way. The overwhelming part of the financial support for this study was provided by the National Science Foundation (ARC-0520578, ARC-0632400, ARC-0856864, ECO-MODI), and by the State of Alaska.

Finally, I would like to acknowledge my family members. In particular, I want to thank my wife, Natavan, for her support and assistance. I am grateful for my mother, Afaq, and my mother-in-law, Samaya, for their constant support, believe and enormous help. I dedicate my work to my son Mikayil and my dear wife Natavan.

Chapter 1
Introduction

1.1 Permafrost distribution in Alaska

In this thesis, permafrost is defined as ground that stays at or below 0^oC for a continuous period of at least two consecutive years, regardless of location, soil texture, ice content or soil moisture content. In the most recent permafrost map of Alaska (Fig. 1.1), the state is divided into the following zones: "continuous permafrost," "discontinuous permafrost," "sporadic permafrost," "isolated permafrost" and "no permafrost."

Continuous permafrost is defined as a layer of frozen ground that underlies at least 90% of the land surface in a given area. Continuous permafrost covers almost the entire northern one-third of Alaska. The mean annual air temperature in the continuous zone ranges from -12^oC to -6^oC, and permafrost thicknesses range from fifty to several hundred meters. The maximum reported thickness occurs in the Prudhoe Bay area, where permafrost extends to depths of 600 to 660 meters [Jorgenson et al., 2008]. In the continuous zone, permafrost is predominantly characterized by polygonal surface structures. The structures originate from a network of ice wedges[1] that define the boundaries of geometric polygons in plan view. Another feature that dominates the continuous permafrost landscape is the pingo [2]. There are two types of pingos: open-system and closed-system. These terms refer to the nature of the water supply involved in pingo formation. Many closed-system pingos in Alaska lie in the low northern plains of the continuous zone [Walker et al., 1985], where they form when the boundaries of drying lakes freeze [Davis, 2001].

The Brooks Range in Alaska tends to define the boundary between the continuous and discontinuous permafrost zones. In this region, north-facing hillsides and lowlands receive different amounts of solar radiation than south-facing slopes. South-facing slopes receive more solar radiation, which influences active layer thicknesses[3]. As a result, the active layer is generally thinner on north-facing slopes. The vegetation biome in this area is tundra.

[1] Ice wedges are massive, generally wedge-shaped bodies that taper downwards, composed of foliated or vertically banded ice [van Everdingen Robert, 1998].

[2] A perennial frost mound consisting of a core of massive ice, produced primarily by injection of water, and covered with soil and vegetation [van Everdingen Robert, 1998].

[3] An active layer in permafrost regions is traditionally defined as a surficial layer overlying the permafrost layer, which undergoes seasonal freeze-thaw cycles [van Everdingen Robert, 1998].

Discontinuous permafrost is widespread in most of Interior Alaska (Fig. 1.1). In the discontinuous zone, permafrost breaks into islands. Separate masses of permafrost cover more than 50% of the land area, and permafrost thickness is highly variable, ranging from 5 to 110 meters. Generally, however, permafrost thickness tends to decrease from the north to the south. A considerable number of Alaska's open-system pingos are concentrated in this zone. They typically lie in valley bottoms or on valley slopes, and form when groundwater flows downhill and becomes trapped underneath the permafrost. The amount of ground ice in this zone varies from low-moderate to high (greater than 40% by volume). In Alaska, the boreal forest region broadly overlaps the discontinuous permafrost zone. This vegetation biome is defined as a taiga. The mean annual air temperature distribution for the discontinuous permafrost zone is -6^oC to -2^oC.

The rest of the southern and southwestern parts of Alaska are underlain with sporadic, isolated islands of permafrost, or contain no permafrost at all. Sporadic and isolated islands of permafrost are generally categorized on the basis of percentage of area occupied by permafrost. The zone of sporadic permafrost is 10% to 50% permafrost by land area, while the zone of isolated permafrost is less than 10% permafrost by land area. The mean annual air temperature distribution for the sporadic permafrost zone ranges from -2^oC to 0^oC. The existence of permafrost in this zone is highly dependent on the thickness of the organic soil layer. This layer acts as a buffer between ground and air, and protects underlying permafrost from warm summer temperatures [Shur and Jorgenson, 2007]. The mean annual air temperatures in the isolated islands and no-permafrost areas range between 0^oC and $+4^oC$. Southern and southeastern areas of Alaska have wide patches of no-permafrost zones, including the areas around Anchorage, Valdez, Kenai and Juneau, as well as the Aleutian Islands.

1.2 Factors that determine permafrost thermal state

Although permafrost is a product of cold climates, its occurrence is the combined outcome of the interplay between a number of environmental factors. These factors include topography, snow cover, vegetation cover, soil type, open water bodies, wildfires and anthropogenic influences. Climatic and environmental factors act separately and synergistically to control the distribution, thermal state, and thickness of permafrost, as well as the thick-

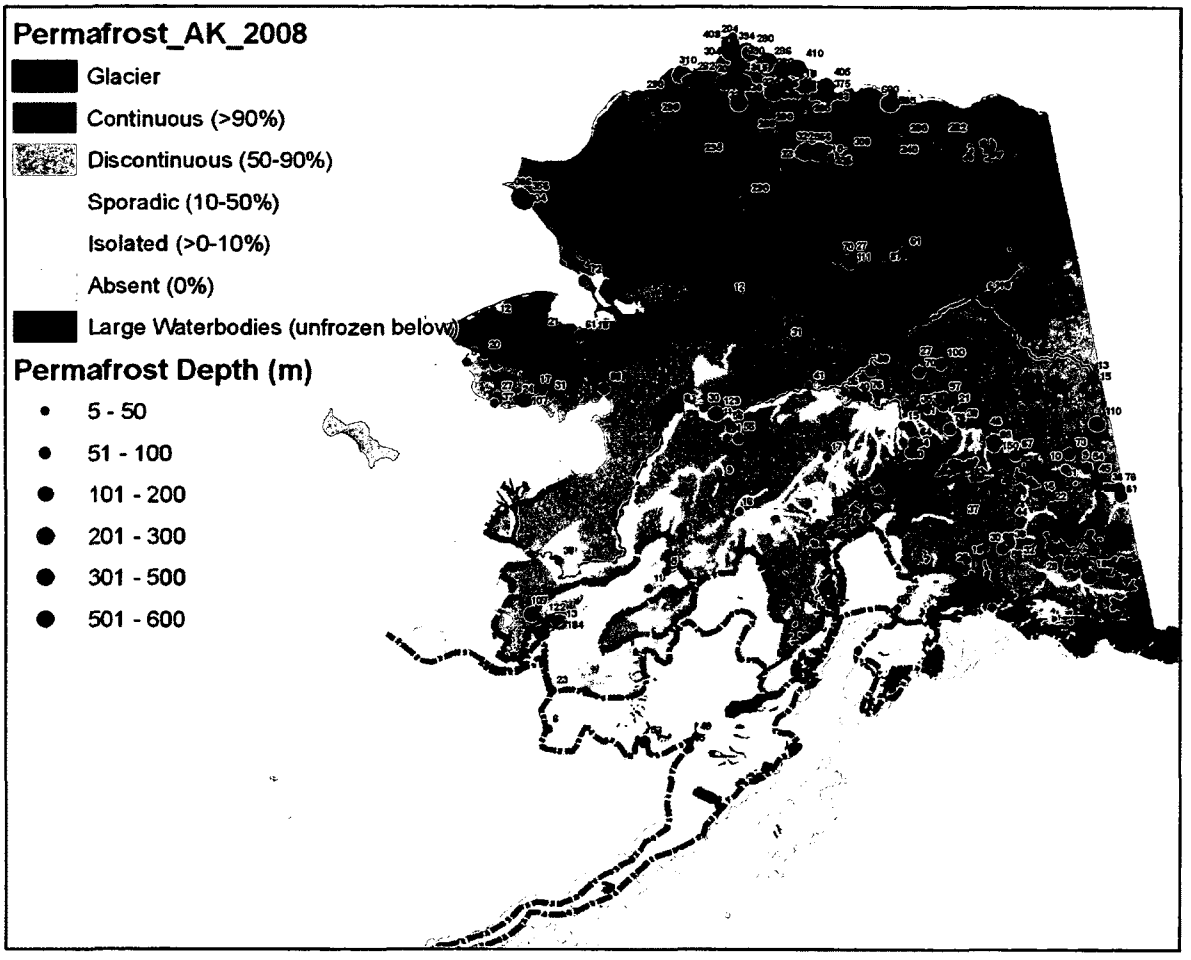

Figure 1.1. Spatial map of permafrost in Alaska. *Source:* Jorgenson et al. [2008]

ness and properties of the active layer. The effects of these individual components and their variations in time and space are manifested in the variations of permafrost existing today.

1.2.1 Snow

The importance of snow cover on the presence of frozen ground in cold regions has been widely recognized [Smith, 1975; Zhang et al., 2001; Zhang, 2005]. In some areas, variation in mean annual ground temperature is determined primarily by snow depth [Nicholson and Granberg, 1973]. Due to its highly insulative properties, newly-fallen snow can

impede heat loss from the ground surface. Alternatively, well-compacted snow has a reduced insulating effect. The insulating properties of snow cover affect the distribution of permafrost by causing substantial changes to heat exchange between the ground and the atmosphere. In discontinuous and sporadic permafrost regions, snow cover may be responsible for the presence or absence of permafrost. In continuous permafrost regions, it may affect the active layer thickness [Street and Melnikov, 1990]. The overall effect of snow cover on heat exchange is complicated and mostly depends on climate and topography.

1.2.2 Topography

The topography of the landscape defines the temperature regime of the ground, which in turn controls the depth of the active layer overlying the permafrost. In mountainous regions, aspect and steepness are important factors that can determine the presence or absence of permafrost. Low inflow of solar energy in the winter makes south- and north-facing slopes equally cold at high latitudes. During the summer period, however, south-facing slopes receive more solar energy, facilitating the formation of a deeper active layer than on north-facing slopes. Topography is also an important factor controlling the redistribution of snow.

1.2.3 Vegetation

Vegetation is one of the terrain features that can have a direct or indirect effect on underlying permafrost. In the summer, vegetation insulates the soil from heating and casts shadows that reduce the effects of solar radiation. In the winter, shrubs capture snow, increasing thermal insulation and changing the quantity of heat that is absorbed and released by the ground. Vegetation canopies also reduce the amount of solar radiation reaching the ground and affect the depth and persistence of snow cover [Luthin and Guymon, 1974; Rouse, 1982]

1.2.4 Organic and mineral soils

The influences of organic layers on ground thermal conditions have been well documented [Alexeyev and Birdsey, 1982; Bonan and Shugart, 1989; Yoshikawa et al., 2003]. In arctic

regions, organic soil contributes to an increase in soil moisture and provides insulation against summer heat [Kryuchkov, 1978]. Therefore, organic soil layers play an important role in the energy exchange between the air and the ground. Heat exchange within organic soils is mainly controlled by the amount of available soil moisture. For example, the thermal conductivity of a thawed moss layer is $0.01 - 0.07\ Wm^{-1}K^{-1}$, which is 1.5 to 2 times lower than the thermal conductivity of a frozen moss layer [Yershov and Garagulya, 2001]. Removal of vegetation and moss layers leads to higher amplitudes of annual temperature fluctuations at the ground surface, resulting in a deepening permafrost table[4].

In certain locations, the existence of permafrost is associated with a soil peat layer. Like snow cover, peat can act as both an insulator and a cooler. Unlike snow cover, however, peat is not a seasonal occurrence. It is present year-round, but its thermal properties vary seasonally as moisture conditions change. In the summer, when peat is dry, its thermal conductivity is low. The ground below the peat layer is insulated from the summer heat, and it stays cooler [Williams and Smith, 1989]. Higher water content in the peat layer causes a greater difference between its frozen and thawed conductivities. With a higher water content, the ability of peat to prevent underlying ground from heating in the summer becomes greater than its ability to prevent the yield of heat in the winter. When peat freezes, it exhibits its highest conductivity and keeps the soil underneath cold. Consequently, the mean annual ground temperatures in peat-covered regions are lower than in peat-free regions. Active layer thicknesses are also lower.

The effects of mineral soils on permafrost depend on soil texture, i.e. the size range of particles in the soil. The sizes and shapes of particles in a soil layer determine how much water is contained within the pore spaces of the soil. Not all pore water freezes at 0 ^oC; some unfrozen water remains in the soil even at very low temperatures. The unfrozen water can influence the thermal regime, and affect heat and mass transport processes including heat fluxes in the active layer and permafrost [Romanovsky and Osterkamp, 2000].

1.2.5 Open water bodies

In high latitudes, open bodies of water that remain unfrozen at depth in winter may have a significant effect on ground temperatures and eventually on underlying permafrost. Wa-

[4]The permafrost table is the upper surface of a permafrost layer.

ter transmits shortwave radiation and retains longwave radiation. The presence of a water body thus constitutes a heat source contributing to the heat flow and temperature conditions in the ground [Williams and Smith, 1989]. Depending on the size and depth of the lake, a talik[5] may or may not develop beneath it. In the continuous permafrost zone, if a lake is deep and large enough, a talik might extend through the entire permafrost column. In general, if a lake is deeper than 2-2.5 meters, the bottom deposits remain unfrozen year-round [Yershov, 1998]. In Alaska, permafrost is reported to be absent or lie at great depths beneath deep lakes and ponds [Hopkins et al., 1955; Ling and Zhang, 2004; West and Plug, 2008].

1.2.6 Wildfires

Wildfires can severely disturb the surface thermal regime by burning surface materials and altering the balance of subsurface energy transfers. Any changes in surface conditions will trigger changes in the ground thermal regime. A severe burn in a soil organic layer can increase mean surface temperatures and eventually lead to thawing of the upper layer of permafrost [Williams and Smith, 1989; Yoshikawa et al., 2003]. In Alaska, the boreal forest widely overlaps the area of discontinuous permafrost. The area of discontinuous permafrost where annual mean temperatures are close to 0^oC are the most sensitive to fire disturbances. The presence and thickness of the organic layer in this zone is crucial for preserving permafrost [Viereck, 1983]. The amount of soil moisture and the severity of the fire are two important factors that control the amount of organic material left after a forest fire. Fires in the boreal forest have both immediate and long-term impacts on the ecosystem due to their effects on the surface energy balance, the water balance, and underlying permafrost. The rate of thaw depth increase after a fire is directly proportional to fire severity [Yoshikawa et al., 2003]. In the first and second years after a fire, mass wasting or landslides frequently occur on hill slopes, which are more prone to failure due to their increased soil moisture contents [Brown and Grave, 1979; Brown, 1983; Tiedemann et al., 1979]. Several decades after a fire, thermokarst[6] formation may occur as a result of

[5] A talik is an unfrozen soil layer that lies between discontinuous blocks of frozen soil or between the permafrost table and the bottom of the active layer.

[6] A thermokarst is a topographic depression resulting from the thawing of ground ice.

the thawing of ice-rich permafrost [Brown, 1983; Viereck, 1979].

1.2.7 Anthropogenic influences

Anthropogenic disturbances in permafrost regions have resulted in marked permafrost degradation and thaw subsidence. Engineering constructions, oil and gas production, mining and agriculture can change geothermal, geochemical, hydrogeological, and geophysical conditions [Yershov, 1998]. Human activities such as land clearance and removal of the organic layer can cause warming of the ground, which increases thaw depth and degrades permafrost. For example, removal of vegetation cover for agricultural and construction purposes in Yakutia, Russia, caused severe land subsidence [Fedorov and Konstantinov, 2008]. Similarly, mean annual ground temperatures increases caused settlement of the pavement on Farmers Loop Road and other roads in the Fairbanks area after land was cleared for road construction. In the end, any type of economic development within the permafrost zone will cause its own disturbances.

1.3 Permafrost under a warmer climate

One of the earliest attempts to predict permafrost temperature dynamics and changes to the active layer thickness dates back to 1940 [Sumgin et al., 1940]. M.I. Sumgin put forward a theory of permafrost degradation in which permafrost is regarded not as eternal and static but as once formed and later continuously changing. The ability to predict near-surface temperatures in response to a changing climate is critical to three main efforts: 1) determining the impact on the economy due to the additional repair costs of public infrastructure [Larsen et al., 2008]; 2) estimating the greenhouse effect from decomposed organic soils [Schuur et al., 2008]; and 3) evaluating changes in the hydrologic response of watersheds [Hinzman and Kane, 1992].

It is a common assumption that the formation and evolution of permafrost goes back to cold glacial periods. During the last glacial maximum (around 20ka BP), a significant portion of North American Arctic shelves were dry and exposed to extremely cold climate conditions [Velichko and Faustova, 2009; Hubberten and Romanovskii, 2001]. During this period, thick terrestrial permafrost was formed. Climatic and environmental factors affected permafrost during the transition period from glacial to interglacial conditions.

Warm global temperatures following the last ice age created unfavorable conditions for permafrost in many regions. Nevertheless, the permafrost zone in the Arctic was generally stable with no widespread thaw. Several thousand years after the Holocene optimum, permafrost started to thaw from the bottom up in the continuous permafrost zone [Osterkamp and Gosink, 1991].

Over the past several decades, observations reveal an increase in permafrost temperatures in many locations around the globe. There is evidence to suggest that the permafrost in northern Alaska has warmed in response to warming air temperatures, including 30-year permafrost records that show a net increase in permafrost temperatures of $0.5 - 3\,^{o}C$ [Osterkamp, 2008; Romanovsky et al., 2010].

Global Circulation Models project an increase in mean annual air temperatures and an increase in the amount of precipitation in the Arctic, which could accelerate permafrost warming [Callaghan et al., 2011]. With climate warming, present-day continuous permafrost will become discontinuous. Changes in discontinuous permafrost will depend on whether organic layers can provide additional resilience to thaw. Terrains that are not well-protected with organic layers will be more vulnerable to climate change.

Areas with ice-rich, near-surface permafrost could develop thermokarst lakes. Thermokarst formation, thermal erosion, and various slope processes may also destroy organic layers and significantly accelerate permafrost degradation. Permafrost degradation could affect slope instability by increasing the amount of rockfalls and rockslides, and increase rates of rock glacier movement. Warming of permafrost may also increase coastal erosion in areas with coastal permafrost [Callaghan et al., 2011].

The organic soils of the boreal forest cover more than one-third of the landscape in Alaska [Cleve and Viereck, 1983] and store the largest reservoir of global terrestrial carbon [McGuire et al., 1995; Alexeyev and Birdsey, 1998]. Thawing of permafrost would increase the depth of the active layer and lower the water table, which could accelerate the rate of carbon loss in arctic ecosystems [Schuur et al., 2009]. Studies have shown that higher air temperatures associated with longer snow-free seasons result in the largest relative soil organic carbon losses ($\sim 5.3\ kgCm^{-2}$), and high fire-severity regimes associated with warmer and drier conditions could magnify these losses ($\sim 6.2\ kgCm^{-2}$) [O'Donnell et al., 2011].

1.4 Research objectives

The goal of this research was to improve modeling of permafrost evolution by better addressing the effects of environmental factors on permafrost characteristics. As mentioned previously, better assessment of permafrost dynamics is important for socioeconomic planning and development in the State of Alaska. It is well-known that climate is the main driver of change in the thermal state of permafrost. There are other environmental controls, however, that can be critical in influencing permafrost characteristics. The primary objective of this study was to develop a spatially-distributed, process-based numerical model that is able to simulate permafrost dynamics throughout the entire State of Alaska in high spatial resolution. The aim of this model was to explore the effects of soil organic layers, soil texture, snow, soil moisture, and forest fires on permafrost thermal regime. Specifically, the following were research objectives of this study:

- Retrieve snow thermal properties using inverse modeling
- Improve ground temperature modeling using retrieved snow thermal properties
- Identify the controlling factors that affect post-fire permafrost dynamics
- Identify burn severity thresholds, conditions that are most likely to trigger changes in ecosystem stability or induce rapid permafrost degradation
- Develop an effective computational algorithm in order to calculate permafrost distribution in high spatial resolution
- Analyze advantages and uncertainties of the projected high spatial resolution permafrost map of Alaska.

1.5 Research questions

Based on the objectives of the study, the following research questions were formulated:

1. *Can snow properties obtained by employing an inverse technique improve ground temperature simulations?* Heat exchange within the snow layer is a difficult and complex process to model. Continuous records of snow thermal properties, specifically thermal conductivity for a particular seasonal snow, are not readily available. A time series

of snow thermal conductivities is crucial in order to better model ground temperature dynamics. The method developed in this study allows indirect determination of snow thermal conductivity by using measured air and ground surface temperatures and snow depths.

2. *Which factors provide the strongest controls on post-fire ground temperatures in boreal forest ecosystems?* Identifying the factors influencing post-fire subsurface thermal regimes in boreal forest ecosystems is necessary for developing a better overall prognosis of permafrost dynamics. Changing climate is a major factor influencing the post-fire permafrost thermal state. However, assessment of organic layer development and its negative feedback on permafrost degradation is currently not well-established.

3. *Under which burn severity scenarios can ecological thresholds be reached?* It is important to know under which environmental conditions ecological thresholds after forest fires can be reached. Reaching these thresholds could affect local spatial permafrost distribution and even impact adjacent permafrost regions. This could change the ecosystem succession cycle (black spruce forest to deciduous).

4. *Can Alaskan permafrost dynamics be mapped in high spatial resolution and be useful for better assessment of the social impacts of climatic changes and economic development?* Due to heterogeneity of the landscape and scarcity of measured ground temperature data, mapping permafrost spatial distribution is a complex problem. Ground data from borehole stations are mainly available from geophysical surveys or pipeline corridors, and are relatively expensive. The method developed in this study uses Geographical Information System (GIS) maps of snow, soil and vegetation in order to project permafrost spatial distribution and dynamics at high spatial resolution. A composite of five Global Circulation Model (GCM) datasets downscaled to a 2 x 2 km spatial resolution and averaged on a monthly time scale was used to simulate permafrost spatial dynamics in the 21th century for the entire State of Alaska.

1.6 Outline of Chapters

The next three chapters of this thesis are organized as a series of manuscripts designed to address the research questions described above. Each of these manuscripts represents

a step towards the improvement and further development of a numerical model capable of simulating permafrost dynamics in a thermal conduction-dominated environment. Climate is a major factor influencing permafrost, but the complex interactions between different environmental factors could be significant in determining the presence and thermal conditions of permafrost. In chapter 2 of this thesis, the effects of snow on ground temperatures are addressed. The objectives of this chapter were to 1) improve ground surface temperature modeling via better snow parameterization, and 2) develop an inverse method in order to recover snow thermo-physical properties. Changing in time and space thermal properties of snow layer make it a complex substance to model [Sturm et al., 1997]. Simple and effective snow heat exchange models are important components of permafrost modeling [Goodrich, 1982; Douville et al., 1995]. Applying constant snow layer thermal parameters is not always a good way to model ground temperatures. Therefore, a better parameterization of snow layer thermal properties is needed. In this chapter, we proposed a method that uses daily changing snow thermal properties. By varying snow thermal properties, we can better model ground surface temperatures.

In chapter 3, the effects of forest fires on permafrost in boreal forest ecosystems are addressed. Forest fires are major factors that can influence organic layer thickness [Yoshikawa et al., 2003]. The severity of the forest fire is determined by the amount of organic layer that was burned during the fire [Flannigan and Harrington, 1988; Johnson, 1992]. The objectives of this chapter were to 1) identify the burn severity thresholds after which permafrost continues to thaw, and 2) determine which factors most influence post-fire permafrost thermal conditions. Post-fire permafrost dynamics are considered for upland and lowland ecosystem settings obtained from Bonanza Creek Long Term Ecological Research stations. The influences of climate warming, fire severity, organic soils and soil moisture content were tested for each ecosystem. The results under certain restrictions can be extrapolated to the wider areas within the boreal forest region.

The problem of permafrost spatial mapping is addressed in chapter 4. Previously, Marchenko et al. [2008] used a numerical model to map permafrost thermal states in Alaska at 0.5^{o} spatial resolution. Daanen et al. [2011] applied a modified version of the same numerical model in order to map permafrost dynamics in Greenland. To map permafrost dynamics in Alaska in finer spatial resolution (2 x 2 km), we used a climate dataset

provided by the Scenarios Network for Alaska and Arctic Planning. Other input datasets such as surficial geology, initial temperature, and organic layer distribution maps were prepared and digitized using ArcGIS mapping software. Results improve the projected earlier permafrost spatial dynamics in Alaska.

In the final chapter, I summarize the results from each chapter, state their limitations, and outline future implications. This chapter also includes the difference between simulated, decadally averaged mean annual ground temperatures at 1 meter depth for the beginning and end of the 21st century. This figure is based on the results from Chapter 4, and serves as additional support for the statements in the concluding chapter.

Bibliography

Alexeyev, V. A. and Birdsey, R. A.: Control of Depth to Permafrost and Soil Temperature by Forest Floor in Black Spruce/Feather Moss Communities, US Department of Agriculture Research Note PNW-396, Portland, OR, 1982.

Alexeyev, V. A. and Birdsey, R. A.: Carbon storage in forests and peatlands of Russia, Gen. Tech. Rep. NE, U.S.D.A. Forest Service Northeastern Research Station, Radnor., 244, 1998.

Bonan, G. B. and Shugart, H. H.: Environmental factors and ecological processes in boreal forests, Annu. Rev. Ecol. Syst., 20, 1–28, 1989.

Brown, J. and Grave, N. A.: Physical and thermal disturbance and protection of permafrost, CRREL Rep. 79-5, p. 42, 1979.

Brown, R. J. E.: Effects of fire on permafrost ground thermal regime, in The Role of Fire in Northern Circumpolar Ecosystems, edited by R. W. Weinand D. A. MacLean, pp. 97–110, 1983.

Callaghan, T. V., Johansson, M., Anisimov, O., Christiansen, H. H., Instanes, A., Romanovsky, V., and Smith, S.: Chapter 5: Changing permafrost and its impacts. In: Snow, Water, Ice and Permafrost in the Arctic (SWIPA), Arctic Monitoring and Assessment Programme (AMAP), p. 62, 2011.

Cleve, K. V. and Viereck, L. A.: A comparison of successional sequences following fire on permafrost-dominated and permafrost-free sites in interior Alaska, Permafrost: Proceeding of the Fourth International Conference. National Academy Press, Fairbanks, Alaska, Geographical Review, pp. 1286–1291, 1983.

Daanen, R. P., Ingeman-Nielsen, T., Marchenko, S. S., Romanovsky, V. R., Foged, N., Stendel, M., Christensen, J. H., and Svendsen, K. H.: Permafrost degradation risk zone assessment using simulation models, The Cryosphere, 5, 1043–1056, 2011.

Davis, M.: Permafrost, a Guide to Frozen Ground in Transition, Universisty of Alaska Press, Fairbanks, Alaska, 2001.

Douville, H., Royer, J. F., and Mahfouf, J. F.: A new snow parameterization for the Meteo-France climate model., Climate Dynamics, 12, 21–35, 1995.

Fedorov, A. N. and Konstantinov, P. Y.: Recent changes in ground temperature and the effect on permafrost landscapes in Central Yakutia, In: Proceedings Ninth International Conference on Permafrost, Edited by D. L. Kane and K. M. Hinkel. Fairbanks. Institute of Northern Engineering, University of Alaska Fairbanks, June 29-July 3, Fairbanks, Alaska, 1, 433–438, doi:10.1641/B580807, 2008.

Flannigan, M. D. and Harrington, J. B.: A Study of the Relation of Meteorological Variables to Monthly Provincial Area Burned by Wildfire in Canada (1953–80), J. Appl. Meteor., 27, 441–452, 1988.

Goodrich, L. E.: The influence of snow cover on the ground thermal regime., Canadian Geotechnical Journal., 19, 421–432, 1982.

Hinzman, L. D. and Kane, D. L.: Potential Response of an Arctic Watershed During a Period of Global Warming, Journal of Geophysical Research - Atmospheres, 97, 2811–2820, 1992.

Hopkins, D. M., Karlstrom, T., Black, R., Williams, J., Pewe, T., Fernold, A., and Muller, E.: Permafrost and ground ice in Alaska, a shorter contribution to the general geology, Permafrost and ground ice in Alaska, a shorter contribution to the general geology, U.S. Geol. Surv. Prof., p. 264, 1955.

Hubberten, H. W. and Romanovskii, N. N.: Terrestrial and offshore permafrost evolution of the Laptev Sea region during the last Pleistocene-Holocene glacial-eustatic cycle, Paper presented at Permafrost response to economic development, environmental security and natural resources. Proceedings of NATO-ARW, Kluwer, pp. 43–60, 2001.

Johnson, E. A.: Fire and vegetation dynamics: studies from the North American boreal forest, Cambridge, 1992.

Jorgenson, T., Yoshikawa, K., Kanevskiy, M., Shur, Y., Romanovsky, V., Marchenko, S., Grosse, G., Brown, J., and Jones, B.: Permafrost Characteristics of Alaska - A new permafrost map of Alaska, Ninth International Conference on Permafrost., 2008.

Kryuchkov, V. V.: The effect of permafrost on the northern tree line, Second International Permafrost Conf., pp. 136–138, 1978.

Larsen, P. H., Goldsmith, S., Smith, O., Wilson, M. L., Strzepek, K., Chinowsky, P., and Saylor, B.: Estimating future costs for Alaska public infrastructure at risk from climate change, Global Environmental Change, 18, 442–457, 2008.

Ling, F. and Zhang, T.: A numerical model for surface energy balance and thermal regime of the active layer and permafrost containing unfrozen water, Cold Regions Science and Technology, 38, 1–15, 2004.

Luthin, J. and Guymon, G.: Soil moisture-vegetation-temperature relationships in central Alaska, Journal of Hydrology, 23, 233–246, doi:10.1016/0022-1694(74)90005-5, 1974.

Marchenko, S., Romanovsky, V., and Tipenko, G.: Numerical modeling of spatial permafrost dynamics in Alaska, in: In Proceedings of the Eighth International Conference on Permafrost, pp. 190–204, Willey, Institute of Northern Engineering, University of Alaska, Fairbanks, 2008.

McGuire, A. D., Melillo, J. W., Kicklighter, D. W., and Joyce, L. A.: Equilibrium responses of soil carbon to climate change: empirical and process-based estimates, Journal of Biogeography, 22, 785–796, 1995.

Nicholson, F. H. and Granberg, H. B.: Permafrost and snowcover relationships near Schefferville, 2nd Int. Conf. on Permafrost, Yakutsk, North American Volume:, pp. 151–158, 1973.

O'Donnell, J. A., Harden, J. W., McGuire, A. D., and Romanovsky, V. E.: Exploring the sensitivity of soil carbon dynamics to climate change, fire disturbance and permafrost thaw in a black spruce ecosystem, Biogeosciences, 8, 1367–1382, doi:10.5194/bg-8-1367-2011, URL `http://www.biogeosciences.net/8/1367/2011/`, 2011.

Osterkamp, T. E.: Thermal state of permafrost in Alaska during the fourth quarter of the twentieth century, Paper presented at Ninth International Conference on Permafrost, pp. 1333–1338, 2008.

Osterkamp, T. E. and Gosink, J. P.: Variations in permafrost thickness in response to changes in paleoclimate, J. Geophys. Res, 96, 4423–4434, 1991.

Romanovsky, V. E. and Osterkamp, T. E.: Effects of unfrozen water on heat and mass transport processes in the active layer and permafrost., Permafrost Periglacial Process., 11, 219–239, 2000.

Romanovsky, V. E., Smith, S. L., and Christiansen, H. H.: Permafrost thermal state in the polar Northern Hemisphere during the international polar year 2007–2009: a synthesis, Permafrost and Periglacial Processes, 21, 106–116, doi:10, 2010.

Rouse, W. R.: Microclimate of low arctic tundra and forest at Churchill, Manitoba, In: Proc 4th Can Permafrost Conf, National Research Councll, Ottawa, pp. 68–80, 1982.

Schuur, E. A. G., Bockheim, J., Canadell, J., Euskirchen, E., Field, C. B., Goryachkin, S. V., Hagemann, S., Kuhry, P., Lafleur, P., Lee, H., Mazhitova, G., Nelson, F. E., Rinke, A., Romanovsky, V., Shiklomanov, N., Tarnocai, C., Venevsky, S., Vogel, J. G., and Zimov, S. A.: Vulnerability of Permafrost Carbon to Climate Change: Implications for the Global Carbon Cycle, BioScience, 58, 701–714, doi:10.1641/B580807, 2008.

Schuur, E. A. G., Vogel, J. G., Crummer, K. G., Lee, H., Sickman, J. O., , and Osterkamp, T. E.: The effect of permafrost thaw on old carbon release and net carbon exchange from tundra, Nature, 459, 556–559, 2009.

Shur, Y. L. and Jorgenson, M. T.: Patterns of permafrost formation and degradation in relation to climate and ecosystems, Permafrost and Periglacial Processes, 18, 7–19, doi: 10.1002/ppp.582, URL `http://dx.doi.org/10.1002/ppp.582`, 2007.

Smith, M. W.: Microclimatic influences on ground temperatures and permafrost distribution, Mackenzie Delta, Northwest Territories, Can. Jnl Earth Sci., 12, 1421–1438, 1975.

Street, R. B. and Melnikov, P. I.: Seasonal snow cover, ice, and permafrost, In: Climate Change: The IPCC Impacts Assesment [McG. Tegart, W.J., G.W. Sheldon, and D.C. Griffiths (eds.)]. Australian Government Publishing Service, Imprimatur Press, Canberra, Australia, pp. 7–1–7–33, 1990.

Sturm, M., Holmgren, J., Konig, M., and Morris, K.: The thermal conductivity of seasonal snow, Journal of Claciology, 43, 1997.

Sumgin, M. I., Kachurin, S. P., Tolstikhin, N. I., and Tumel, V. F.: Obshchee merzlotovedenie. [General Permafrostology], Akademiia Nauk SSR, Leningrad-Moscow, 1940.

Tiedemann, A. R., Conrad, C. E., Dieterich, J. H., Hurnbeck, J. W., Megahan, W. F., Viereck, L. A., and Wade, D. D.: Effects of fire on water: A state-of-knowledge review, Gen. Tech. Rep. WO-10, p. 28, 1979.

van Everdingen Robert: Multi-language glossary of permafrost and related ground-ice terms, Boulder, CO: National Snow and Ice Data Center/World Data Center for Glaciology., revised May 2005, 1998.

Velichko, A. A. and Faustova, M. A.: Glaciation during the Late Pleistocene, Paleoclimates and paleoenvironments of extra-tropical area of the Northern Hemisphere. Late Pleistocene - Holocene, GEOS, Moscow, pp. 32–42, 2009.

Viereck, L. A.: Ecological effects of river flooding and forest fires on permafrost in the taiga of Alaska, in Permafrost: The North American Contribution to the 2nd International Conference, July 1973, Yakutsk, USSR,, pp. 60–67, 1979.

Viereck, L. A.: The effects of fire in black spruce ecosystems of Alaska and northern Canada, In The role of fire in northern circumpolar ecosystems. Edited by R.W. Wein and D.A. MacLean. Wiley, Chichester, UK., pp. 201–220, 1983.

Walker, D. A., Walker, M. D., Everett, K. R., and Webber, P. J.: Pingos of the Prudhoe Bay Region, Arctic and Alpine Research, 17, 321–336, 1985.

West, J. J. and Plug, L. J.: Time-dependent morphology of thaw lakes and taliks in deep and shallow ground ice, J. Geophys. Res., 113, F01 009, 2008.

Williams, P. J. and Smith, M. W.: The Frozen Earth: Fundamentals of Geocryology, Cambridge University Press, 1989.

Yershov, E. D.: General Geocryology, Cambridge University Press, 1998.

Yershov, E. D. and Garagulya, L. S.: Basics of geocryology. Part 4:Dynamical geocryology, Moscow, in russian edn., 2001.

Yoshikawa, K., Bolton, W. R., Romanovsky, V. E., Fukuda, M., and Hinzman, L. D.: Impacts of wildfire on the permafrost in the boreal forests of Interior Alaska, J. Geophys. Res., 107, doi:10.1029/2001JD000438, 2003.

Zhang, T.: Influence of the seasonal snow cover on the ground thermal regime: An overview, Rev. Geophys., 43, RG4002, doi:10.1029/2004RG000157, 2005.

Zhang, T., Barry, R. G., and Haeberli, W.: Numerical simulations of the influence of the seasonal snow cover on the occurrence of permafrost, Norwegian Journal of Geography, 55, 261–266, 2001.

Chapter 2

The effect of snow: How to better model ground surface temperatures[§]

Abstract

We present a method that reconstructs daily snow thermal conductivities using air and ground temperature measurements. We employ an inverse approach to recover daily snow thermal conductivities over the entire snow season. By using reconstructed snow conductivities, we can improve the modeling of ground surface temperatures. The method was applied to four permafrost observation stations in Alaska. Estimated snow thermal conductivities for the interior stations indicated low conductivity values that reached their maximum towards the end of the snow season, while the northern stations showed high conductivity values that reached their maximum towards the middle of the snow season. The differences in snow conductivities between the interior and northern stations are most likely due to wind compaction, which is more pronounced in the northern Arctic lowlands of Alaska.

2.1 Introduction

Snow influences the hydrological cycle, the atmosphere, and the subsurface heat exchange in Arctic climates [Bonan, 2002; Gallimore et al., 2005]. It is one of the main factors responsible for controlling heat exchange between the ground and the atmosphere, ground temperature dynamics, and the thickness of the active layer [e.g., Goodrich, 1982; Shiklomanov and Nelson, 1999; Sazonova and Romanovsky, 2003]. Due to its highly insulative properties, snow effectively lowers the rate of heat loss from the ground, thereby maintaining higher winter soil temperatures [Zhang, 2005]. Morin et al. [2010] define the effective thermal conductivity of snow as the conductivity that accounts not only for heat conduction through the ice crystals within the snowpack but also heat conduction in air voids and latent heat transfer.

Thermo-physical properties of snow cover are critical in moderating the energy exchange between the air and the ground. Thermal properties of seasonal snow strongly depend on numerous factors such as temperature, density, and grain structure, and vary with

[§] E. E. Jafarov, D. J. Nicolsky, V. E. Romanovsky, and J. E. Walsh, in Preparation to be submitted to The Cryosphere.

time and position within the snow layer. Various studies of the thermo-physical properties of snow include field observations, laboratory experiments, and theoretical frameworks [Yen, 1962; Mellor, 1977; Fukusako, 1990; Sturm et al., 1997]. To measure snow thermal conductivity, for example, Abel [1893] used in-situ temperatures, Pitman and Zuckerman [1967] employed the guarded hot-plate method, and Sturm et al. [2002] used the needle probe method. All of the above methods use a common approach: the parameterization of heat capacity and thermal conductivity as functions of snow density [e.g., Goodrich, 1982; Douville et al., 1995; Sturm et al., 1997].

The Geophysical Institute Permafrost Laboratory (GIPL) numerical transient model [Sergueev et al., 2003; Marchenko et al., 2008; Jafarov et al., 2012] simulates ground temperature distribution and uses parameterized snow thermal properties and measurements collected from permafrost observation stations. The input data used in the model was collected at permafrost observation stations in Alaska, and includes snow depth, air temperatures and ground temperatures. Air temperature and snow depth are used as upper boundary conditions in simulations of permafrost temperature dynamics [Marchenko et al., 2008; Jafarov et al., 2012]. To achieve a close correspondence between measured and simulated ground temperatures, Romanovsky and Osterkamp [2000] and Nicolsky et al. [2007, 2009] developed the so-called calibration technique. It's goal is to find a physically-based optimal parameterization of the thermal properties of the active layer and permafrost by minimizing the difference between simulated and in-situ temperature observations at and below the ground surface. One limitation of the calibration technique is that it relies on ground temperature observations and does not reconstruct thermal properties of the snow cover. However, it is typical to simulate the present and future thermal state of permafrost by using only air temperatures and the snow depth, i.e. output variables from large-scale GCMs. Large discrepancies in thermal properties of the snow cover lead to errors in the simulation of ground temperatures and cause modeling biases between measured and simulated ground temperatures. Therefore, to improve the overall quality of permafrost dynamics simulations, we need to find an optimal parameterization of snow layer thermal properties. In this article we suggest a technique to find thermal properties of the snow cover, if temperature observations are available.

Sergienko et al. [2008] reconstructed snow thermal diffusivity from snow temperatures

by using inverse methods to find the diffusivity distribution that best allows a solution of the heat diffusion equation which matches observed temperatures. We propose a similar approach, originally introduced by Tipenko and Romanovsky [2002], which reconstructs daily snow thermal conductivities using both air and ground temperature measurements. Using this method, we obtain a time series of optimal daily snow conductivities over the entire snow season. Obtained snow thermal conductivities improve simulation of the ground temperature dynamics during a snow season.

The structure of this article is as follows. In Sect. 2.2, we describe a commonly used physical model of temperature changes in snow layers and near-surface permafrost. In Sect. 2.3, we outline an inverse approach used to recover snow density and conductivity. In Sect. 2.4, we evaluate the proposed inverse approach using three synthetic experiments. Sect. 2.5 presents a brief description of the four stations in Alaska to which the current method was applied. In Sect. 2.6, we apply our method to estimate the thermal properties of snow layers at the four sites located in Alaska. In Sect. 2.7, we discuss limitations and shortcomings of the proposed algorithm. Finally, in Sect. 2.8, we provide conclusions and describe our main results.

2.2 Physical model

To simulate observed ground temperatures, we used the GIPL transient numerical model, which incorporates the effects of air temperature, snow, soil moisture and multi-layered soil thermal properties [Marchenko et al., 2008]. The model simulates ground temperatures and the seasonal freezing/thawing layer dynamics, and has been successfully validated using ground temperature measurements in shallow boreholes across Alaska [Romanovsky and Osterkamp, 2000; Nicolsky et al., 2009].

The GIPL model solves the 1-D heat equation with phase changes [Carslaw and Jaeger, 1959]:

$$C\frac{\partial T(x,t)}{\partial t} + L\frac{\partial \theta(x,T)}{\partial T}\frac{\partial T}{\partial t} = \frac{\partial}{\partial x}\left(k\frac{\partial T(x,t)}{\partial x}\right), \tag{2.1}$$

where $T(x,t)$ is the temperature and L $[Jm^{-3}]$ is the volumetric latent heat of water fusion. Here, t stands for time and $x \in (x_u, x_l)$ is the spatial variable such that the ground surface is at $x = 0$. The upper boundary $x_u = x_u(t)$ depends on time in order to track the evolution of snow cover. The quantity $x_u(t)$ is equal to the snow cover depth when snow is present,

or is 0 otherwise. The lower boundary x_l is fixed and represents a certain depth below the active layer. Equation (4.1) is complemented with boundary $T(x_u,t) = T_{air}$, $T(x_l,t) = T_l$, and initial conditions $T(x,0) = T_0(x)$. Here, $T_0(x)$ is the temperature at $x \in [0,x_l)$ at time $t = 0$; T_{air} and T_l are observed temperatures at the ground (snow) surface $x = x_u(t)$ and at the depth $x = x_l$, respectively. The volumetric water content in equation (4.1) $\theta(x,T)$ for ground material $0 \le x < x_l$ is defined as:

$$\theta(x,T) = \eta(x)\phi(T,x), \quad \phi(T,x) = \begin{cases} 1, & T \ge T_* \\ |T_*|^b |T|^{-b}, & T < T_* \end{cases}, \tag{2.2}$$

where $\phi(T,x)$ represents the liquid pore water fraction, η is the soil porosity, T_* is the so-called freezing point depression, and b is a dimensionless parameter obtained from unfrozen water curve fitting [Romanovsky and Osterkamp, 2000]. The volumetric water content in equation $\theta(x,T)$ for snow layer, i.e. $x_u \le x < 0$, is equal to zero. The quantities $k = k(x,T)$, $[Wm^{-1}K^{-1}]$ and $C = C(x,T)$ $[Jm^{-3}K^{-1}]$ are thermal conductivity and the volumetric heat capacity, respectively, and are defined in the following way:

$$\begin{aligned} &C = C_s, && k = k_s, && x_u < x < 0, \\ &C = C_t\phi + C_f(1-\phi), && k = k_t^{\phi} k_f^{1-\phi}, && 0 \le x < x_l \end{aligned} \tag{2.3}$$

where $C_s = C_s(t)$ and $k_s = k_s(t)$ are the volumetric heat capacity and bulk thermal conductivity of snow, respectively. The quantities marked with the sub-scripts "t" and "f" represent effective thermal properties of the ground material for the frozen and thawed states. Unlike the thermal properties of snow, effective heat capacity and thermal conductivity are assumed to be time-independent and to vary only with depth. The soil column in the model consists of several soil layers, with every soil layer having its own thermo-physical properties: C_t, C_f, k_t and k_f.

The snow layer in the GIPL model is represented as a homogeneous substance with changing thickness during the snow season. To obtain the temperature distribution within the snow layer, the GIPL solves the heat equation (4.1), where $k_s = k_s(t)$ and $C_s = C_s(t)$ are snow thermal parameters that may change in time but do not change within a snow layer at any given time. So, in order to simulate measured ground surface temperatures, it is important to assign proper daily snow thermal properties.

It is common to define snow heat capacity and thermal conductivity as a function that depends on snow density (Abel [1893], Anderson [1976], Yen [1981], Ostin and Andersson [1991], and many others). Goodrich [1982] and Douville et al. [1995] represented snow heat capacity as a linear function of snow density in order to calculate frozen ground thermal states. Given that the differences between the snow heat capacity formulas used by Goodrich [1982] and Douville et al. [1995] are not significant, we assigned snow heat capacity according to Douville et al. [1995].

$$C_s = C_i \cdot \rho_s / \rho_i, \tag{2.4}$$

where C_i is the heat capacity of ice, and $\rho_s = \rho_s(t)$ and ρ_i $[g \cdot cm^{-3}]$ are densities of snow and ice respectively. Snow thermal conductivity k_s was set according to Sturm et al. [1997]'s empirical formula:

$$k_s = \begin{cases} 0.138 - 1.01\rho_s + 3.233\rho_s^2 & 0.156 \leq \rho_s \leq 0.6, \\ 0.023 + 0.234\rho_s & \rho_s < 0.156, \end{cases}, \tag{2.5}$$

so that both the thermal conductivity and the heat capacity of snow depend on snow density. We ran the model using a vertical grid spatial domain starting from the ground or snow surface to 1 m in depth. We utilized a fine grid resolution (0.01 m) between nearby points for both the snow and the ground layer.

2.3 Data assimilation technique

In this section, we describe key components of the data assimilation technique. The main idea of the data assimilation technique is to optimize the set of model parameters in order to minimize the difference between the modeled and measured temperatures. Here, we supplement the assimilation algorithm to reconstruct thermal properties of the ground material [Romanovsky and Osterkamp, 2000; Nicolsky et al., 2007, 2009] using estimates of the thermal properties of the snow cover. Therefore, for the rest of this manuscript, we assume that the thermal properties k_t, k_f, C_t, C_f, the soil porosity η, and the parameterization of the unfrozen water content a, b are known and can be utilized to simulate the temperature dynamics below the ground surface.

One of the methods to find a snow density $\rho_s = \rho_s(t)$ that can optimally improve the ground surface temperature simulation is to minimize the cost function J [Tarantola, 2005].

This cost function J could be defined according to Beck and Arnold [1977]; Tikhonov and Leonov [1996] as

$$J(\rho_s) = J_1 + J_2, \tag{2.6}$$

where

$$\begin{aligned} J_1 &= \frac{1}{\delta T^2} ||T_m - T(\rho_s)||^2 \\ &= \frac{1}{\delta T^2} \frac{1}{t_f} \int_0^{t_f} [T_m(\tau) - T(0, \tau; \rho_s)]^2 d\tau. \end{aligned} \tag{2.7}$$

is the discrepancy between the measured $T_m(t)$ and simulated $T(0,t;\rho_s)$ ground surface temperatures computed according to equation 4.1 with snow density equal to $\rho_s = \rho_s(t)$, when snow covers the ground surface over the period $[0, t_f]$, and

$$J_2 = \frac{1}{\delta\rho^2} ||\rho_s - \tilde{\rho}_s||^2 = \frac{1}{\delta\rho^2} \frac{1}{t_f} \int_0^{t_f} (\rho_s - \tilde{\rho}_s)^2 d\tau \tag{2.8}$$

is the regularization term. Here, $\tilde{\rho}_s = \tilde{\rho}_s(t)$ is *a priori* information. The coefficient δT in equation (2.6) is the uncertainty in temperature measurements by the sensor at the ground surface [Marchenko et al., 2008; Jafarov et al., 2012], and $\delta\rho$ is the uncertainty in the estimates of density which was determined by fitting the model to the data.

This problem is difficult to solve, since we need to recover the function $\rho_s = \rho_s(t)$, where snow density is a daily changing parameter. It is common to assume that snow density ρ_s is constant. Then the effective snow density can be found for the entire snow season $[0, t_f]$:

$$\hat{\rho}_s = \min_{\rho_s}(J(\rho_s)). \tag{2.9}$$

The constant snow density value, however, does not reflect changes with time due to compaction. To recover daily snow density as a function of time, we propose to modify the cost function (eq. 2.6) in the following form:

$$\begin{aligned} J(\rho_s(t)) = &\frac{1}{\delta T^2} \frac{1}{t - \tilde{t}} \int_{\tilde{t}}^{t} (T_m(\tau) - T(0, \tau; \rho_s))^2 d\tau \\ &+ \frac{1}{\delta\rho^2} \frac{1}{t - \tilde{t}} \int_{\tilde{t}}^{t} (\rho_s - \tilde{\rho}_s)^2 d\tau, \end{aligned} \tag{2.10}$$

Here $T_m(t)$ is the measured and $T(0,t;\rho_s)$ is the simulated daily ground surface temperature, and time interval $\Delta t = t - \tilde{t}$ is the number of days over which the difference between simulated and measured at the ground surface temperatures has been minimized (later in the paper we will refer to it as the "minimization time interval.") The snow density $\rho_s(t)$ is assumed to be constant within the minimization time interval Δt. The main difference between cost functions (2.10) and (2.6) is the minimization time interval Δt. An average snow density $\bar{\rho}_s(t)$ on time interval $[\tilde{t}, t]$, Eq. (2.10) becomes

$$\bar{\rho}_s(t) = \frac{1}{t-\tilde{t}} \int_{\tilde{t}}^{t} \rho_s d\tau. \tag{2.11}$$

Similar to Eq. (2.6), the first part of Eq. (2.10) minimizes a difference between measured and simulated ground surface temperatures, and the second term does not let the daily snow density be significantly different from the average of previously obtained densities. Assuming low density of the freshly fallen snow as an initial approximation, we start with snow density equal to 0.1 $g \cdot cm^{-3}$. Then we calculate ground surface temperature by solving equation (4.1) with the current snow density. Using the calculated ground surface temperature, we find an optimal snow density

$$\hat{\rho}_s(t) = \min_{\rho_s}(J(\rho)). \tag{2.12}$$

for every time moment t from $[0, t_f]$ by minimizing cost function (eq. 2.10). In order to find the optimal daily snow density $\hat{\rho}_s(t)$, we use the nonlinear optimization method by Lagarias et al. [1998]. When the optimal snow density is found, we proceed to the next day. As a result, we obtain a reconstructed snow density time series over the whole snow season. We provide an evaluation of the this method next.

2.4 Method evaluation

To evaluate the method performance, we chose data during winter 2009-2010 measured at the recently installed Deadhorse Permafrost Observation Station. The data from this station is published on-line and includes up-to-date, high precision measurements of snow depth and ground temperatures. We calibrated ground thermal properties according to the measured ground temperatures within a 1 m soil column starting from the ground

surface. In the current numerical experiment, we calculated ground surface temperatures for three different cases. In the first case, we used rounded measured air temperatures and constant snow depth $d_{snow} = 30cm$ (Fig. 2.1, Case 1). In the second case, we used rounded measured air temperatures and measured snow depth (Fig. 2.1, Case 2). In the final (third) case, we used measured air temperatures and measured snow depth (Fig. 2.1, Case 3). For all three cases we considered the following two sub-cases: A) constant snow density $\rho_A(t) = 0.25\ g \cdot cm^{-3}$ (Fig. 2.2-A); and B) exponentially growing [Verseghy, 1991] and then varying snow density $\rho_B(t)$ (Fig. 2.2-B).

First, we calculated ground surface temperatures by using prescribed snow densities for all three cases. Then, we assigned calculated ground surface temperatures as described above. The uncertainty of the ground temperature measurements includes the uncertainties from the thermistor calibration in the ice bath, uncertainties from the field measurements, and uncertainties from the probes that might also disturb the soil temperature around them. Uncertainty of the ground surface temperature measurements $\delta T = 0.1$ and uncertainty in the estimate of density $\delta\rho = 0.1$.

For all three cases, the initial snow density was set to $0.1\ g \cdot cm^{-3}$ and the minimization time interval Δt was set to 30 days. Recovered snow density functions for Cases 1 and 2 (Fig. 2.2, Case 1,2-A,B) corresponded well with actual densities from sub-cases (A) and (B), except for small fluctuations in reconstructed snow densities for Case 2-A,B, which can be attributed to the non-homogeneous snow depth. Recovered snow densities for Case 3 (Fig. 2.2, Case 3-A,B) had higher amplitude fluctuations compared with Case 2, which were caused by strong fluctuations in the measured air temperature.

To estimate the uncertainty of the method, we calculated an error covariance of the estimated snow density according to Thacker [1989], which involves calculating the inverse of the Hessian matrix (in our case the second derivative of the cost function Eq.. 2.10) by applying a finite difference formula [Schröter, 2010]. The computed daily method uncertainty is shown in Fig. 2.3. Average uncertainty for the estimated snow densities was $0.06\ g \cdot cm^{-3}$.

To reduce unrealisticly high frequency oscillations in reconstructed snow densities for Case 3-B (Fig. 2.2, Case 3-B), we applied different minimization time intervals $\Delta t = \{1, 30, 60, 90, 120\}$ (eq. 2.10). As the result, we were able to decrease the amplitude of the oscillations

in reconstructed snow densities (Fig. 2.4,A). To evaluate the accuracy, we calculated the discrepancies

$$||\Delta\rho_s|| = ||\hat{\rho}_s - \rho_B|| \tag{2.13}$$

between the reconstructed $\hat{\rho}_s(t)$ and prescribed $\rho_B(t)$ snow densities according to Eq. (2.8). Additionally, we calculated discrepancies between the synthetic and simulated ground surface temperatures $||\Delta T||$ (Fig. 2.4,C)

$$||\Delta T|| = ||T_m - T(\hat{\rho}_s)|| \tag{2.14}$$

according to the equation (2.7). An increase in the minimization time interval Δt improved discrepancies between reconstructed and prescribed snow densities for Δt =30, 60 and 90 days (Fig. 2.4,B). The smallest difference between simulated and synthetic ground surface temperatures was obtained for the 30-day minimization time interval (Fig. 2.4,C).

This analysis showed that method is able to reconstruct prescribed snow densities. Nevertheless, high fluctuations in measured air temperatures affected reconstructed snow densities. Therefore, we rounded reconstructed snow densities for minimization time intervals Δt =30 and 60 days, using a moving-average filter corresponding to the minimization time interval day span, i.e. a 30-day span for Δt = 30 and a 60 day-span for Δt = 60 (Fig. 2.4,D). Simulated ground surface temperatures using reconstructed snow densities for a minimization time interval of 30 days and rounded with a 30-day moving-average filter showed the smallest discrepancies in terms of snow density and temperature (Fig. 2.4,B-C). The rounded snow density lies within uncertainty intervals (Fig. 2.3); therefore, later in the study, we use a Δt = 30 days minimization time interval and a 30-day moving-average filter to round reconstructed snow densities. Accordingly, snow thermal conductivities were obtained from reconstructed snow densities.

To identify how the choice of initial snow density affects the overall shape of the reconstructed snow density $\hat{\rho}_s(t)$, we used different initial densities at the beginning of the time interval. Selection of a proper initial snow density is important, since it ensures that the recovered snow density is close to the actual snow density from the first day of snow fall. Numerical experiments show that reconstructed snow densities obtained using different initial approximations may vary for the first few days of the snow season, but then remain similar to one another for the rest of the time interval.

2.5 A brief description of the sites

To evaluate the model, we chose two permafrost observation stations from the North Slope (Deadhorse and Franklin Bluffs) and two from Interior Alaska (Bonanza Creek and Smith Lake). These sites were chosen because each has continuous snow depth measurements available for the simulation time periods. Northern permafrost observation stations were equipped with Campbell Scientific SR50 Sonic Ranging Sensors that were connected to the data logger at the climate stations. Interior stations do not include snow measuring sensors. The snow depth for the Smith Lake site was obtained from the Alaska Climate Data Browser[1] and corresponds to the Fairbanks International Airport station. The snow data for the Bonanza Creek site were obtained from the Bonanza Creek Long Term Ecological Research data-server. Each permafrost observation station represents a small climate station which includes high-precision air and ground temperature sensors (Campbell Scientific L107 thermistor) and up to three Hydra Probe soil moisture sensors. Ground temperatures were measured down to 1 m depth with sensors located about every 10 cm. All measurements were taken at one-hour time intervals. The thermistor sensors were calibrated in an ice bath prior to installation to an accuracy of 0.01^oC. More detailed information on data logger installation can be found in [Osterkamp and Romanovsky, 1999; Romanovsky and Osterkamp, 2001; Osterkamp, 2003; Romanovsky et al., 2003].

The Deadhorse (DH) permafrost observation site is located in the continuous permafrost zone, 2.5 km south of the Deadhorse airport (Alaska) along the Dalton Highway. The Franklin Bluffs (FB) permafrost observation site is also located along the Dalton Highway, about 47 km south of Deadhorse on a low terrace of the Sagavanirktok River. At both of these sites, the mean annual air temperature was approximately -12^oC and annual precipitation levels ranged from 150 mm to 250 mm, where most of the precipitation falls as snow. The vegetation at DH and FB is characterized as moist tundra [Walker et al., 2008]. This continuous vegetation consists mostly of graminoids (mainly sedges) and sparse dwarf shrubs. Dwarf shrubs are common for FB and sparse at DH. The ground surface is flat with occasional frost boils. Continuous data from the DH station are available from July 2007 to July 2012, and from July 2002 to July 2006 for the FB station.

The Smith Lake (SL) station is located at the University of Alaska Fairbanks campus

[1] http://climate.gi.alaska.edu

in the discontinuous permafrost zone. The vegetation in this region is taiga evergreen needle-leafed forest. Typical plants at this site include black spruce. According to the Alaska Climate Center, mean annual air temperature averaged for the last 10 years in the Fairbanks vicinity is approximately -2^oC, with mean annual precipitation of about 261 mm, a large amount of which falls as rain during the summer. Continuous data from the SL station are available from June 1997 to June 2012; for the numerical experiment we chose the 1999 to 2005 time period.

The Bonanza Creek (BZ) station is located in the discontinuous permafrost zone within the Bonanza Creek Long Term Ecological Research (LTER) site on the Tanana River floodplain, 26 km southwest of Fairbanks. This site experienced a severe forest fire in 1983. Vegetation includes small black spruce trees with shrubs. Continuous data from the BZ station are available from June 2000 to June 2004.

2.6 Results

Before estimating snow thermo-physical properties, we calibrated ground thermal properties according to the measured ground temperatures in a 1 m soil column starting from the ground surface for all four stations. The snow density recovery method was applied to four permafrost observation stations: two northern stations located in North Slope Alaska in the continuous permafrost zone and two interior stations near Fairbanks located in the discontinuous permafrost zone. We calculated snow thermal conductivities using Eq. 2.5, and calculated the corresponding uncertainties assuming that snow thermal conductivities are not subject to uncertainty [Taylor, 1997]. Obtained snow thermal conductivities for the two northern stations (Figures 2.5,2.6) exhibited similar behavior: positive trends during every snow season with high peaks towards the end of the season. The reconstructed snow thermal conductivities for the two interior stations (Figures 2.7,2.8) showed a smaller positive trend for the Bonanza Creek station and near-constant conductivities for the Smith Lake station.

To obtain the averaged snow thermal conductivity time series for each of four stations, we spanned reconstructed thermal conductivities over the same time domain (Fig 2.9). To identify the time evolution during the snow season, we named the spans "beginning," "middle," and "end," which correspond to the beginning, middle and ending of the snow

season, respectively. The high peaks in the averaged reconstructed thermal conductivities toward the end of the snow season were neglected, since the model cannot be used when snow is experiencing a phase transition such as melting or freezing.

The highest snow thermal conductivity was 0.42 $Wm^{-1}K^{-1}$, obtained at the most northern station, Deadhorse. Approximately 47 km south of this station is the Franklin Bluffs station, where the highest average snow conductivity was 0.26 $Wm^{-1}K^{-1}$. At both of these stations, snow conductivity reached its maximum value in the middle of the snow season (Fig 2.9-A,B). The maximum averaged snow thermal conductivities for the Bonanza Creek and Smith Lake interior stations were equal to 0.18 and 0.09 $Wm^{-1}K^{-1}$, respectively. Unlike at the northern sites, the maximum snow conductivity values for the two interior stations were reached towards the end of the snow season (Fig 2.9-C,D).

Finally, in addition to the reconstructed snow thermal conductivities, we calculated constant optimal conductivity for every snow season for all four stations. The constant snow thermal conductivities were calculated from constant densities obtained by minimizing the cost function (eq. 2.6) during entire snow season. Calculated constant conductivities for every station were averaged over the total number of snow seasons for each station.

Averaged reconstructed daily time series and constant snow thermal conductivities were used to simulate ground surface temperatures for all four stations. The root mean square errors (RMSE) between the measured and the simulated ground surface temperatures (eq. 2.14) with both the averaged daily time series (Fig. 2.9) and constant conductivities during the entire snow season were calculated for every station in every snow season.

Overall, obtained RMSEs (Fig. 2.10) showed that the use of a reconstructed averaged daily snow thermal conductivity time series (Fig. 2.9) improved simulation of the ground surface temperatures in comparison with an average constant conductivity for the whole snow season. High discrepancies for DH in 2007 and 2008 (Fig. 2.10-A) were due to unusually shallow snow depths over entire snow season in comparison to other years. The reconstructed average snow thermal conductivities for the SL station (Fig. 2.10-D) had almost constant shape and, therefore, simulated ground surface temperatures using constant and averaged reconstructed snow thermal conductivities did not significantly differ.

2.7 Discussion

Snow thermal conductivities obtained for the DH station have high values: $k_s > 0.4\ Wm^{-1}K^{-1}$ (Fig. 2.5 and Fig. 2.9-A). There are two major factors that may have caused high conductivity values for this station. First, our observations show that the soil at the DH site is highly saturated and a pool of water commonly forms on the ground surface. If the standing water freezes, a thin ice layer could form and cover the temperature measuring sensor at the surface. This ice layer could contribute to the high values of snow effective thermal conductivity retrieved by this method. Another important factor that can affect snow conductivities is wind. Heat convection created by high airflow in the snow layer could increase effective snow thermal conductivity values by factor of 2 to 3 [Sturm, 1991; Sturm and Johnson, 1991].

To show that the proposed method is able to recover expected snow conductivities, we applied it to the other site within the Deadhorse area. Here, high-accuracy data were collected by M. Sturm during the 1991-1992 snow season and include snow depth, air temperatures, ground surface temperatures, and heat flux measured at the ground surface (Fig. 2.11-A).

Since the data did not include temperatures measured below the ground surface, we modified the model by setting measured heat flux at the ground surface. The reconstructed snow thermal conductivities using our method, and the conductivities calculated by dividing measured heat flux by the temperature gradient within the snow layer, showed close correspondence with one another (Fig. 2.11-B). This experiment confirms the importance of prescribing the proper heat flux at the ground surface.

In the method evaluation section, we showed that the high-frequency oscillations in the reconstructed thermal conductivity profile were mainly a consequence of high fluctuations in the daily measured air temperature, and to a smaller degree changes in snow depth. It is important to note that, during time intervals when the temperature gradient within the snow layer was equal to zero, snow thermal conductivity could not be optimally reconstructed. The cost function is especially sensitive to the small temperature gradient at the boundary points and is not always able to converge (e.g. Smith Lake 2000-01, Fig. 2.8). The increase in snow conductivity towards the end of the season could be associated with snow melt, which may last longer for the northern stations than for the interior stations.

The two northern stations are characterized by tundra-type snow [Sturm et al., 1995] and have high thermal conductivity values (Fig 2.9-A,B). High thermal conductivity values can be caused by wind, which compacts the snow layer and produces so-called "wind slab" layers within the snowpack. These layers have high density and thermal conductivity. The interior sites (Fig. 2.9-C,D) are characterized by taiga snow type [Sturm et al., 1995] and are located in the boreal forest. The effect of wind in this area is not so pronounced, and the snow layer consists mainly of chains of depth hoar with lower density and thermal conductivity. The trees at the SL site are able to intercept falling snow and reduce the wind effect. Alternatively, the BZ site is located in the recent (1983) forest fire area, where the trees are still small and the effect of wind is more pronounced, which could be responsible for differences in thermal conductivity maximum values between the two interior stations (Fig. 2.9-C,D).

In the GIPL model, snow is represented as a homogeneous layer that changes in depth with time. A caveat to our approach is the assumption of the conductive nature of energy transfer within the snow layer. Actual snow undergoes compaction via changes in temperature, wind or humidity, effectively changing the density and thermal properties of the snow layer as a function of time. In general, snow melts from the top. Melt-water penetrates the snow column and refreezes close to the ground surface. This mechanism enables advective heat transfer and causes a rapid increase in soil temperature [Kane et al., 2001]. Thus, other heat flow mechanisms such as convection and radiation may become significant [Sturm et al., 1997], meaning that the heat flow within the snow layer is no longer dominated by conduction.

An advantage of our model lies in its ability to reveal changes in snow thermal conductivity based primarily on the availability of snow depth data and air and ground temperature measurements. The developed method shows that better snow thermal properties parameterization can reduce bias in modeling ground temperatures. Further work is necessary to obtained a regional snapshot of the snow thermal conductivity distribution, including high-precision data sets on snow depth, air and ground temperatures.

2.8 Conclusions

The objective of this study was to improve parameterization of snow thermal properties and to better model ground temperature dynamics. Estimated snow thermal conductivities (Fig. 2.9) showed higher values at the northern sites, which could be associated with differences in climatic factors and in particular with compaction due to wind effects. The snow at the two interior stations was not subject to as much wind, and therefore had lower conductivities (Fig. 2.9-C,D). A thin ice layer may have formed at the ground surface and caused high snow conductivities at the Deadhorse station.

The model cannot be applied to areas where the seasonal snowpack is experiencing frequent phase changes (melting or freezing). A 1D heat flow model used to reconstruct snow densities and thermal conductivities also does not include other processes, such as latent heat and water vapor diffusion, which could have an impact on the overall heat exchange within the snowpack. The snow thermal conductivity estimated by our method, however, can be described as an effective snow thermal conductivity and, therefore, includes the effects of nonconductive heat exchange until the process is primarily dominated by conduction.

2.9 Acknowledgements

We are very thankful to M. Sturm for sharing his data with us and for his advice, critiques and reassurances along the way. We also thank J. Stroh and S. Higgins for their valuable comments and corrections. This research was funded by the State of Alaska and by the National Science Foundation under grant ECO-MODI.

2.10 Figures

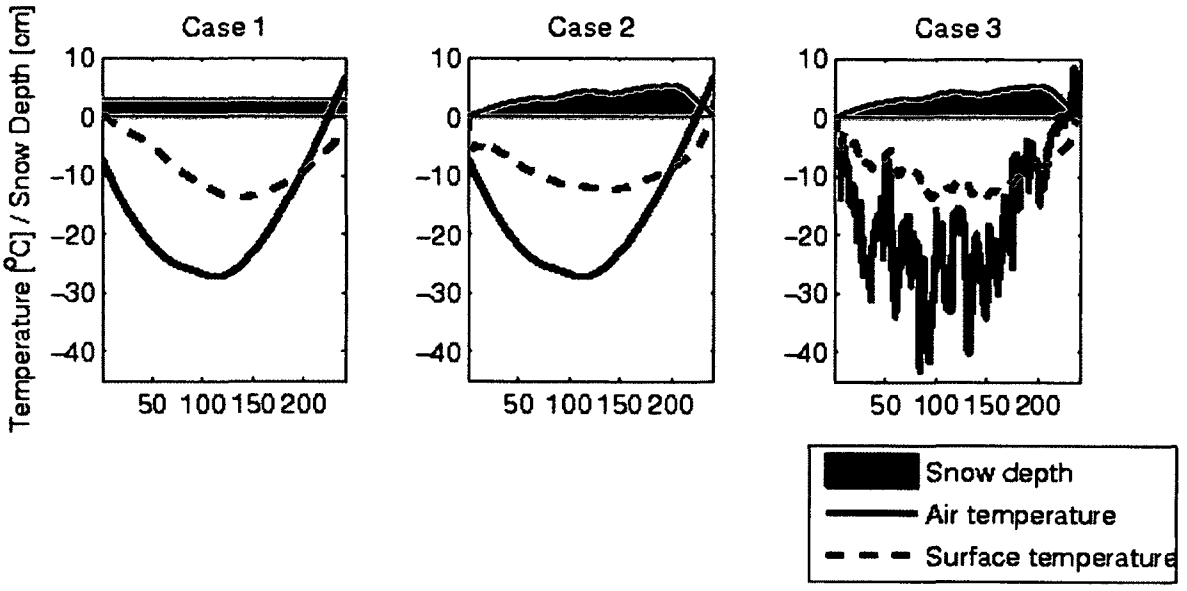

Figure 2.1. Three cases experiment set up to evaluate proposed method. The subplot marked by Case 1 include constant snow depth $d_s = 30\ cm$, rounded air temperature and simulated surface temperature. The subplot marked by Case 2 include measured snow depth, rounded air temperature and simulated surface temperature. The subplot marked by Case 3 include measured snow depth, measured air temperature and simulated surface temperature. For all three subplots from Fig. 2.1 the upper column cyan colored shape represents snow depth, solid blue curve corresponds to the air temperature and dotted red curve corresponds to the simulated ground surface temperature.

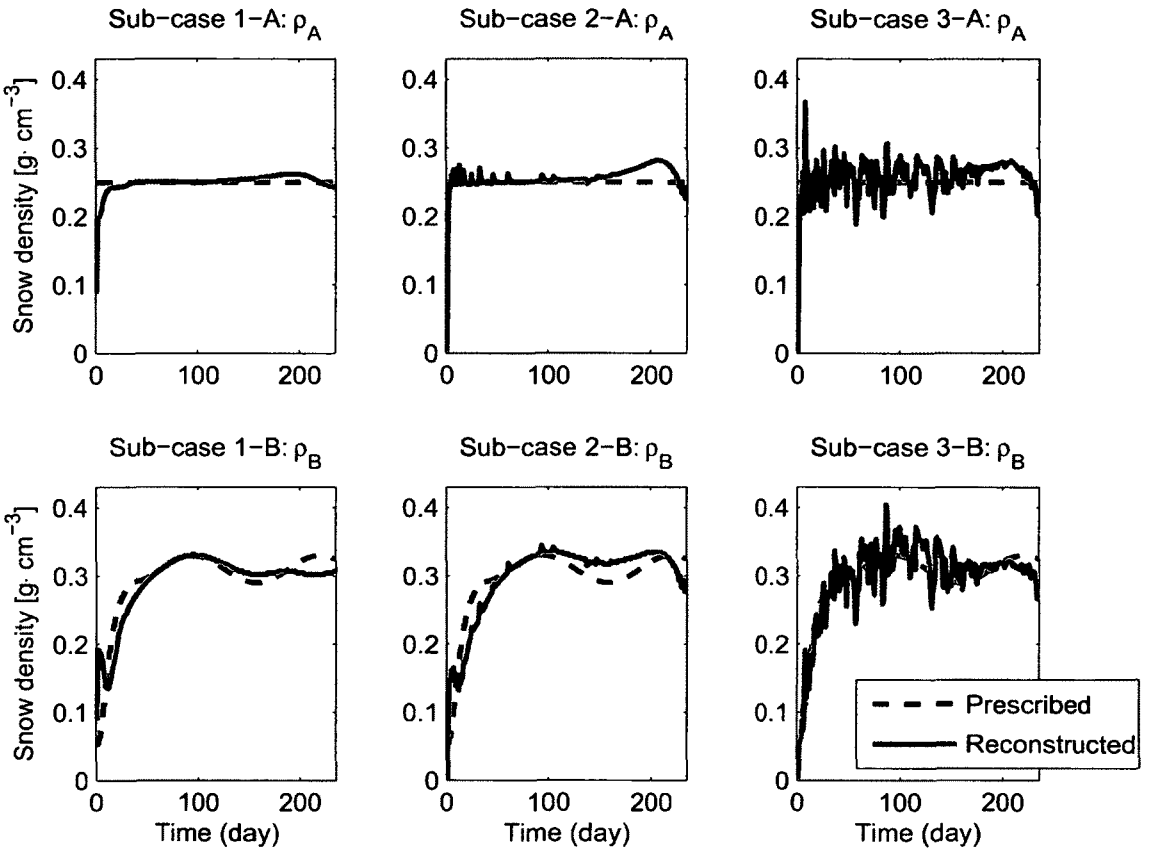

Figure 2.2. Estimated and prescribed snow thermal conductivities for three cases experiments. The subplots marked by letter (A) correspond to constant snow density and subplots marked by letter (B) correspond to the exponentially growing and then varying snow density. In subplots marked by letter (A) and (B) the dash black curve corresponds to the prescribed snow density and solid green curve corresponds to the reconstructed snow density. The subplots marked by letters (A) and (B) are the sub-cases of Case 1,2 and 3.

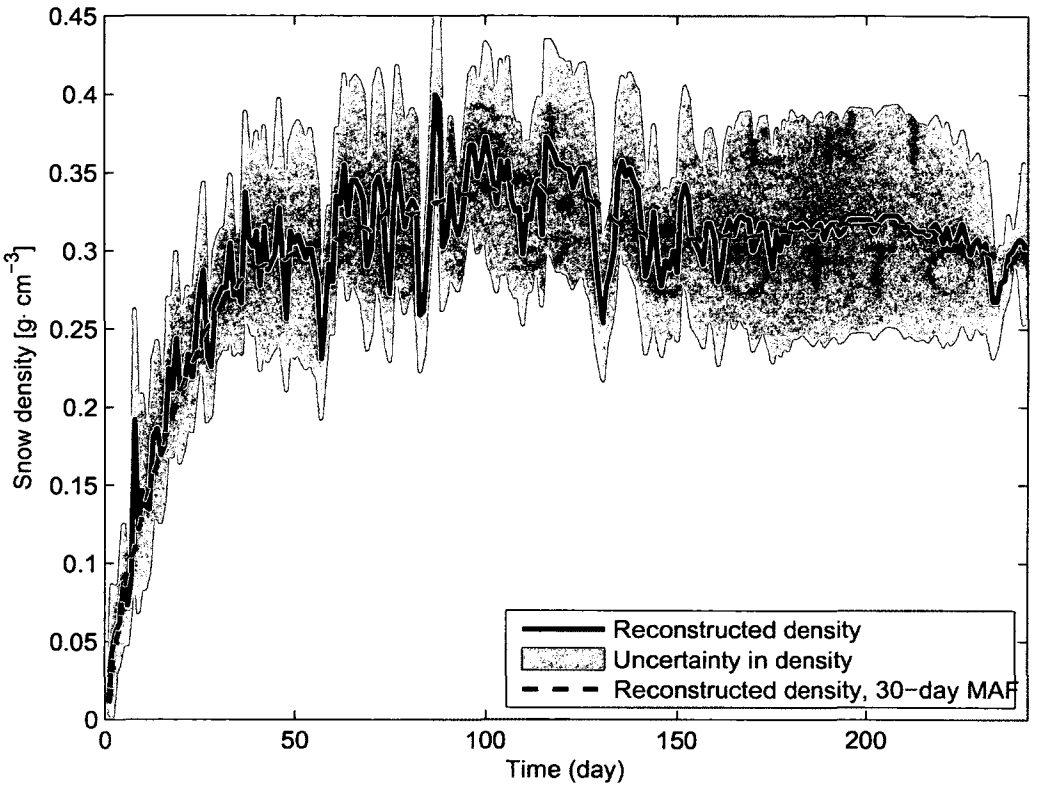

Figure 2.3. The estimated snow density (black solid curve) and calculated uncertainties (solid cyan) for the reconstructed snow densities for CASE 3, scenario 2 (Fig. 2.2, CASE 3-C) obtained using time average interval Δt = 30 days, and rounded snow densities (dashed red curve) for minimization time interval Δt = 30 days using moving average filter with the corresponding day span.

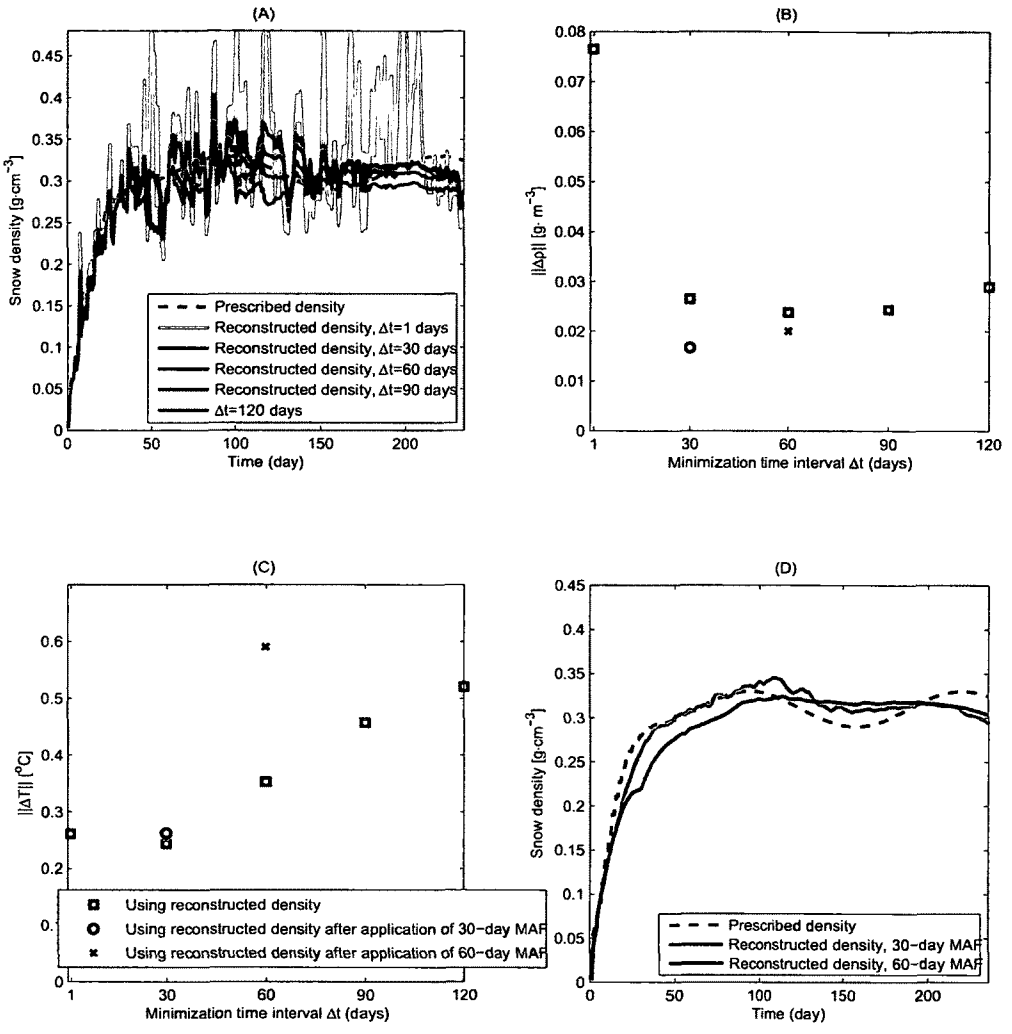

Figure 2.4. Evaluation of the reconstructed snow densities. Top left: the reconstructed snow densities for CASE 3, sub-case (B) (Fig. 2.2, Case 3-B) obtained using different minimization time average intervals $\Delta t = \{1, 30, 60, 90, 120\}$; Top right: the red squares correspond to the difference $||\Delta\rho||$ between prescribed and recovered snow densities and blue circles correspond to the discrepancy between prescribed and rounded snow densities. Bottom left: the red squares correspond to the difference $||\Delta T||$ between measured and simulated ground surface temperatures obtained using recovered snow densities and blue circles correspond to the difference between measured and simulated ground surface temperatures obtained using rounded snow densities. Bottom right: Rounded snow densities for minimization time intervals Δt equal to 30 and 60 days using moving average filter (MAF) with the corresponding day span.

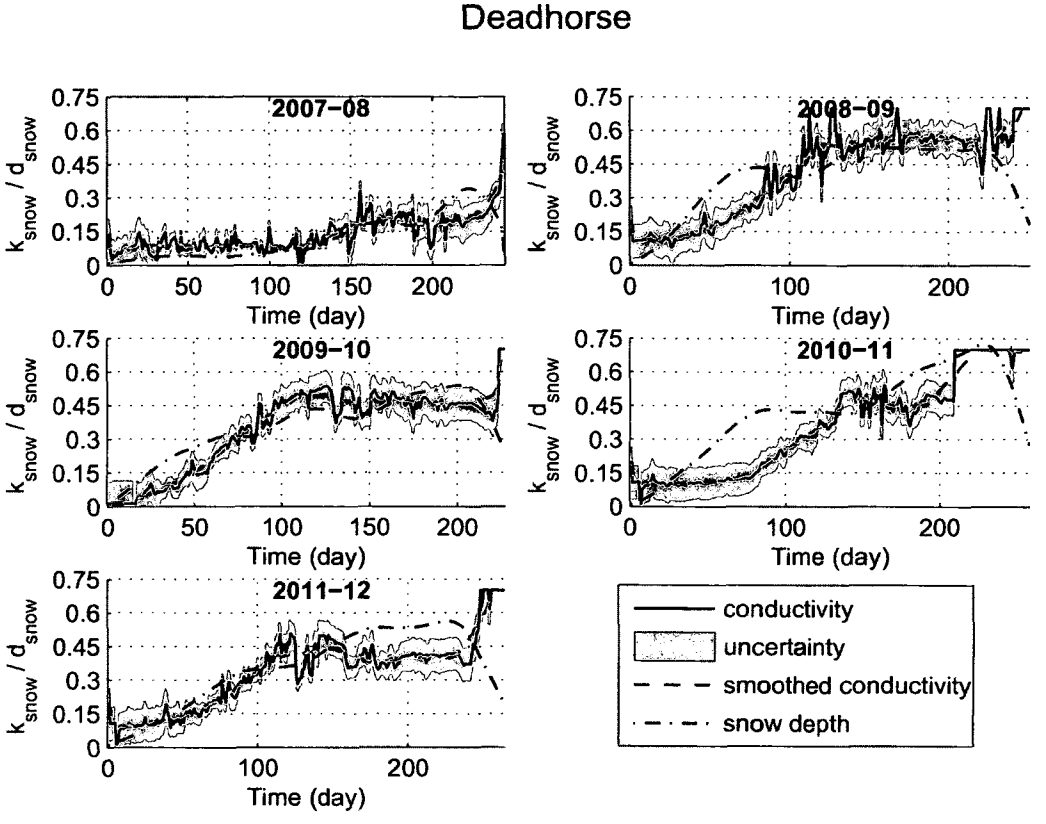

Figure 2.5. The estimated snow thermal conductivities $[Wm^{-1}K^{-1}]$ (black solid curve) at the Deadhorse permafrost station and the corresponding uncertainties (solid cyan) for 2007-2012 snow seasons. The dash red curve corresponds to the rounded thermal conductivities and the dot-dash blue curve corresponds to the snow depth $[m]$.

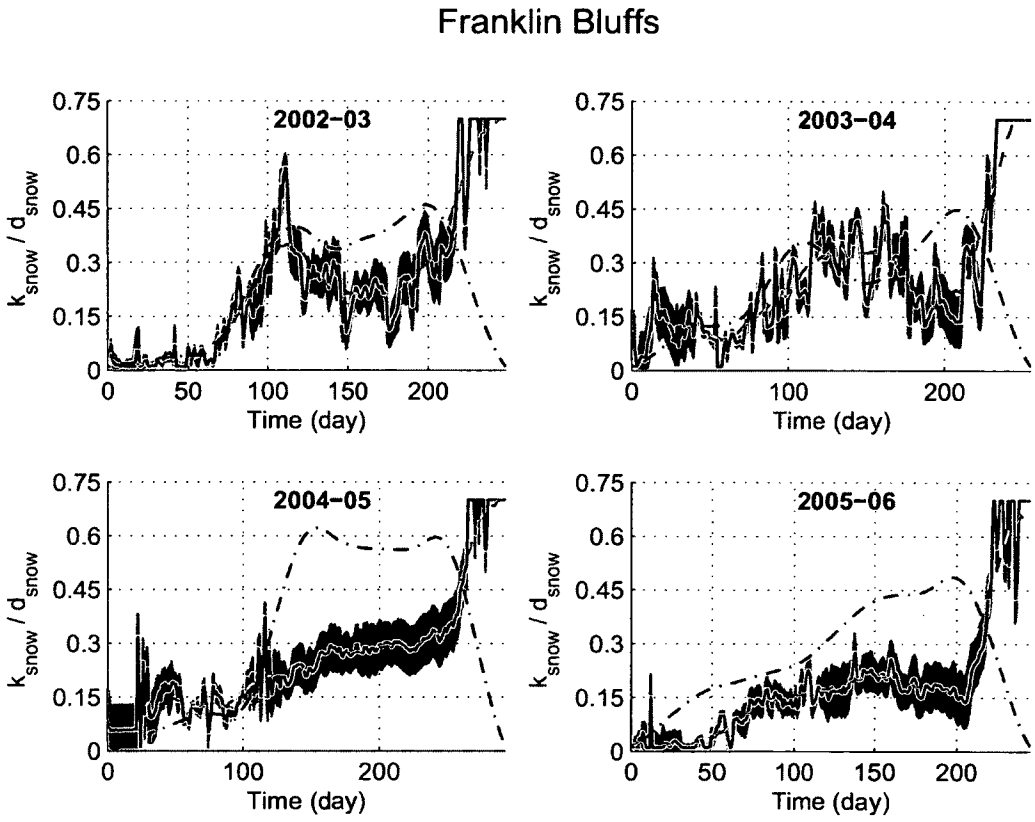

Figure 2.6. The estimated snow thermal conductivities $[Wm^{-1}K^{-1}]$ (black solid curve) at the Franklin Bluffs permafrost station and the corresponding uncertainties (solid cyan) for 2002-2006 snow seasons. The dash red curve corresponds to the rounded thermal conductivities and the dot-dash blue curve corresponds to the snow depth $[m]$.

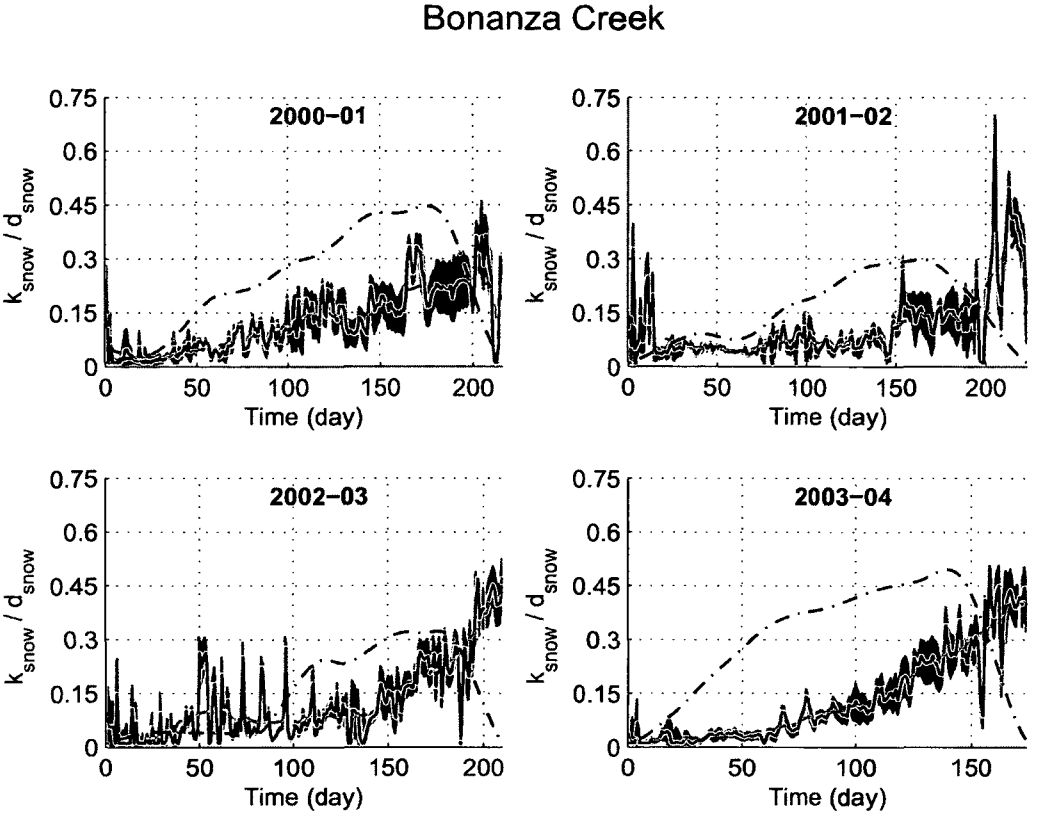

Figure 2.7. The estimated snow thermal conductivities $[Wm^{-1}K^{-1}]$ (black solid curve) at the Bonanza Creek permafrost station and the corresponding uncertainties (solid cyan) for 2000-2004 snow seasons. The dash red curve corresponds to the rounded thermal conductivities and the dot-dash blue curve corresponds to the snow depth $[m]$.

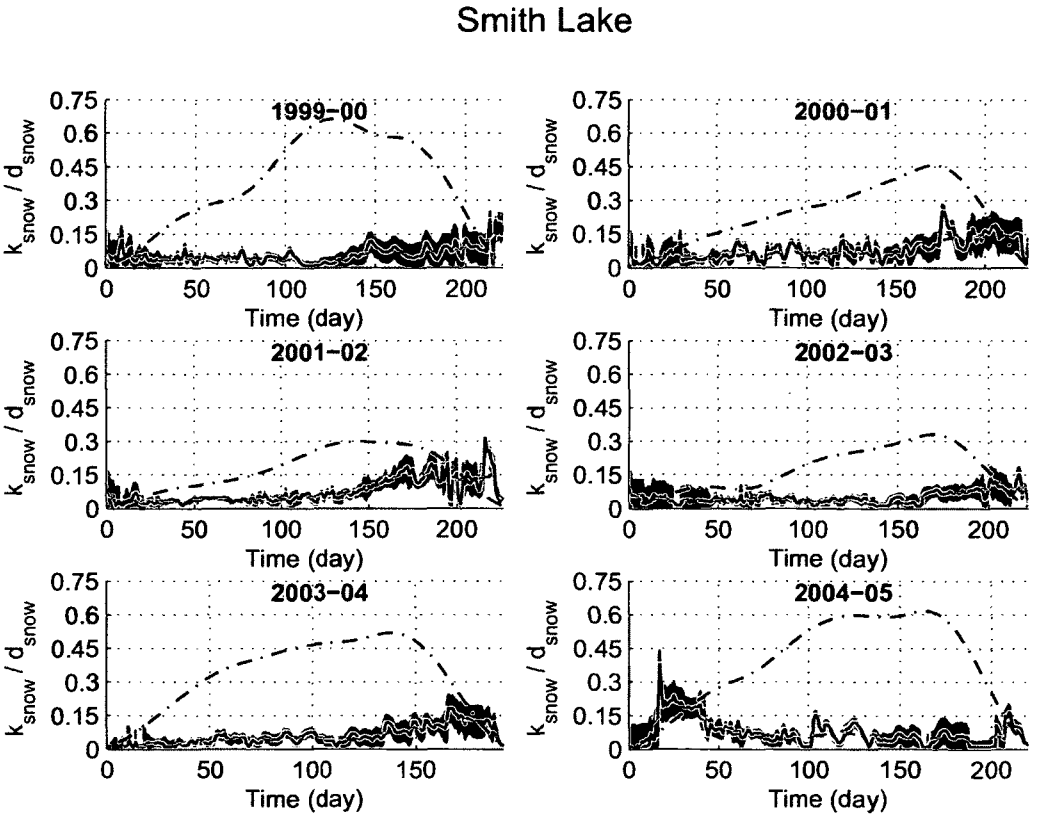

Figure 2.8. The estimated snow thermal conductivities $[Wm^{-1}K^{-1}]$ (black solid curve) at the Smith Lake permafrost station and the corresponding uncertainties (solid cyan) for 1999-2005 snow seasons. The dash red curve corresponds to the rounded thermal conductivities and the dot-dash blue curve corresponds to the snow depth $[m]$.

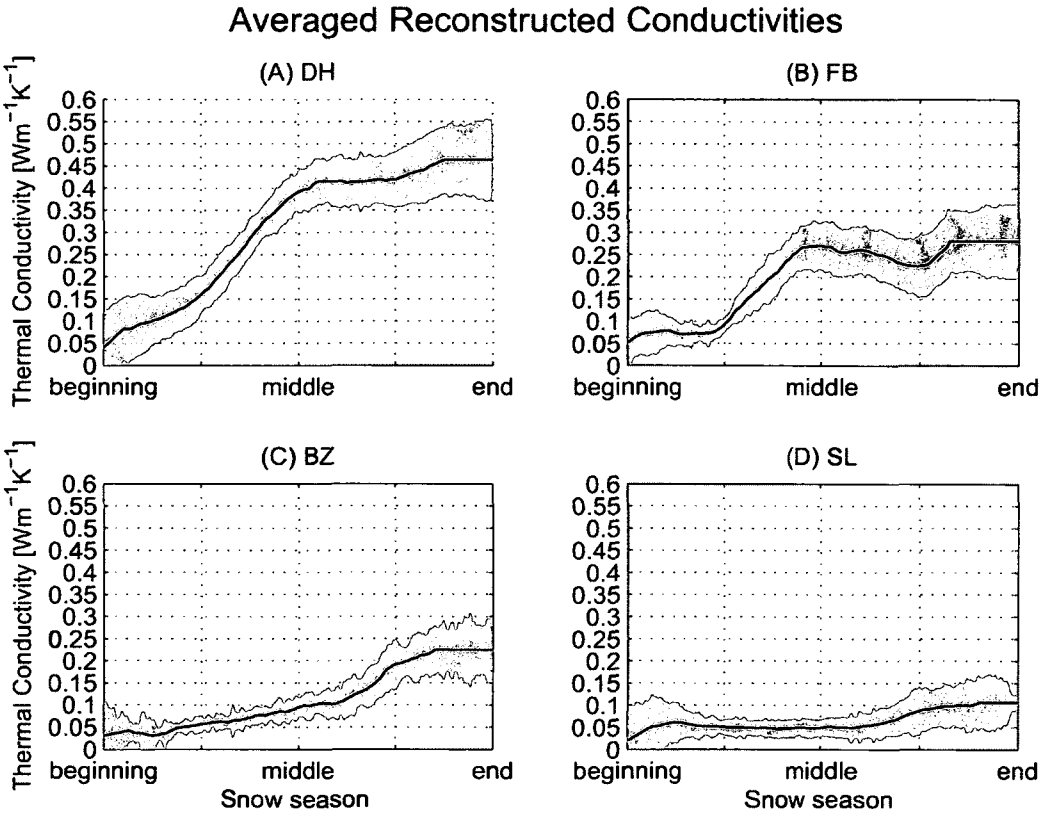

Figure 2.9. Averaged snow thermal conductivities (solid black curve) obtained from average of rounded thermal conductivities (Figures 2.5-2.8) over each snow season for (A) Deadhorse, (B) Franklin Bluffs, (C) Bonanza Creek and (D) Smith Lake stations, and their corresponding uncertainties (solid cyan).

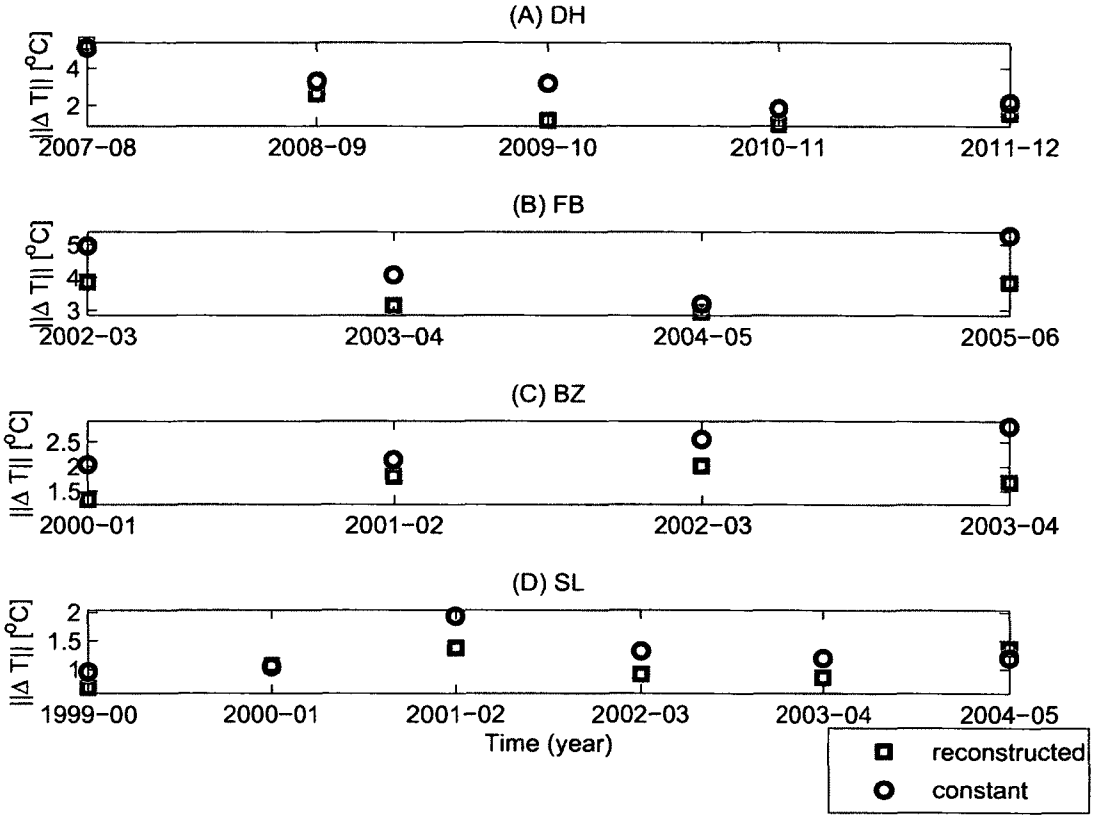

Figure 2.10. The root mean square errors between measured and simulated ground surface temperatures obtained using averaged reconstructed and averaged constant snow thermal conductivities calculated yearly for (A) Deadhorse, (B) Franklin Bluffs, (C) Bonanza Creek, (D) Smith Lake stations.

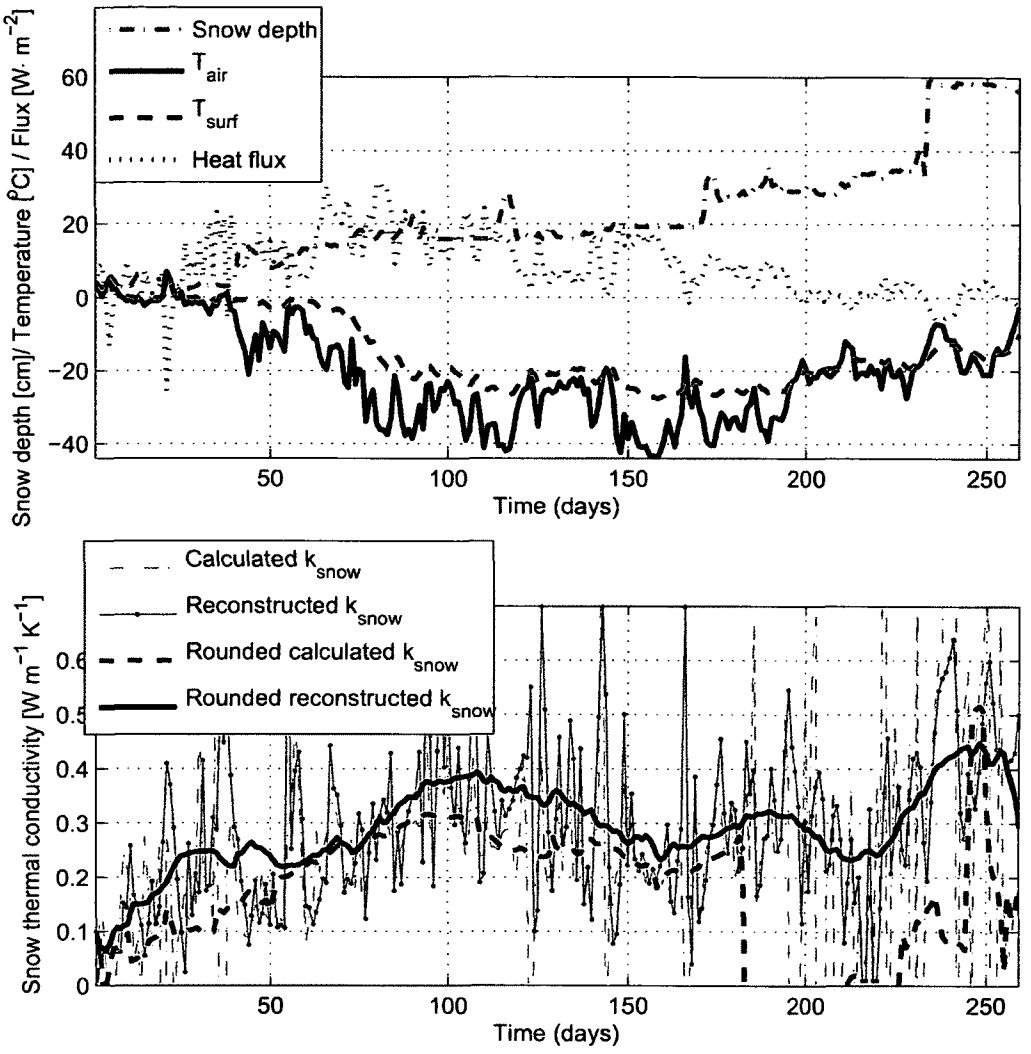

Figure 2.11. The compasion between calculated from measured heat flux and estimated snow thermal consuctivities. (A) Snow depth (red curve), heat flux from the ground to the atmosphere (cyan curve), air (blue curve) and ground surface (green curve) temperatures measured daily at the Prudhoe station within the Deadhorse area (B) Estimated using field data (cyan) and reconstructed using our method (green) snow thermal conductivity time series. Calculated from observed heat flux and temperature gradient thermal conductivities rounded over 30 days using moving average filter (MAF) (dash black curve) and reconstructed snow thermal conductivities rounded over 30 days using MAF (solid blue curve).

Bibliography

Abel, G.: Daily variations of temperature in snow and the relation between the thermal conductivity of snow and its density., Meteorologiskii Vestnik., 3, 31–75, 1893.

Anderson, E. A.: A point energy and mass balance model of a snow cover, NOAA Tech. Rep., pp. NWS–19, 1976.

Beck, J. and Arnold, K.: Parameter Estimation in Engineering and Science, New York, 1977.

Bonan, G. B.: Ecological Climatology: Concepts and Applications., Cambridge University Press, p. 678 pp, 2002.

Carslaw, H. and Jaeger, J.: Conduction of Heat in Solids, London, 1959.

Douville, H., Royer, J. F., and Mahfouf, J. F.: A new snow parameterization for the Meteo-France climate model., Climate Dynamics, 12, 21–35, 1995.

Fukusako, S.: Thermophysical properties of ice, snow, and sea ice., Int. J. Thermophys., 11, 353–372, 1990.

Gallimore, R., Jacob, R., and Kutzbach, J.: Coupled atmosphere–ocean–vegetation simulations for modern and mid-Holocene climates: Role of extratropical vegetation cover feedbacks., Climate Dyn., 25, 755–776, 2005.

Goodrich, L. E.: The influence of snow cover on the ground thermal regime., Canadian Geotechnical Journal., 19, 421–432, 1982.

Jafarov, E. E., Marchenko, S. S., and Romanovsky, V. E.: Numerical modeling of permafrost dynamics in Alaska using a high spatial resolution dataset, The Cryoshpere, 6, 613–624, 2012.

Kane, D., Hinkel, K., Goering, D., Hinzman, L., and Outcalt, S.: Non-conductive heat transfer associated with frozen soils, Global and Planetary Change, 29, 257–292, 2001.

Lagarias, J. C., Reeds, J. A., Wright, M. H., and Wright, P. E.: Convergence Properties of the Nelder-Mead Simplex Method in Low Dimensions, SIAM Journal of Optimization, 9, 112–147, 1998.

Marchenko, S., Romanovsky, V., and Tipenko, G.: Numerical modeling of spatial permafrost dynamics in Alaska, in: In Proceedings of the Eighth International Conference on Permafrost, pp. 190–204, Willey, Institute of Northern Engineering, University of Alaska, Fairbanks, 2008.

Mellor, M.: Engineering properties of snow., J. Glaciol., 19, 15–66, 1977.

Morin, S., Domine, F., Arnaud, L., and Picard, G.: In-situ monitoring of the time evolution of the effective thermal conductivity of snow, Cold Regions Science and Technology, 64, 73–80, 2010.

Nicolsky, D. J., Romanovsky, V. E., and Tipenko, G. S.: Using in-situ temperature measurements to estimate saturated soil thermal properties by solving a sequence of optimization problems, The Cryosphere, 1, 41–58, 2007.

Nicolsky, D. J., Romanovsky, V. E., and Panteleev, G. G.: Estimation of soil thermal properties using in-situ temperature measurements in the active layer and permafrost., Cold Reg. Sci. Technol., 55, 120–129, 2009.

Osterkamp, T. and Romanovsky, V.: Evidence for Warming and Thawing of Discontinuous Permafrost in Alaska, Permafrost and Periglacial Processes, 10, 17–37, 1999.

Osterkamp, T. E.: Establishing Long-term Permafrost Observatories for Active-layer and Permafrost Investigations in Alaska: 1977–2002, Permafrost and Periglacial Processes, 14, 331–342, 2003.

Ostin, R. and Andersson, S.: Frost growth parameters in a forced air stream, Int. J. Heat Mass Trallsfer., 34, 1009–1017, 1991.

Pitman, D. and Zuckerman, B.: Effective thermal conductivity of snow at -88, -27 and -5C, J. Appl. Phys., 38, 2698–2699, 1967.

Romanovsky, V. E. and Osterkamp, T. E.: Effects of unfrozen water on heat and mass transport processes in the active layer and permafrost., Permafrost Periglacial Process., 11, 219–239, 2000.

Romanovsky, V. E. and Osterkamp, T. E.: Permafrost: Changes and Impacts, in: R. Paepe and V. Melnikov (eds.), "Permafrost Response on Economic Development, Environmental Security and Natural Resources", Kluwer Academic Publishers, pp. 297–315, 2001.

Romanovsky, V. E., Sergueev, D. O., and Osterkamp, T. E.: Temporal variations in the active layer and near-surface permafrost temperatures at the long- term observatories in Northern Alaska, In: Permafrost, Phillips, M., Springman, S. and L. U. Arenson (eds), Swets & Zeitlinger, Lisse, 989–994, 2003.

Sazonova, T. and Romanovsky, V.: A Model for Regional-Scale Estimation of Temporal and Spatial Variability of the Active Layer Thickness and Mean Annual Ground Temperatures, Permafrost and Periglacial Processes, 14, 125–139, 2003.

Schröter, J.: Oceanic Circulation Models: Combining Data and Dynamics., In: Anderson, D.L., Willebrand, J. (Eds.), Ch. Driving of Nonlinear Time Dependent Ocean Models by Observation of Transient Tracers – A Problem of Constrained Optimization. Kluwer Academic, pp. pp. 257–285, 2010.

Sergienko, O. V., MacAyeal, D. R., and Thom, J. E.: Reconstruction of snow/firn thermal diffusivities from observed temperature variation: application to iceberg C16 (Ross Sea, Antarctica), Ann. Glaciol., 49, 2004–07, 2008.

Sergueev, D., Tipenko, G., Romanovsky, V., and Romanovskii, N.: Mountain permafrost thickness evolution under the influence of long-term climate fluctuations (results from numerical simulation), in: In 8th International Conference on Permafrost, edited by Swets & Zeitlinger: Lisse, Z., pp. 1017–1021, Phillips M, Springman S, and Arenson L, 2003.

Shiklomanov, N. I. and Nelson, F. E.: Analytic representation of the active layer thickness field, Kuparuk River Basin, Alaska, Ecological Modeling, 123, 105–125, doi: 10.1016/S0304-3800(99)00127-1, 1999.

Sturm, M.: The role of thermal convection in heat and mass transport in the subarctic snow cover, CRREL Rep., pp. 91–19, 1991.

Sturm, M. and Johnson, J. B.: Natural convection in heat and mass transport in the subarctic snow cover, J. Geophys. Res., 96, 11 657–11 671, 1991.

Sturm, M., Holmgren, J., and Liston, G. E.: A Seasonal Snow Cover Classification System for Local to Global Applications, J. Climate, 8, 1261–1283, 1995.

Sturm, M., Holmgren, J., Konig, M., and Morris, K.: The thermal conductivity of seasonal snow, Journal of Claciology, 43, 1997.

Sturm, M., Perovich, D. K., and Holmgren, J.: Thermal conductivity and heat transfer through the snow on the ice of the Beaufort Sea, J. Geophys. Res., 107, 8043, 2002.

Tarantola, A.: Inverse problem theory and methods for model parameter estimatio, SIAM, 2005.

Taylor, J. R.: An Introduction to Error Analysis: The Study of Uncertainties in Physical Measurements, University Science Books, 2nd edn., 1997.

Thacker, W.: The role of the Hessian matrix in fitting models to measurements, Journal of Geophysical Research, 94, 6177–6196, 1989.

Tikhonov, L. and Leonov, A.: Nonlinear Ill-posed Problems, Applied Mathematics and Mathematical Computation Series, 14, 1996.

Tipenko, G. S. and Romanovsky, V. E.: Simulations of soil freezing and thawing: impact of snow cover and unfrozen water content, ARCSS All Hands Meeting, 2002.

Verseghy, D. L.: ClassA Canadian land surface scheme for GCMS. I. Soil model, International Journal of Climatology, 11, 111–133, doi:10.1002/joc.3370110202, URL `http://dx.doi.org/10.1002/joc.3370110202`, 1991.

Walker, D. A., Epstein, H. E., Romanovsky, V., Ping, C. L., Michaelson, G. J., Daanen, R., Shur, Y., Peterson, R. A., Krantz, W. B., Raynolds, M. K., Gould, W. A., Gonzalez, G., Nicolsky, D. J., Vonlanthen, C. M., Kade, A. N., Kuss, P., Kelley, A. M., Munger, C. A., Tamocai, C. T., Matveyeva, N. V., and Daniels, F. J. A.: Arctic patterned-ground ecosystems: A synthesis of field studies and models along a North American Arctic Transect, Journal of Geophysical Research-Biogeosciences, 113, –, 2008.

Yen, Y. C.: Effective thermal conductivity of ventilated snow., J. Geophys. Res., 67, 1091–1098, 1962.

Yen, Y. C.: Review of thermal properties of snow, ice and sea ice., CRREL Rep., pp. 81–10, 1981.

Zhang, T.: Influence of the seasonal snow cover on the ground thermal regime: An overview, Rev. Geophys., 43, RG4002, doi:10.1029/2004RG000157, 2005.

Chapter 3

The effects of fire on the thermal stability of permafrost in lowland and upland black spruce forests of interior Alaska in a changing climate[§]

Abstract

Fire is an important factor controlling the composition and thickness of the organic layer in the black spruce forest ecosystems of Interior Alaska. Fire that burns the organic layer can trigger dramatic changes in the underlying permafrost, leading to accelerated ground thawing within a relatively short time. In this study, we addressed the following questions: (1) which factors determine the post-fire ground temperature dynamics in lowland and upland black spruce forests? and (2) what level of burn severity will cause irreversible permafrost degradation in these ecosystems?

We evaluated these questions in a transient modeling-sensitivity analysis framework in order to assess the sensitivity of permafrost to climate, burn severity, soil organic layer thickness, and soil moisture content in lowland (thick organic layers) and upland (thin organic layers) black spruce ecosystems. The results indicate that climate warming accompanied by fire disturbances could significantly accelerate permafrost degradation. Permafrost in upland black spruce environments under a stable climate with an organic soil layer up to 30 *cm* thick could completely degrade in an 18 *m* soil column within 120 years of a severe fire. In contrast, permafrost in a lowland black spruce environment with an 80 *cm* thick soil organic layer is capable of being sustained under different scenarios of burn severity and climate warming.

3.1 Introduction

The largest reservoir of global terrestrial carbon is stored within organic soils of the boreal forest [Apps et al., 1993; McGuire et al., 1995; Zoltai and Martikainen, 1996; Alexeyev and Birdsey, 1998]. Black spruce is the dominant tree type in interior Alaska boreal forest environments, covering approximately 44% of the landscape [Cleve and Viereck, 1983]. Most of the black spruce forest is underlain by permafrost, which protects organic carbon from decomposition. Soil organic layers insulate the deeper soil permafrost from warm

[§] E. E. Jafarov, V. E. Romanovsky, H. Genet, A. D. McGuire, and S. S. Marchenko, in preparation, to be submitted to the Journal of Environmental Research Letters.

temperatures during summer and from cold temperatures during winter [Alexeyev and Birdsey, 1982; Bonan and Shugart, 1989; Yoshikawa et al., 2003]. The existence and thickness of these organic layers are important factors controlling temperature of permafrost in the discontinuous permafrost region.

Climate is a major factor that can directly influence the thermal stability of permafrost [Camill, 2005; Callaghan et al., 2011]. Statistical analyses of climatic records (1930-2010) for Fairbanks indicate that mean annual air temperatures (MAATs) have increased by $1.79^{o}C$ during the last 80 years (Fig. 3.1A), and that there is no trend in snow depth change over the same time period (Fig. 3.1B). Global Climate Models (GCMs) predict large temperature increases in high latitude regions of the Northern Hemisphere during the 21st century [Solomon et al., 2007]. For the moderate A1B carbon emissions scenario, GCMs project annual mean temperature changes in northern high latitudes of +2.5 to $+7^{o}C$ [Overland et al., 2011]. A comparison of GCM projections for Alaska indicates lower uncertainty in temperature increases [Walsh et al., 2008].

In addition to the direct effects of climate on permafrost, fire can influence the thermal state of frozen ground by burning the soil organic layer [Zhuang et al., 2002; Yoshikawa et al., 2003]. The effects of fire on permafrost thermal dynamics depend on the thickness of the organic soil layer remaining after fire. Burn severity is defined by the depth of burning and the consumption of surface soil organic matter, which in turn depends on both weather and climate [Flannigan and Harrington, 1988; Johnson, 1992]. The most severe fires often occur late in the growing season when the active layer is deepest and upper soils are dry [Kasischke et al., 2010]. Fire frequency is expected to increase in Alaska during the remainder of the 21st century [Balshi et al., 2009]. Alteration of soil organic layers in response to a changing fire regime may trigger long-term changes in permafrost stability under some conditions. However, a soil organic layer could recover its pre-fire state within about 100 years [Cleve and Viereck, 1981] and provide some resilience against permafrost degradation in the face of warming climate and increased fire frequency and severity.

The post-fire dynamics of soil moisture are another factor that can affect soil thermal dynamics after fire. Fire tends to increase soil moisture content because of decreased evapotranspiration [Klock and Helvey, 1976; Tiedemann et al., 1979; Moore and Keeley, 2000]. Increased soil moisture content in valleys and lowlands after fires can also be observed

using remote sensing [Kasischke et al., 2007]. In-situ measurements of soil moisture at burn sites indicate higher moisture contents compared to unburned sites [Yoshikawa et al., 2003]. The increase in soil moisture content is more pronounced immediately after the fire, and slowly decreases through the following decade [Yoshikawa et al., 2003]. Lowland black spruce forests may provide a favorable environment for the persistence of permafrost in the face of changing climate and fire regimes. The low rates of evapotranspiration in lowland black spruce forests [Bonan, 1991; Liu et al., 2005] can cause the forest-floor to hold more moisture, which is necessary for deep accumulation of the soil organic layer over time [Fenton et al., 2005]. The accumulation of soil organic layers in mesic to moist boreal forest ecosystems is associated with feedbacks among cool and moist soils, low rates of decomposition and nutrient cycling, and high moss productivity [Johnstone et al., 2010b]. The boreal forest ecosystem with shallow organic layers and drier soil conditions has higher rates of decomposition and higher vascular plant productivity, which reduces moss accumulation [Johnstone et al., 2010b].

Our primary goal in this study was to better understand the effects of climate warming, burn severity, post-fire recovery of the organic soil layer, and post-fire patterns of soil moisture on the thermal stability of permafrost in lowland and upland black spruce ecosystems in Interior Alaska. To assess the effects of each factor, we used soil properties observed at upland and lowland sites in the Bonanza Creek Experimental Forest near Fairbanks, Alaska, where a severe forest fire occurred in the summer of 1983. In this study, we addressed the following questions: (1) which factors determine the post-fire ground temperature dynamics in lowland and upland black spruce forests? and (2) what level of burn severity will cause irreversible permafrost degradation in these ecosystems?

3.2 Methods

To evaluate the effects of climate warming and fire disturbance on permafrost in the black spruce forests of Interior Alaska, we examined the following factors: 1) the effect of climate warming with no fire disturbance; 2) the effect of different burn severity levels under a stable climate; 3) the effect of dynamic post-fire soil organic layers under a stable climate; 4) the effect of post-fire soil moisture dynamics under stable climate; and 5) the effect of climate warming with fire disturbance in combination with dynamic organic soil layers

and soil moisture. To simulate the effects of each these factors on permafrost, we used the Geophysical Institute Permafrost Laboratory (GIPL) numerical transient model [Sergueev et al., 2003; Nicolsky et al., 2007; Marchenko et al., 2008; Jafarov et al., 2012]. We simulated changes in soil organic layers with the Dynamic Organic Soil version of the Terrestrial Ecological Model (DOSTEM) [Yi et al., 2009, 2010; Yuan et al., 2012].

The GIPL model simulates the effects of snow and subsurface soil thermal properties on ground temperatures by solving the 1-D heat diffusion equation with phase change. The phase change associated with freezing and thawing process occurs within a range of temperatures below 0^oC, and is represented by the unfrozen water curve [Romanovsky and Osterkamp, 2000]. The model employs a finite difference numerical scheme over a specified domain. The soil column is divided into several layers (moss, fibrous, amorphous, mineral and rock), each with distinct thermo-physical properties. The overall soil column thickness was 20 m, where zero temperature gradient was set at the lower boundary. The GIPL model has been successfully validated using ground temperature measurements in shallow boreholes across Alaska [Romanovsky and Osterkamp, 2000; Nicolsky et al., 2009].

In this study, we addressed the effects of the Rosie Creek fire, a human-caused wildfire that burned 8,600 acres including one-third of the Bonanza Creek Long Term Experimental Forest (LTER) [Glenn, 2010]. Bonanza Creek is located about 20 km southwest of Fairbanks, Alaska. To distinguished the effects of fire on shallow versus deep organic layers, we considered upland and lowland sites from Bonanza Creek LTER [Jorgenson et al., 2010]. The organic soil profile at each site includes three organic layers (moss, dead moss, and peat), which we classify as moss, fibrous, and amorphous soil layers (Table 3.1). The rest of the soil column includes mineral soil and rock layers.

We set the upper boundary conditions to be equal to daily averaged air temperatures and snow depths from 1983. To mimic the effect of a stable climate, we replicated averaged daily air temperatures and snow depths over 120 years. The 120-year time interval was chosen as a fire return frequency interval for the black spruce forest [Johnstone and Kasischke, 2005; Johnstone et al., 2010a]. The ground temperature and active layer dynamics were simulated for 120 years after the fire. Prior to the simulation run, using pre-burn soil properties (Table 3.1), we equilibrated initial ground temperatures by spinning-up the model until mean annual ground temperature at every depth was stabilized.

1. In the first stage of the numerical experiment, we tested the effects of a warming climate without fire disturbances. We imposed a linear warming trend by adding a yearly positive increment to daily air temperatures. We tested both 1°C and 2°C of total warming, imposed gradually over 120 years. To introduce the effects of increased snow fall on the thermal stability of permafrost, we linearly increased snow depth by 20% over the fire frequency interval.

2. To quantify burn severities, we reduced overall organic layer thickness. In both the upland and lowland cases, we assumed a dry organic layer by the end of summer, so that the most severe fire burned the amount of organic layer equal to the active layer thickness. For example, if the overall organic layer thickness was 80 *cm* at the lowland site and the active layer thickness before the fire was 48 *cm*, then the maximum burn severity corresponds to 48 *cm* of organic layer removal. We applied different burn severity levels to the upland and lowland sites in order to identify thresholds after which permafrost degradation was irreversible. Organic soil layer removal associated with fire occurrence was implemented after ground temperatures reached their equilibrium state. Fire was implemented at the end of summer when the active layer depth was close or equal to its maximum value. Once the burn severity thresholds were identified, the next control factor was added into the analysis.

3. To address the effects of new organic layer accumulation, we simulated the dynamics of three different organic soil carbon layers (moss, fibrous, and amorphous layers; Table 3.1), and used the DOSTEM [Yi et al., 2009, 2010] version of the TEM model [Raich et al., 1991; McGuire et al., 1992; Melillo et al., 1993]. We used the DOSTEM to simulate post-fire organic layer re-accumulation rates for moss, fibrous and amorphous soil layers (Fig. 3.2) for the upland and lowland sites from Table 3.1. Organic soil layer accumulation rates were simulated for the equilibrium run of the DOSTEM model [Yi et al., 2010]. Soil carbon pools and decomposition rates for lowland and upland ecosystems were calibrated according to the sample records from Bonanza Creek LTER.

The DOSTEM calculates moss layer thickness (Fig. 3.2A) according to an empirical function [Yi et al., 2009]:

$$d_{moss} = d_{moss,max} \cdot y_{sf} / (y_{sf} - y_{half}) \tag{3.1}$$

where d_{moss} is the thickness of moss (cm), $d_{moss,max}$ is the maximum thickness of moss (*cm*),

y_{sf} is the number of years since the fire, and y_{half} is the number of years needed for moss to reach half of $d_{moss,max}$. For the upland and the lowland sites, we assigned $d_{moss,max}$ equal to 4 *cm* and 6 *cm* respectively, according to our observations, and y_{half} = 5 based on Yi et al. [2009].

The DOSTEM simulates thicknesses of fibrous and amorphous layers (Fig. 3.2C,B) using the soil carbon content, C, of each soil layer:

$$d = (C/a)^{1/b} \tag{3.2}$$

where C is the carbon content (gC/cm^2) of an organic layer, d is organic layer thickness (cm), and a and b are fitted coefficients for the fibrous or amorphous layers [Yi et al., 2009]. We inserted the organic soil thicknesses simulated by TEM (Fig. 3.2) into the GIPL numerical model in order to investigate the effect on permafrost post-fire dynamics.

4. During the fourth stage of the numerical experiment, we tested the impact of soil moisture on active layer depth. The effect of soil moisture was tested together with growing organic layers. We increased the upper soil layer moisture content to full saturation in the year following the fire, then linearly decreased the soil moisture saturation to its pre-fire condition over 10 years. Note that in the GIPL model, soil moisture content is not coupled with soil organic layer thermal properties.

5. Finally, we tested the effects of a warming climate on post-fire permafrost thermal dynamics, combined with changes in soil moisture and dynamic organic layer recovery in the 10 years following a fire. Climate warming scenarios applied to the upland and lowland sites were similar to the ones used in the first stage of the analysis with no fire disturbances.

3.3 Results

The results of active layer thickness (ALT) simulations under different climate warming scenarios without fire disturbance indicate gradual thickening of the active layer for every warming scenario at the upland and lowland black spruce sites without changing snow thickness (Fig. 3.3). For the upland simulation, with increased snow thickness (+2 ^{o}C mean annual temperature warming over 120 years with a 20% increase in snowfall), there was rapid increase in permafrost degradation at approximately year 105, when snow had

increased 17.5%. The thickening of the active layer was weaker at the lowland site with a thicker organic layer for all warming scenarios, and there was no rapid increase in permafrost degradation for the scenario with increasing snow thickness (Fig. 3.3B).

Fire disturbance with no climate change and no organic layer regrowth had a substantial impact on permafrost thermal stability. At the upland black spruce site, permafrost started to thaw progressively when burn severity was equal to 12 *cm* of organic layer removal (Fig. 3.4A). In contrast, permafrost did not progressively thaw at the lowland site until burn severity was equal to 24 *cm* of organic layer removal (Fig. 3.4B). Fire disturbance at the lowland site did not immediately degrade permafrost after 24 *cm* of the organic layer was burned; permafrost degradation began after approximately 100 years had passed. It is notable that the rate of permafrost degradation for the highest burn severity at the lowland site was less pronounced than for 15 *cm* burn severity at the upland site.

The next step in the numerical experiment was the implementation of dynamic change in the organic soil layer horizons in the GIPL model after fire, under a stable climate scenario. When the organic soil dynamics for the both sites were included in the model, the permafrost table thickening threshold was shifted by 10% for upland permafrost (Fig. 3.5A) and 100% for lowland permafrost (Fig. 3.5B). Allowing the regrowth of organic soil layers caused the threshold for permafrost degradation to increase at the upland site by 10% (Fig. 3.5A) and prevented permafrost degradation at the lowland site (Fig. 3.5B). Permafrost at the lowland site was able to fully recover its thermal state and ALT within 40 years after fire (Fig. 3.5B).

Compared with a reference simulation, the simulation with post-fire soil moisture dynamics had a subtle effect on the pattern of ALT dynamics (Fig. 3.6A,B). The increase in soil moisture content retarded active layer thickening until the seasonally thawed layer began refreezing and prevented an unfrozen layer (talik) from forming. In the years after the talik formed at the upland site, an unfrozen layer that survived winter contributed to warmer ground temperatures. Therefore, a slightly deeper permafrost table formed when soil moisture dynamics were included in the simulation (Fig. 3.6A). In contrast, at the lowland site, a talik did not form and an excess of soil moisture in the 10 years after the fire slowed the thickening of the active layer (Fig. 3.6B).

More detailed analyses of the soil moisture factor indicate that an increase in soil mois-

ture content reduces ground temperature amplitude during the year following a fire (Fig. 3.7A) compared with no change in soil moisture (Fig. 3.7B). In the current formulation, changes in soil moisture introduce the effect of the latent heat of water fusion on permafrost and do not connect with changes in soil thermal properties [Jorgenson et al., 2010]. Latent heat corresponds to the energy that needs to be spent in order to freeze or thaw the excess ground water available as a result of decreases in evapotranspiration. This latent heat effect reduces the ground temperature amplitude (Fig. 3.7A). At the upland site, during 15 *cm* of organic layer burn, changes in soil moisture content accelerated the development of the thaw layer and therefore increased the warming effect of the ground. An increase in soil moisture affected the active layer depth and caused the ground to refreeze more slowly. Ground temperature freeze-up dates simulated with increased post-fire soil moisture contents indicate a faster transition from seasonally thawed active layer to talik. This can be better seen on the freeze-up day graph (Fig. 3.8A), which indicates that freeze-up ceased four years after the fire. Therefore, the threshold between a freeze-up year and a no freeze-up year occurred between year four and year five. This threshold marks the time of the beginning of talik formation, which allows heat to remain in the ground longer and contributes to its further warming. In the case with no changes in soil moisture, it took two years longer for the talik to form (Fig. 3.8B), which reduced the effects of ground warming and therefore reduced the depth of the permafrost table (Fig. 3.6A). At the lowland site, increased soil moisture also delayed the freeze-up date, but freeze-up still occurred and no talik formed (Fig. 3.8B). The ability of the lowland permafrost to completely refreeze the soil column contributed to the shallow ALT within 10 years after the fire (Fig. 3.6B).

For the final simulation, we included climate warming, fire disturbance with post-fire organic layer dynamics, and soil moisture dynamics. Results indicate substantial permafrost degradation at the upland site for burn severity equal to 15 *cm* (Fig. 3.9A) compared with no fire (Fig. 3.3A). In contrast, at the lowland site for the most severe burn (equal to 48 *cm* of organic soil removal), permafrost was able to recover its pre-fire thermal condition under almost every warming scenario, except the highest warming scenario with an increase in snow thickness (Fig. 3.9B). For the entire organic layer burn at the upland site, active layer thickness dramatically increased to 8 *m* within 30 years after the fire for the no climate change scenario, with further deepening to 18 *m* within the next 70

years (Fig. 3.10). For the $+2^oC$ and increased snow depth scenario, permafrost completely disappeared in a 20 m soil column 67 years after a fire (Fig. 3.10).

3.4 Discussion

Resilience of permafrost is the capacity to maintain frozen temperatures and similar ground ice contents and morphologies, while vulnerability is the extent to which permafrost thaws vertically and laterally and how much thaw settlement occurs during thawing of ground ice [Jorgenson et al., 2010]. In the current analysis, we define the vulnerability and resilience of the permafrost based primarily on changes in its temperatures and ALT. Permafrost vulnerability in the black spruce forest is the combination of resilience and exposure, whereas climate change and burn severity are components of exposure.

Fire is a major disturbance in the high-latitude boreal forest. It influences vegetation and permafrost [Balshi et al., 2009], and is in turn strongly influenced by climate and human activity [Kasischke et al., 2000]. Balshi et al. [2009] provide evidence that fire frequency as well as the amount of area burned by wildfires will increase by 2050. The burning of vegetation, moss and a portion of the surface peat layer by fire leads to degradation of permafrost and an increase in active layer thickness, which could be irreversible in areas with shallow organic soil layers (Fig. 3.10). Permafrost degradation could trigger changes in the ecosystem succession cycle, i.e. transition of black spruce forests to deciduous forests [Johnstone and Kasischke, 2005; Johnstone et al., 2010a]. Thawing of permafrost increases the depth of the active layer and lowers of the water table, which could accelerate the rate of carbon loss in Arctic ecosystems [Schuur et al., 2009]. Studies show that warmer air temperatures associated with longer snow-free seasons result in the largest relative soil organic carbon losses ($\sim 5.3\ kgCm^{-2}$), whereas high burn severity regimes associated with warmer and drier conditions could magnify organic carbon losses ($\sim 6.2\ kgCm^{-2}$) [O'Donnell et al., 2011].

The magnitudes of the climate warming and burn severity effects can be different due to differences in soil texture, thermal properties, degree of soil saturation, and snow depth. An increase in snow depth increases the warming effect on the ground due to the insulating properties of snow. However, the overall effect of snow after fire is not well understood. For example, snow compaction could be increased after a fire due to wind com-

paction effects, which could decrease the insulation of the ground. When trees regrow, they can intercept falling snow and improve permafrost stability.

The ability of a system to recover depends on the organic layer thickness left after a fire. According to our simulations, organic layer recovery after a fire increases permafrost resilience for both boreal forest sites. Different rates of organic layer recovery can have different impacts on the permafrost. Numerical experiments indicate that recovery of the permafrost thermal conditions after moderate to severe fires could be initiated as soon as moss layers start to re-accumulate. Thus, the amount of organic layer left after a fire and the re-accumulation of the soil organic layer are two major negative feedbacks that could slow permafrost degradation.

The results of the current analysis could be generalized for upland boreal forest ecosystems with a thin (up to 30 *cm*) organic layer. Our results indicate that, for Interior Alaska (Fairbanks) with MAATs of about $-2\,^{o}C$, a fire that burns 15 *cm* or more of the soil organic layer could trigger immediate permafrost degradation. South of Fairbanks, less severe fires could trigger permafrost degradation. Permafrost resilience increases to the north, meaning that thicker organic soil layers need to be burned before permafrost degradation occurs. Upland sites with significantly deeper organic soil layers may not necessarily demonstrate similar permafrost degradation rates. Similarly, lowlands with shallow organic layers could have less resilience to climatic changes and fire disturbances. Dry areas with shallow organic layer thicknesses and MAATs of about $-2\,^{o}C$ have no resilience to severe fires and can lose their underlying permafrost within a relatively short time-frame. The vegetation succession cycle in these areas could change due to changes in the soil conditions. Areas with deep, wet organic soil layers in regions with MAATs of about $-2\,^{o}C$ have high degrees of resilience, and the vegetation succession cycle in these areas will most likely be preserved.

3.5 Conclusions

Thawing of permafrost could have a significant impact on soil hydrology, vegetation succession and the global carbon balance. The results of the current simulations indicate high-order permafrost vulnerability in black spruce forests with thin (up to 30 *cm*) organic soil layers. Our numerical experiments show that soil organic layers play a crucial role in per-

mafrost recovery after fire disturbances. Predicted increases in forest fire frequency and severity will primarily affect areas with shallow and dry organic soil layers, where fire will accelerate permafrost degradation and most likely introduce changes in post-fire vegetation. The amount of soil organic matter left unburned after a fire and the rate of its recovery will determine permafrost degradation and later aggregation rates. Wet soil provides a better environment for moss layers to regrow, and therefore improves permafrost resilience. An increase in post-fire soil moisture content and changes in soil thermal properties could potentially accelerate ALT. The hydrological factor was not well-addressed in the current version of the GIPL model, since changes in soil moisture were not coupled with changes in soil thermal properties. Instead, we addressed the effect of latent heat on post-fire permafrost dynamics. This work emphasizes the high-order sensitivity between soil organic layer thickness, burn severity and climate warming. The effect of organic layer development needs to be better addressed in the permafrost models. To better simulate the spatial effect of forest fires on permafrost, it is necessary to couple the GIPL, DOSTEM and fire generation numerical models. Future work is necessary to improve the results of spatial permafrost modeling in the black spruce forests of the discontinuous permafrost zone.

3.6 Acknowledgements

We are very thankful to S. Higgins for valuable comments and corrections. This research was funded by the National Science Foundation under grant ECO-MODI.

3.7 Tables

Table 3.1. Thermal properties used in ground temperature simulations for the unburned upland and lowland sites.

Soil type	VWC	UWC (a,b)	C_t/C_f (10^6)	k_t/k_f	Thickness (m)
Upland soil layers					
moss	0.101	0.001/-0.1	1.8/1.6	0.08/0.13	0.04
fibrous	0.185	0.002/-0.1	1.9/1.7	0.12/0.26	0.13
amorphous	0.56	0.48/-0.38	2.6/2.2	0.35/0.54	0.13
mineral	0.50	0.53/-0.38	2.5/1.7	1.0/2.1	2.7
rock	0.2	0.01/-0.1	1.8/1.6	2.2/2.8	17.0
Lowland soil layers					
moss	0.08	0.001/-0.1	1.8/1.6	0.08/0.13	0.06
fibrous	0.12	0.002/-0.1	1.9/1.7	0.18/0.36	0.12
amorphous	0.62	0.48/-0.38	2.6/2.2	0.56/1.6	0.62
mineral	0.50	0.53/-0.38	2.5/1.7	1.0/2.1	2.2
rock	0.2	0.01/-0.1	1.8/1.6	2.2/2.8	17.0

VWC - Volumetric water content (fraction of 1)

UWC - Unfrozen water coefficients

C_t/C_f - Thawed/frozen volumetric heat capacities $[Jm^{-3}K^{-1}]$

k_t/k_f - Thawed/frozen thermal conductivities $[Wm^{-1}K^{-1}]$

3.8 Figures

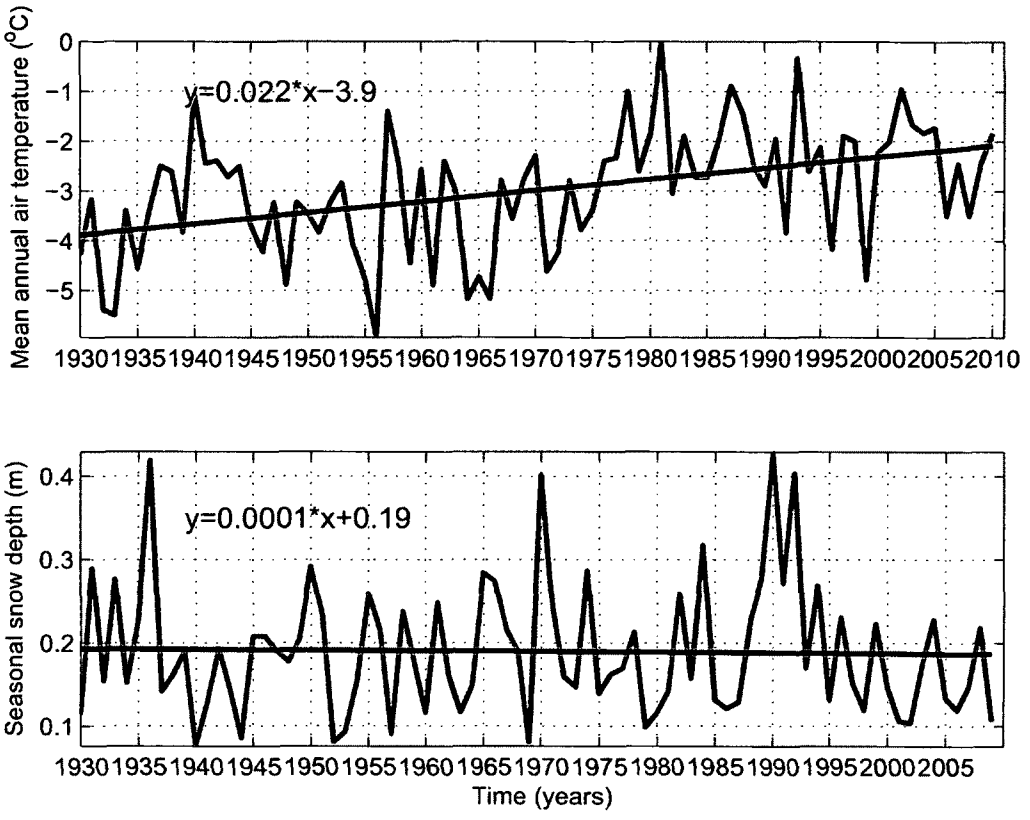

Figure 3.1. Climatological data from the Fairbanks International Airport station: (A) mean annual air temperature in ^{o}C and (B) seasonal averaged snow depth in meters. ACRC: Alaska Climate Research Center, Fairbanks Alaska Climatology, Geophysical Institute, Univ. of Alaska Fairbanks, AK, http://climate.gi.alaska.edu, 2010.

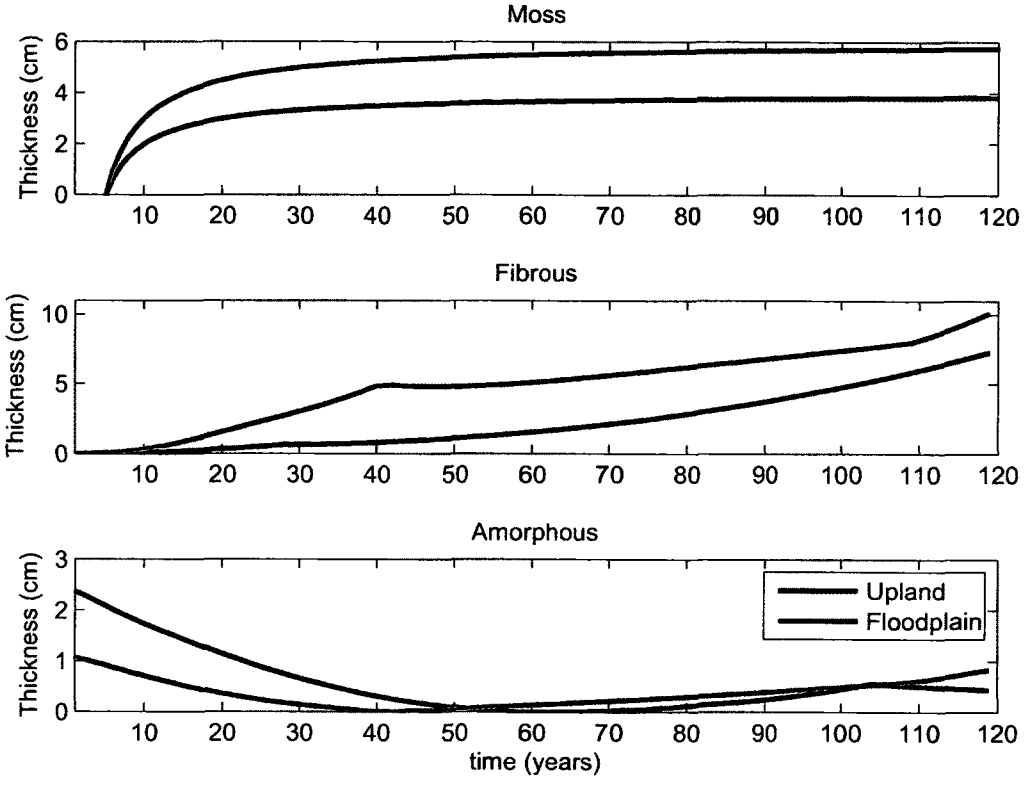

Figure 3.2. The postfire dynamics rates of (A) moss, (B) fibrous, and (C) amorphous organic soil layers simulated by DOSTEM model during the equilibrium run.

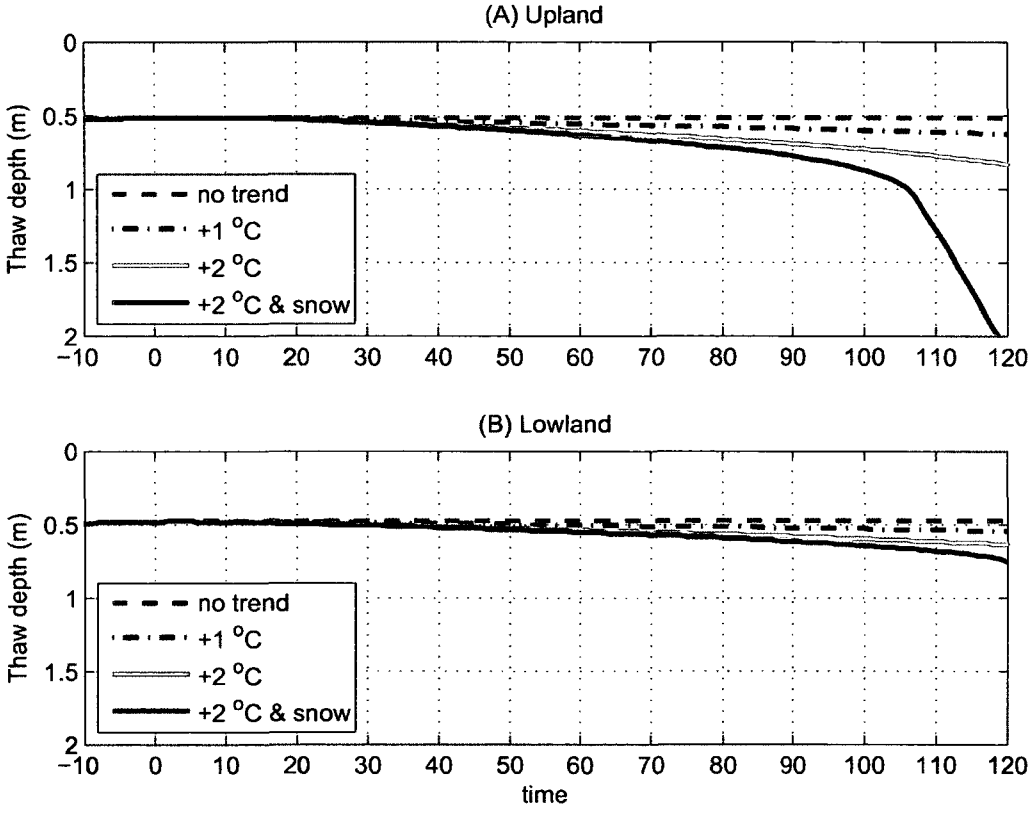

Figure 3.3. Simulations of the active layer thickness for the (A) upland and (B) lowland boreal forest sites for different warming scenarios with no fire disturbances. Time interval [-10,0] corresponds to the equilibrium run, and [0,120] time interval corresponds to the transient run.

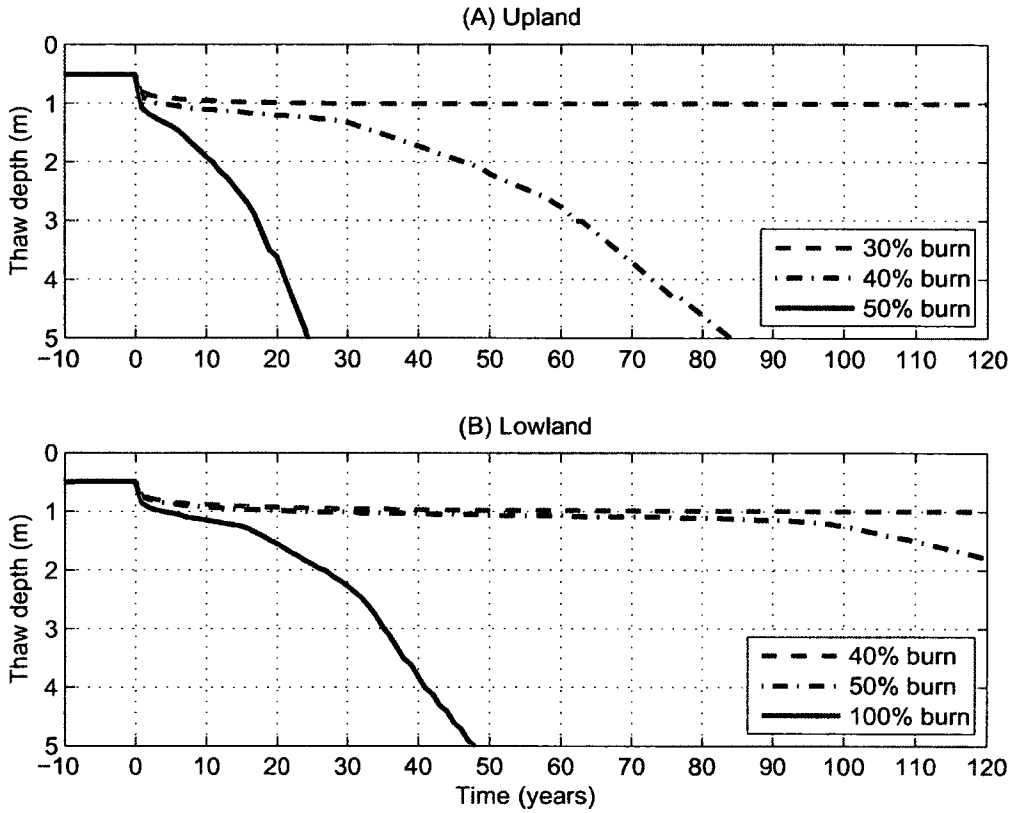

Figure 3.4. Simulations of the permafrost table depth for the (A) upland and (B) lowland boreal forest sites for different fire severities during stable climate (mean annual air temperatures $-2^{o}C$). Time interval [-10,0] corresponds to the equilibrium run, and [0,120] time interval corresponds to the transient run, where 0 is year of a fire ignition.

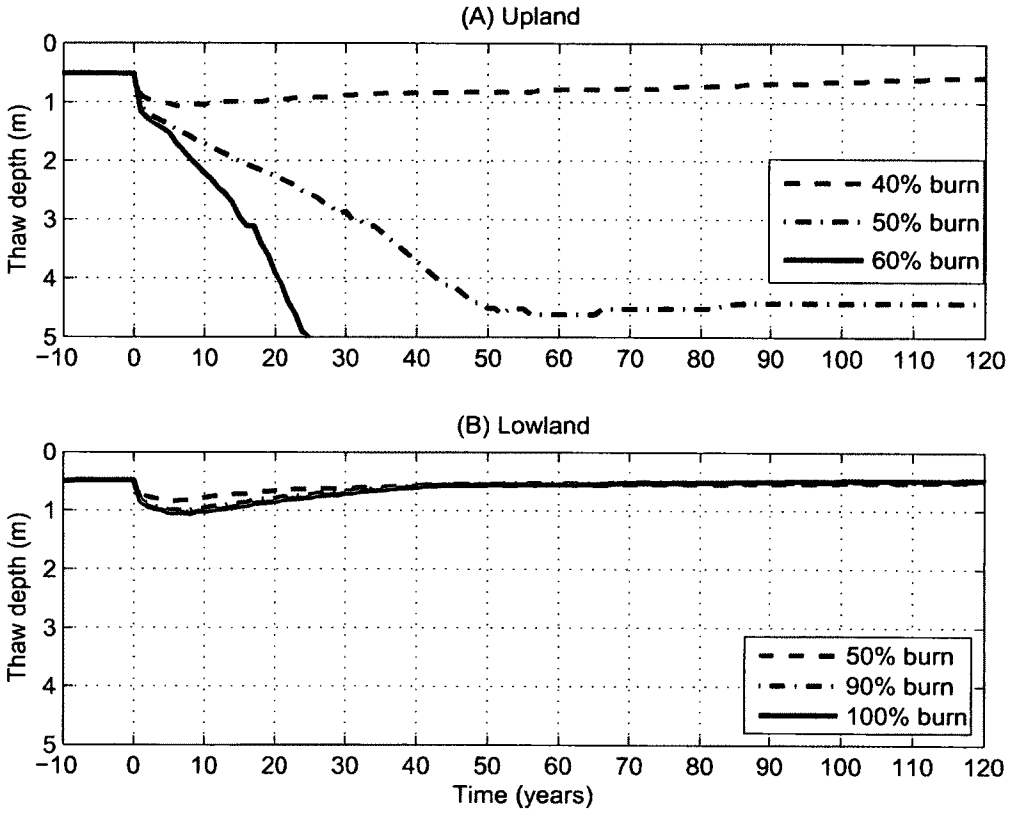

Figure 3.5. Simulations of the permafrost table depth for the (A) upland and (B) lowland boreal forest sites for different fire severities during stable climate (mean annual air temperatures -2^oC) using dynamic organic soils recovery rates. Time interval [-10,0] corresponds to the equilibrium run, and [0,120] time interval corresponds to the transient run, where 0 is year of a fire ignition.

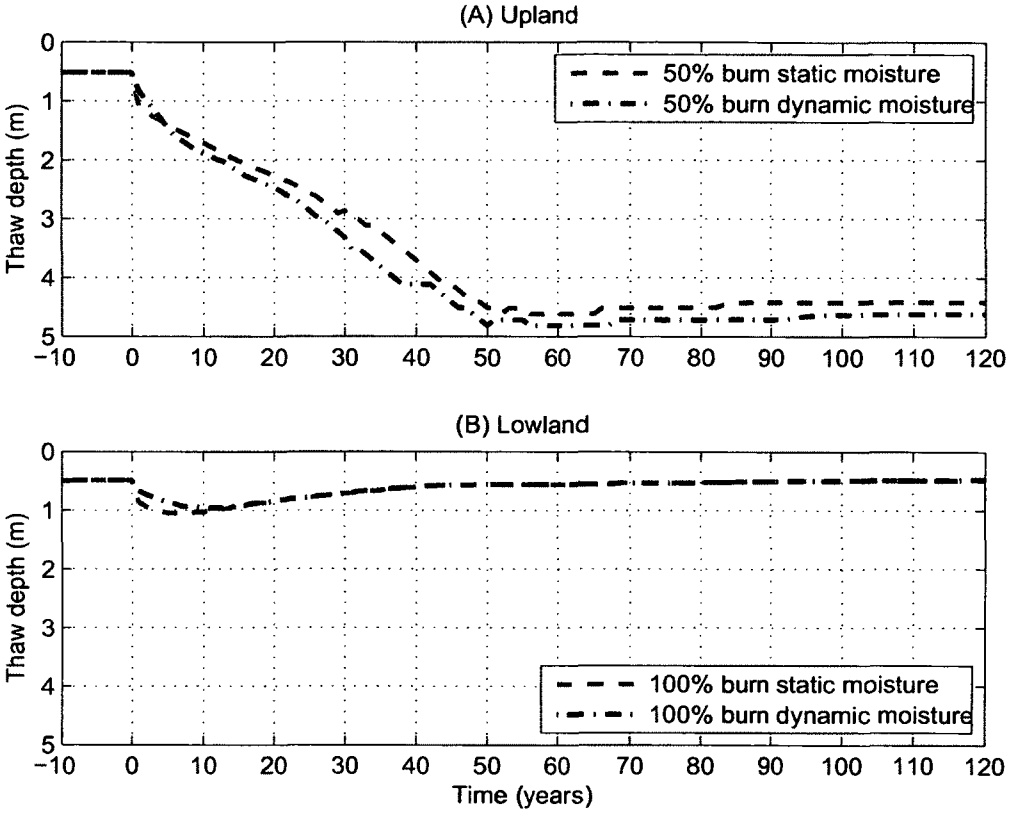

Figure 3.6. Simulated permafrost table dynamics with and without changes in the soil moisture content within 10 years after fire for (A) upland (B) lowland sites during stable climate (mean annual air temperatures -2^oC) using dynamic organic soils recovery rates generated by the Dynamic Organic Soil Terrestrial Ecosystem Model. Time interval [-10,0] corresponds to the equilibrium run, and [0,120] time interval corresponds to the transient run, where 0 is year of a fire ignition.

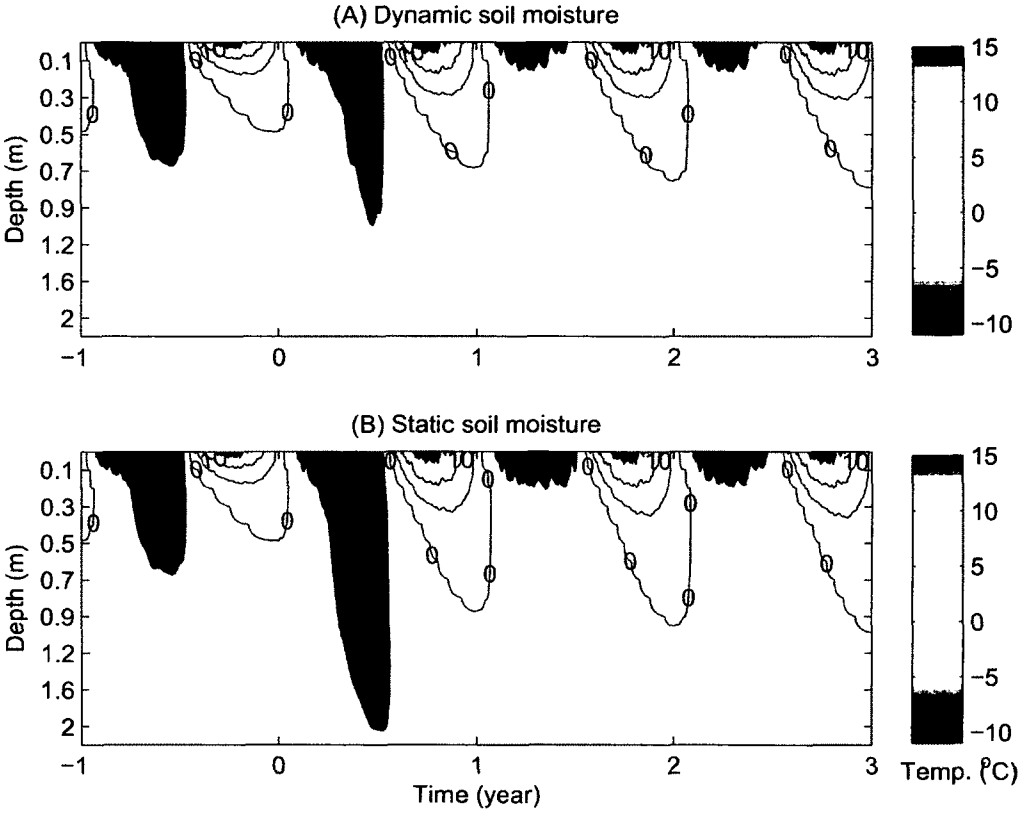

Figure 3.7. Contour plots of the ground temperature dynamics with depth over time for the lowland permafrost site simulated with (A) and without (B) changes in the soil moisture content 2 years after fire.

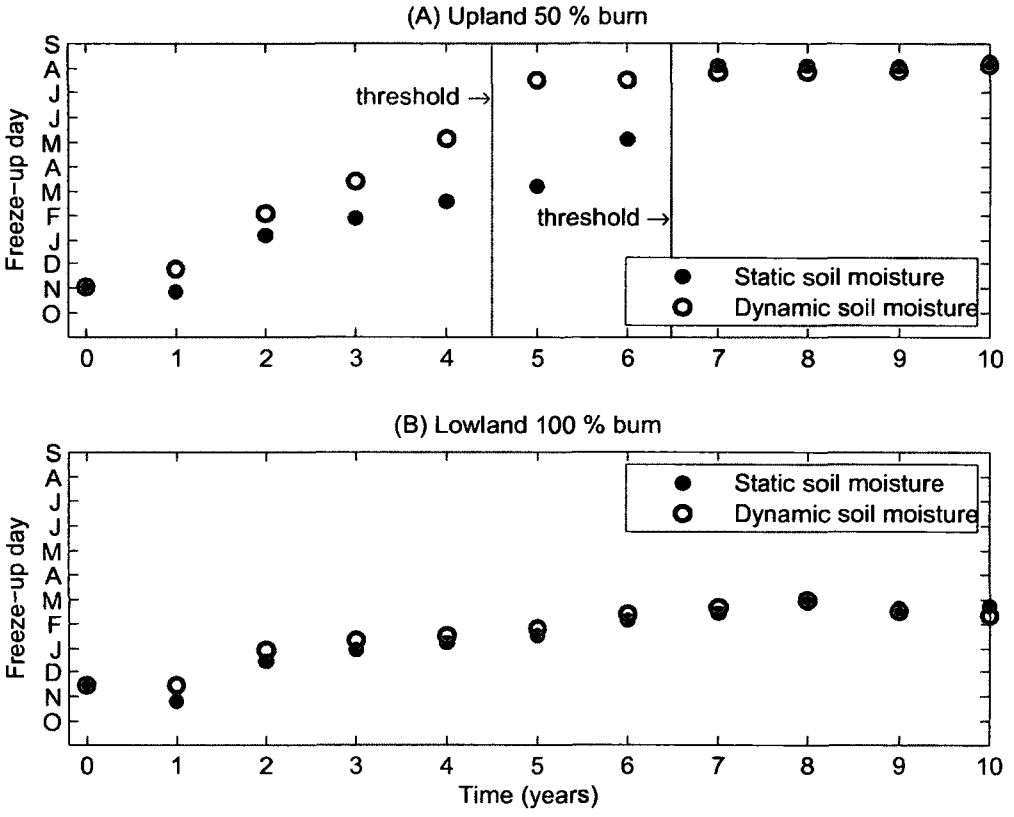

Figure 3.8. Freeze-up time for (A) the upland permafrost site after 15 *cm* of the organic layer burn and (B) the lowland permafrost site after 48 *cm* of the organic layer burn sites.

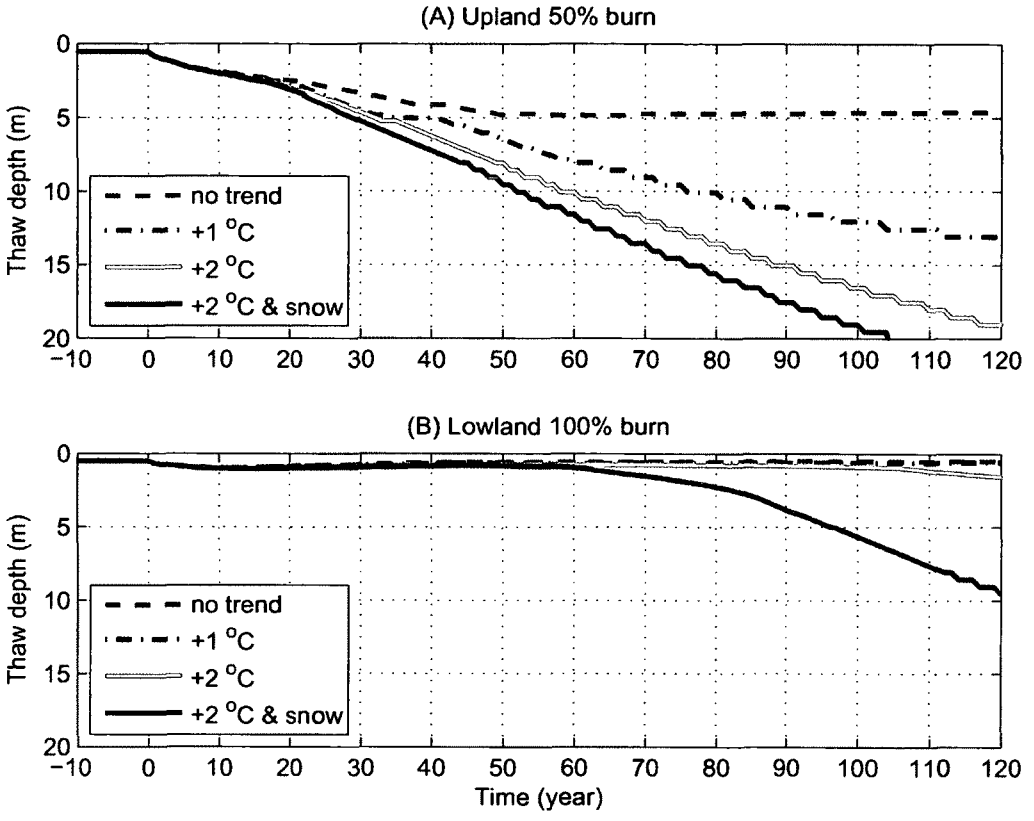

Figure 3.9. Simulated permafrost table dynamics after (A) 15 *cm* of the organic layer burn for the upland and (B) 48 *cm* of the organic layer burn for the lowland boreal forest permafrost sites during different climate warming scenarios using dynamic organic soils recovery rates and changes in soil moisture content. Time interval [-10,0] corresponds to the equilibrium run, and [0,120] time interval corresponds to the transient run, where 0 is year of a fire ignition.

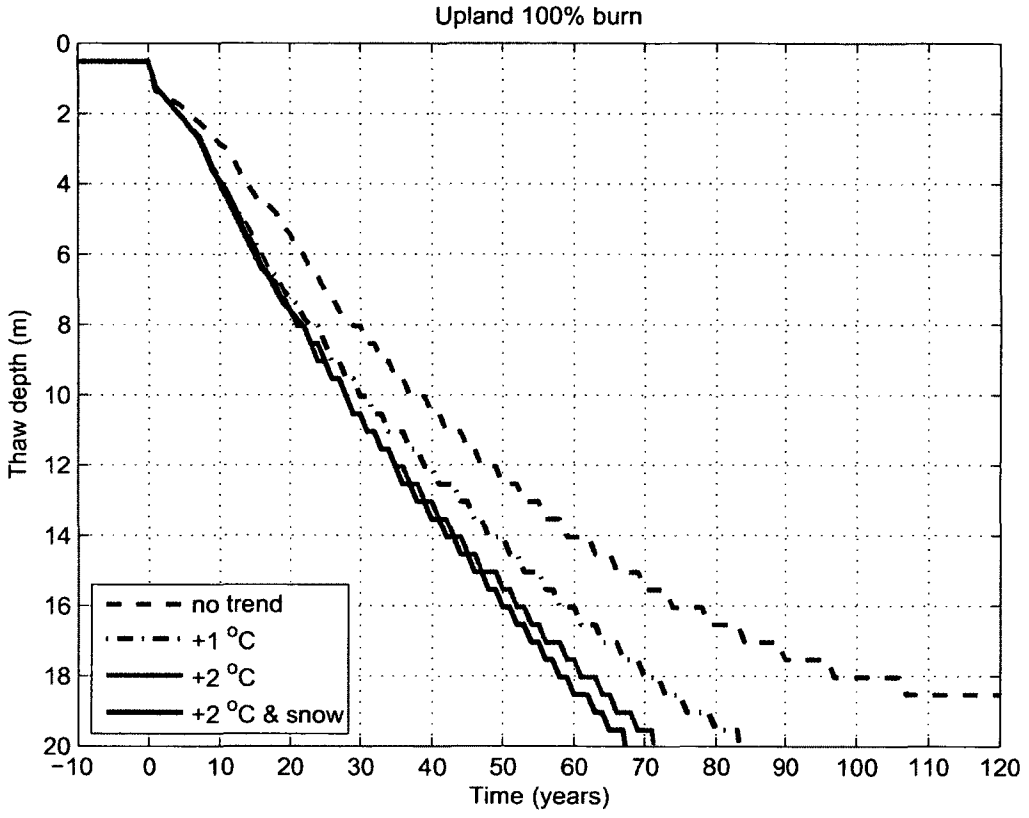

Figure 3.10. Simulated permafrost table dynamics after 100 % organic layer burn for the upland boreal forest permafrost sites during different climate warming scenarios using dynamic organic soils recovery rates and changes in soil moisture content. Time interval [-10,0] corresponds to the equilibrium run, and [0,120] time interval corresponds to the transient run, where 0 is year of a fire ignition.

Bibliography

Alexeyev, V. A. and Birdsey, R. A. (1982). Control of depth to permafrost and soil temperature by forest floor in black spruce/feather moss communities. *US Department of Agriculture Research Note PNW-396, Portland, OR.*

Alexeyev, V. A. and Birdsey, R. A. (1998). Carbon storage in forests and peatlands of Russia. *Gen. Tech. Rep. NE, U.S.D.A. Forest Service Northeastern Research Station, Radnor.*, 244.

Apps, M. J., Kurz, W. A., Luxmoore, R. J., Nilsson, L. O., Sedjo, R. A., Schmidt, R., Simpson, L. G., and Vinson, T. S. (1993). Boreal forests and tundra. *Water, Air and Soil Pollution*, 70(1-4):39–53.

Balshi, M. S., McGuire, A. D., Duffy, P., Flannigan, M., Walsh, J., and Melillo, J. (2009). Assessing the response of area burned to changing climate in western boreal north america using a multivariate adaptive regression splines (mars) approach. *Global Change Biology*, 15(3):578–600.

Bonan, G. B. (1991). A biophysical surface energy budget analysis of soil temperature in the boreal forests of interior Alaska. *Water Resour. Res.*, 27(5):767–781.

Bonan, G. B. and Shugart, H. H. (1989). Environmental factors and ecological processes in boreal forests. *Annu. Rev. Ecol. Syst.*, 20:1–28.

Callaghan, T. V., Johansson, M., Anisimov, O., Christiansen, H. H., Instanes, A., Romanovsky, V., and S, S. S. (2011). Changing permafrost and its impacts. *In: Snow, Water, Ice and Permafrost in the Arctic (SWIPA),Arctic Monitoring and Assessment Programme (AMAP)*, 68:p. 62.

Camill, P. (2005). Permafrost thaw accelerates in boreal peatlands during late-20th century climate warming. *Climatic Change*, 68:135–152.

Cleve, K. V. and Viereck, L. A. (1981). Forest succession in relation to nutrient cycling in the boreal forest of alaska. *In Forest succession, concepts, and application. Edited by D.C. West, H.H. Shugart, and D.B. Botkin. Springer-Verlag, New York.*, pages 184–211.

Cleve, K. V. and Viereck, L. A. (1983). A comparison of successional sequences following fire on permafrost-dominated and permafrost-free sites in interior Alaska. *Permafrost: Proceeding of the Fourth International Conference. National Academy Press, Fairbanks, Alaska, Geographical Review*, pages 1286–1291.

Fenton, N., Lecomte, N., Legare, S., and Bergeron, Y. (2005). Paludification in black spruce (Picea mariana) forests of eastern Canada: potential factors and management implications. *For. Ecol. Manage.*, 213(1-3):151–159.

Flannigan, M. D. and Harrington, J. B. (1988). A study of the relation of meteorological variables to monthly provincial area burned by wildfire in canada (1953–80). *J. Appl. Meteor.*, 27:441–452.

Glenn, J. (2010). Bonanza creek lter photo monitoring. Technical report, Bonanza Creek LTER - University of Alaska Fairbanks.

Jafarov, E. E., Marchenko, S. S., and Romanovsky, V. E. (2012). Numerical modeling of permafrost dynamics in alaska using a high spatial resolution dataset. *The Cryosphere*, 6(3):613–624.

Johnson, E. A. (1992). *Fire and vegetation dynamics: studies from the North American boreal forest*. Cambridge.

Johnstone, J. F., Hollingsworth, T. N., III, F. S. C., and Mack, M. C. (2010a). Changes in fire regime break the legacy lock on successional trajectories in the Alaskan boreal forest. *Glob. Change Biol.*, 16(4):1281–1295.

Johnstone, J. F., III, F. S. C., Hollingsworth, T. N., Mack, M. C., Romanovsky, V., and Turetsky, M. (2010b). Fire, climate change, and forest resilience in interior Alaska. *Can. J. Forest Res.*, 40:1302–1312.

Johnstone, J. F. and Kasischke, E. S. (2005). Stand-level effects of soil burn severity on postfire regeneration in a recently burned black spruce forest. *Can. J. For. Res.*, 35(9):2151–2163.

Jorgenson, M. T., Romanovsky, V., Harden, J., Shur, Y., O'Donnell, J., Schuur, E. A. G., Kanevskiy, M., and Marchenko, S. (2010). Resilience and vulnerability of permafrost to climate change. *Canadian Journal of Forest Research*, 40(7):1219–1236.

Kasischke, E., French, N., ONeill, K., Richter, D., Bourgeau-Chavez, L., and Harrell, P. (2000). Influence of fire on long-term patterns of forest succession in alaskan boreal forests. In Kasischke, E. and Stocks, B., editors, *Fire, Climate Change, and Carbon Cycling in the Boreal Forest*, volume 138 of *Ecological Studies*, pages 214–235. Springer New York.

Kasischke, E. S., Bourgeau-Chavez, L. L., and Johnstone, J. F. (2007). Assessing spatial and temporal variations in surface soil moisture in fire-disturbed black spruce forests in Interior Alaska using spaceborne synthetic aperture radar imagery Implications for post-fire tree recruitment. *Remote Sensing of Environment*, 108:42–58.

Kasischke, E. S., Verbyla, D. L., Rupp, S. T., McGuire, A. D., Murphy, K. A., Jandt, R., J L Barne, E. E. H., Duffy, P. A., Calef, M., and Turetsky, M. R. (2010). Alaskas changing fire regimeimplications for the vulnerability of its boreal forests. *Can. J. For. Res.*, 40(7):1313–1324.

Klock, G. O. and Helvey, J. D. (1976). Soil - water trends following wildfire on the Entiat, Experimental Forest. *Annual Proceedings Tall Timbers Fire Ecologic Conference*, 15:193–200.

Liu, H. P., Randerson, J. T., Lindfors, J., and III, F. S. C. (2005). Changes in the surface energy budget after fire in boreal ecosysems of interior alaska: an annual perspective. *J. Geophys. Res – Atmospheres*, 110:D13101.

Marchenko, S., Romanovsky, V., and Tipenko, G. (2008). Numerical modeling of spatial permafrost dynamics in Alaska. In *In Proceedings of the Eighth International Conference on Permafrost*, pages 190–204, Institute of Northern Engineering, University of Alaska, Fairbanks. Willey.

McGuire, A. D., Melillo, J., Jobbagy, E. G., Kicklighter, D., Grace, A. L., Moore, B., and Vorosmarty, C. J. (1992). Interactions between carbon and nitrogen dynamics in estimating net primary productivity for potential vegetation in North America. *Global Biogeochem. Cycles*, 6:101–124.

McGuire, A. D., Melillo, J. W., Kicklighter, D. W., and Joyce, L. A. (1995). Equilibrium responses of soil carbon to climate change: empirical and process-based estimates. *Journal of Biogeography*, 22:785–796.

Melillo, J. M., McGuire, A. D., Kicklighter, D. W., III, B. M., Vorosmarty, C. J., and Schloss, A. L. (1993). Global climate change and terrestrial net primary production. *Nature*, 63:234–240.

Moore, C. M. and Keeley, J. E. (2000). Long-term hydrologic response of a forested catchment to prescribed fire. *in Proceedings of the American Water Resources Association Spring Specialty Conference, Water Resources in Extreme Environments, edited by D. L. Kane*, pages 37–42.

Nicolsky, D. J., Romanovsky, V. E., and Panteleev, G. G. (2009). Estimation of soil thermal properties using in-situ temperature measurements in the active layer and permafrost. *Cold Reg. Sci. Technol.*, 55(1):120–129.

Nicolsky, D. J., Romanovsky, V. E., and Tipenko, G. S. (2007). Using in-situ temperature measurements to estimate saturated soil thermal properties by solving a sequence of optimization problems. *The Cryosphere*, 1:41–58.

O'Donnell, J. A., Harden, J. W., McGuire, A. D., and Romanovsky, V. E. (2011). Exploring the sensitivity of soil carbon dynamics to climate change, fire disturbance and permafrost thaw in a black spruce ecosystem. *Biogeosciences*, 8(5):1367–1382.

Overland, J. E., Wang, M., Walsh, J. E., Christensen, J. H., Kattsov, V. M., and Chapman, W. L. (2011). Climate model projections for the arctic (swipa). *Arctic Monitoring and Assessment Programme (AMAP)*.

Raich, J. W., Rastetter, E. B., Melillo, J., Kicklighter, D., Steudler, P. A., Peterson, B. J., Grace, A. L., Moore, B., and Vorosmarty, C. J. (1991). Potential net primary productivity in South America: Application of a global model. *Ecol. Appl.*, 1:399–429.

Romanovsky, V. E. and Osterkamp, T. E. (2000). Effects of unfrozen water on heat and mass transport processes in the active layer and permafrost. *Permafrost Periglacial Process.*, 11(3):219–239.

Schuur, E. A. G., Vogel, J. G., Crummer, K. G., Lee, H., Sickman, J. O., and Osterkamp, T. E. (2009). The effect of permafrost thaw on old carbon release and net carbon exchange from tundra. *Nature*, 459:556–559.

Sergueev, D., Tipenko, G., Romanovsky, V., and Romanovskii, N. (2003). Mountain permafrost thickness evolution under the influence of long-term climate fluctuations (results from numerical simulation). In Swets & Zeitlinger: Lisse, Z., editor, *In 8th International Conference on Permafrost*, pages 1017–1021. Phillips M, Springman S, and Arenson L.

Solomon, S., Qin, D., Manning, M., Chen, Z., Marquis, M., Averyt, K. B., Tignor, M., and Miller, H. L. (2007). *Contribution of Working Group I to the Fourth Assessment Report of the Intergovernmental Panel on Climate Change*. Cambridge, United Kingdom and New York, NY, USA.

Tiedemann, A. R., Conrad, C. E., Dieterich, J. H., Hurnbeck, J. W., Megahan, W. F., Viereck, L. A., and Wade, D. D. (1979). Resilience and stability of ecological systems. *Gen. Tech. Rep.*, W0-10:28.

Walsh, J. E., Chapman, W. L., Romanovsky, V., Christensen, H., and Stendel, M. (2008). Global climate model performance over alaska and greenland. *J. Climate*, 21:6156–6174.

Yi, S., McGuire, A. D., Harden, J., Kasischke, E., Manies, K., Hinzman, L., Liljedahl, A., Randerson, J., Liu, H., Romanovsky, V. E., Marchenko, S., and Kim, Y. (2009). Interactions between soil thermal and hydrological dynamics in the response of alaska ecosystems to fire disturbance. *Journal of Geophysical Research – Biogeosciences*, 114:G02015.

Yi, S., McGuire, A. D., Kasischke, E., Harden, J., Manies, K., Mack, M., and Turetsky, M. (2010). A dynamic organic soil biogeochemical model for simulating the effects of wildfire on soil environmental conditions and carbon dynamics of black spruce forests. *J. Geophys. Res.*, 115:G04015.

Yoshikawa, K., Bolton, W. R., Romanovsky, V. E., Fukuda, M., and Hinzman, L. D. (2003). Impacts of wildfire on the permafrost in the boreal forests of Interior Alaska. *J. Geophys. Res.*, 107(8184).

Yuan, F. M., Yi, S. H., McGuire, A. D., Johnson, K. D., Liang, J. J., Harden, J. W., Kasischke, E., and Kurz, W. A. (2012). Assessment of historical boreal forest carbon dynamics in the yukon river basin: Relative roles of climate warming and fire regime changes. *Ecological Applications*, 22:2091–2109.

Zhuang, Q., McGuire, A. D., O'Neill, K. P., Harden, J. W., Romanovsky, V. E., and Yarie, J. (2002). Modeling soil thermal and carbon dynamics of a fire chronosequence in interior alaska. *Journal of Geophysical Research: Atmospheres*, 107(D1):FFR 3–1–FFR 3–26.

Zoltai, S. C. and Martikainen, P. J. (1996). The role of forested peatlands in the global carbon cycle. *In: Apps, M.J., Price, D.T. (Eds.), Forest Ecosystems, Forest Management and the Global Carbon Cycle. NATO ASI. Springer-Verlag, Heidelberg*, pages 47–58.

Chapter 4

Numerical modeling of permafrost dynamics in Alaska using a high spatial resolution dataset[§]

Abstract

Climate projections for the 21st century indicate that there could be pronounced warming and permafrost degradation in the Arctic and sub-Arctic regions. Climate warming is likely to cause permafrost thawing with subsequent effects on surface albedo, hydrology, soil organic matter storage and greenhouse gas emissions.

To assess possible changes in permafrost thermal state and active layer thickness, we implemented the GIPL2-MPI transient numerical model for the entire Alaska permafrost domain. The model input parameters are spatial datasets of mean monthly air temperature and precipitation, prescribed thermal properties of the multilayered soil column, and water content. The parameters are specific to each soil class and geographical location. As a climate forcing, we used a composite of five IPCC Global Circulation Models that was downscaled to 2 by 2 km spatial resolution by the Scenarios Network for Alaska Planning (SNAP) group.

In this chapter, we present modeling results based on this five-model composite with the A1B carbon emission scenario. The model has been calibrated with annual borehole temperature measurements for the State of Alaska. We also performed more detailed calibration for fifteen shallow borehole stations where high quality data are available on a daily basis. To validate the model's performance, we compared simulated active layer thicknesses with observed data from Circumpolar Active Layer Monitoring (CALM) stations. The calibrated model was used to address possible ground temperature changes for the 21st century. The model simulation results show that widespread permafrost degradation in Alaska could begin between 2040 and 2099 within the vast area south of the Brooks Range, except for the high altitude regions of the Alaska Range and Wrangell Mountains.

[§] Jafarov, E. E., Marchenko, S. S., and Romanovsky, V. E.: Numerical modeling of permafrost dynamics in Alaska using a high spatial resolution dataset, The Cryosphere, 6, 613-624, doi:10.5194/tc-6-613-2012, 2012.

4.1 Introduction

According to the State of the Climate in 2010 Report [Richter-Menge and Jeffries, 2011], the Arctic cryosphere is undergoing substantial changes such as loss of sea ice and warmer ocean temperatures, melting of the Greenland Ice Sheet and glaciers, and continuous increase in permafrost temperatures. Permafrost is one of the main components of the cryosphere in northern regions, where it influences hydrological processes, energy exchanges, natural hazards and carbon budgets. The World Meteorological Organization (WMO) identifies permafrost as one of the six cryospheric indicators of global climate change [Brown et al., 2008]. Changes in the thermal state of permafrost in Alaska were reported recently by Romanovsky et al. [2010] and Smith et al. [2010], who observed an increase in permafrost temperatures by $0.5 - 3^{o}C$ over the last 30 years. Thawing of permafrost causes land surface changes, damaging forests, houses, and infrastructure. Changes in permafrost thermal state can have a significant impact on the state's economy due to the additional repair costs of public infrastructure [Larsen et al., 2008].

Mapping of permafrost distribution, especially its thermal state, remains a challenging problem due to the sparsity of observed data. Despite the fact that geophysical surveys and boreholes are the most reliable sources of information about permafrost, they are extremely costly and are mostly available from relatively small areas such as oil fields and transportation corridors.

In the past, one of the most popular methods in permafrost mapping was the use of a frost number or permafrost index [Nelson, 1986], which usually takes into account seasonal air temperature variations explicitly, and does not include other important factors such as snow, soil moisture content, and soil thermo-physical parameters that affect the permafrost thermal state.

Riseborough et al. [2008] divided permafrost models into three main categories: empirical, equilibrium and numerical. Empirical models relate permafrost occurrences to topoclimatic factors and use empirically derived landscape parameters representing the response of the active layer and permafrost to both climatic forcing and local factors, such as soil properties, moisture conditions and vegetation [Nelson et al., 1997; Shiklomanov and Nelson, 2002; Zhang et al., 2005; Shiklomanov et al., 2008]. Equilibrium models employ transfer functions between the air and ground temperatures to define the active layer

depth. The Kudryavtsev Model, N factor, TTOP and GIPL 1.0 models are classified as equilibrium models [Kudryavtsev et al., 1974; Romanovsky and Osterkamp, 1995, 1997; Shiklomanov and Nelson, 1999; Klene et al., 2003; Sazonova and Romanovsky, 2003; Wright et al., 2003]. However, the applicability of equilibrium models is restricted to problems of limited complexity, and cases where transient effects may be neglected or unimportant. Numerical solution methods are generally used to solve freezing and thawing problems over a short (engineering) time scale in which transient effects of phase change are important [see Williams and Smith, 1989, pg. 86]. Therefore, transient numerical modeling with an incorporated phase change effect is the most effective method to simulate and forecast the thermal regime of permafrost over a relatively short time interval. Transient numerical models [e.g., Gruber et al., 2004a,b; Nicolsky et al., 2007; Farbrot et al., 2007; Etzelmuller et al., 2008] have a higher computational cost, but they are more accurate in determining temperature field and phase change boundary dynamics.

In this chapter we propose a method based on numerical modeling, which allows us to map the temporal dynamics and spatial distribution of permafrost with high spatial resolution. To simulate ground thermal regimes, we implement the GIPL2-MPI numerical transient model. The GIPL2 was developed by G. Tipenko and V. Romanovsky [Tipenko et al., 2004] and applied for first time to the entire Alaskan permafrost domain with 0.5^{o} spatial resolution by Marchenko et al. [2008]. In order to quantify the socio-economical impact of permafrost degradation, permafrost distribution maps with higher spatial resolution are required. In the current project, we map the permafrost thermal state with 2 by 2 km spatial resolution, which is 410205 grid points, to cover the entire Alaskan region. Due to an increase in the amount of spatial grid points, the computational load increases as well. To perform calculations efficiently, we developed the GIPL2-MPI version of the GIPL2 model, which runs in parallel on several processors. To run the parallel model, we used the Arctic Region Supercomputing Center facility at the University of Alaska Fairbanks.

The current chapter is constructed in the following order. The mathematical description section gives more detailed information on our methods. In the methods section we outline all necessary input datasets, such as initial temperatures, snow, thermal properties of multi-layered organic and mineral soils, and geothermal heat flux. The model calibra-

tion and validation section provides a detailed description of the model calibration with observed monthly-averaged temperatures available from shallow boreholes stations and validation of the mean annual ground temperatures from deep boreholes, as well as validation of the active layer thickness values with CALM[1] active layer observation stations in Alaska. The "optimization of ground thermal parameters" section illustrates the effect of additional upper layer(s) of organic matter on mean annual ground temperatures. In the results section, we illustrate the model outputs and provide projected decadal warming rates at different depths for the 21st century. The discussion section gives an overview of major physical factors that affect the permafrost thermal regime and outlines how the model can be improved. Finally, the conclusion section outlines major results and concludes the current work.

4.2 Mathematical model

The GIPL2-MPI numerical model solves the Stefan problem [Vasilios and Solomon, 1993] with phase change, which is the problem of thawing or freezing via conduction of heat. The enthalpy formulation used in the solution of Stefan problem is the most common method, which does not require explicit treatment of the moving freeze/thaw boundary [Caldwell and Chan, 2001]. The core of the GIPL2-MPI numerical model is based on the $1-D$ quasi-linear heat conductive equation [Sergueev et al., 2003]:

$$\frac{\partial H(x,t)}{\partial \tau} = \frac{\partial}{\partial x}\left(k(x,t)\frac{\partial t(x,\tau)}{\partial x}\right) \tag{4.1}$$

where $x \in (x_u, x_l)$ is a spatial variable that changes with depth, x_u and x_l are the upper and lower boundaries of the vertical grid, $\tau \in (0,T)$ is a temporal variable, $t(x,\tau)$ is temperature, $k(x,t)$ is thermal conductivity ($Wm^{-1}K^{-1}$), and $H(x,t)$ is an enthalpy function.

$$H(x,t) = \int_0^t C(x,s)ds + L\Theta(x,t) \tag{4.2}$$

where $C(x,s)$ is volumetric heat capacity ($Jm^{-3}K^{-1}$), and $\Theta(x,t)$ is volumetric water content (fraction of 1); L is the volumetric latent heat of freeze/thaw (Jm^{-3}). The Eq. (4.1) is complemented with boundary and initial conditions. The upper part of the domain corresponds to the air layer which is at two meters height above the surface. The fictitious

[1]Circumpolar Active Layer Monitoring Network http://www.udel.edu/Geography/calm/

domain formulation [Marchuk et al., 1986] allows us to incorporate a seasonal snow layer into the current air layer. The Dirichlet type boundary condition was used as an upper boundary condition:

$$t(x_u, \tau) = t_{air} \tag{4.3}$$

where t_{air} is a monthly-averaged air temperature. The geothermal gradient was set at the lower boundary:

$$\frac{\partial t(x_l, \tau)}{\partial x} = g \tag{4.4}$$

where g is geothermal gradient, a small constant number (Km^{-1}). For the initial temperature distribution we used an appropriate ground temperature profile based on the point location

$$t(x, 0) = t_0(x). \tag{4.5}$$

The formula for unfrozen water content $\Theta(x, t)$ is based on empirical experiments and has the following form:

$$\Theta(x, t) = \eta(x) \cdot \begin{cases} 1, & t \geq t_* \\ a|t|^{-b}, & t < t_*. \end{cases} \tag{4.6}$$

Parameters a and b are dimensionless positive constants [Lovell, 1957], and $\eta(x)$ represents the volumetric soil moisture content. The right side of the Eq. (4.6) represents the liquid pore water fraction. The constant $t_* = (1/a)^b$ is a freezing point depression, which from a physical point of view means that ice does not exist in the soil if $t > t_*$. $\Theta(x, t)$ changes with depth and depends on the soil type. The discretized form of Eq. (4.1) can be found in [Sergueev et al., 2003] and [Shiklomanov et al., 2008]. A detailed mathematical description of the model and numerical solution can be found in [Nicolsky et al., 2007].

4.3 Methods

We implemented the Scenarios Network for Alaska Planning (SNAP) dataset as a baseline input for the GIPL2-MPI numerical model. The dataset is composed of five GCMs, which (according to SNAP) perform the best for Alaska [Walsh et al., 2008]. The dataset includes monthly-averaged temperatures and precipitation data for the years 1980-2099, using A1B carbon emission scenario. The outputs from the selected five models were downscaled

to 2 by 2 km resolution by SNAP using the knowledge-based system PRISM[2]. PRISM uses a digital elevation model that contains information describing Alaska's topography (slopes, aspects, elevation) and observed precipitation measurements to determine variations in precipitation as functions of elevation. To calculate snow depth and its thermal conductivity, we developed the following method. Snow density is calculated according to [Verseghy, 1991]

$$\rho_0 = \rho_{smin}, \quad \rho_i = (\rho_{i-1} - \rho_{smax})e^{-\tau_f \Delta\tau} + \rho_{smax}. \tag{4.7}$$

where $\tau_f = 0.24$ corresponds to an e-folding time of about 4 days, ρ_s is the snow density in units of $kg \cdot m^{-3}$, and the value of ρ_s ranges from minimum snow density ρ_{smin} to maximum snow density ρ_{smax} with a time step $\Delta\tau$ of one month. We chose ρ_{smin} and ρ_{smax} from the corresponding snow classes following [Sturm et al., 1995]. Snow depth h_s is calculated by extracting snow water equivalent (SWE) from the downscaled five-GCM composite precipitation dataset:

$$h_s = \frac{SWE}{\rho_s} \tag{4.8}$$

Snow thermal conductivity k_s was calculated according to [Sturm et al., 1997].

$$k_s = 0.138 - 1.01\rho_s + 3.233\rho_s^2. \tag{4.9}$$

Snow water equivalent was extracted from the precipitation dataset by comparing monthly mean temperatures with the water freezing point temperature. If the MMT is less than 0^oC, we accumulate the SWE on a monthly basis (i.e. since snow stays on the ground after it falls, we add existing SWE to the SWE for the current month). When the SWE is obtained, we calculate density, depth and thermal conductivity of the snow by employing equations 4.7-4.9.

We analyzed the ground temperature profiles (ground temperature distribution profiles are available online at Geophysical Institute Permafrost Laboratory[3] and Advanced Cooperative Arctic Data and Information Service[4] websites) in more than 25 relatively deep boreholes from 29 to 89 m in depth [Osterkamp and Romanovsky, 1999; Osterkamp,

[2]Parameter-elevation Regressions on Independent Slopes Model climate mapping system (http://www.prism.oregonstate.edu)

[3]www.permafrostwatch.org

[4]www.aoncadis.org

2003] along the Trans-Alaskan transect. This analysis revealed a ground temperature zonality in Alaska with generally lower permafrost temperatures in the north and higher ground temperatures in the south. Based on this zonality, we extrapolated available initial ground temperature profiles to wider areas and classified them into 18 ground temperature zones (Fig. 4.1). The 18 ground temperature zones represent the 18 classes of temperature distribution with depth and were used as initial conditions for simulation.

The thermo-physical properties (volumetric soil ice/water content, unfrozen water curve parameters, soil heat capacity and thermal conductivity, thickness of soil layers, etc.) for 18 ground temperature zones might be different and depend on many factors including surficial geology. The number of soil type classes we used in these simulations was 26, and each class had its own number of soil and bedrock layers with different thermal properties (e.g. peat, silt, bedrock, gravel etc.). The multilayered soil columns were assigned for each soil class according to the Modified Surficial Geology Map of Alaska [Karlstrom et al., 1964]. The thermo-physical properties were assigned to each ground mineral layer according to surficial geological (soil type) class. The model was calibrated against the ground temperature measurements from the shallow boreholes, which were specific for each soil class and geographical location (the method used and its limitations were described in more detail by Nicolsky et al. [2007]). Organic layers in the model were introduced as a separate layer(s) which could be added to the top of a mineral soil column. For upper organic soil layers, we used the data obtained from the numerous field observations and Ecosystem Map of Alaska from the National Atlas of the United States of America[5]. To further optimize the number and the thermal properties of the organic layers, we developed an algorithm described in the "optimization of ground thermal parameters" section.

Each grid point on the map uses a one-dimensional multilayer soil profile down to a depth of 700 m. The vertical grid has fine resolution between nearby points at the near surface ground layer (0.01 m) and becomes coarser towards the bottom boundary (100 m). The geothermal heat flux was assigned as a lower boundary condition. The values for the geothermal heat flux were generated using Pollack's geothermal heat model [Pollack et al., 1993].

[5]http://www.nationalatlas.gov

4.4 Model calibration and validation

For the initial model calibration, we used measured data from more than fifteen shallow boreholes (1-1.2 m in depth) across Alaska. These high quality ground temperature measurements (precision generally at 0.01^oC) are available from the mid-1990s to 2010. Soil water content and snow depth measurements were also available at most of these boreholes. Figures 4.2 through 4.4 illustrate the results of the model calibration for the three shallow borehole stations. The West Dock site (Fig. 4.2) is located on the outer Arctic Coastal Plain within the Prudhoe Bay oil field. The polygonized "uplands" and drained thaw-lake basins constitute the primary relief at this site. Landcover units include wet nonacidic graminoid- moss tundra. The site was described by Osterkamp [1987] and Romanovsky and Osterkamp [1995]. The SagMat site (Fig. 4.3) is located on a north-facing slope of about 2 degrees. The vegetation cover is a moist acidic tundra [Walker et al., 2008]. The Galbraith Lake site (Fig. 4.4) is located in a previously glaciated mountain valley. Landcover units include graminoid-moss tundra and graminoid, prostrate dwarf-shrub, and moss tundra (wet and moist nonacidic). Further site descriptions can be found in [Ping et al., 2003]. All of these sites were instrumented by at least ten thermistors arranged vertically at depths from 0 to 1 m. A detailed description of the thermistor set up and installation can be found in Nicolsky et al. [2007]. For all the stations, correlations between GCMs and observations are higher than 90% for monthly mean air temperatures (MMATs). Despite the high correlation between downscaled and observed MMATs, the freezing and thawing periods do not always agree well with the downscaled GCM composite. As can be seen from Fig. 4.2, the variances between simulated and measured ground temperatures during the 1999 freezing period increased with depth. The simulated monthly-averaged ground temperatures decrease sharply when the actual ground temperature freezing period is longer. The same pattern can be observed during the thawing periods of 2004 and 2005 in SagMat (Fig. 4.3). Furthermore, there were winter periods in which the actual monthly-averaged ground temperatures were colder than the simulated temperatures (see SagMat thawing period 2002, 2004, 2005, Fig. 4.3, Galbraith Lake winter periods 2004, 2005, Fig. 4.4), which could be due to snow conductivities and snow depth biases over those winter periods. The simulated ground temperatures were, in general, smoother than measured temperatures and did not represent the seasonal effects, which could be a reason for high variabilities

between measured and simulated ground temperatures over certain winter seasons.

To validate the model results, we used annually-averaged temperatures at deeper depths. More than 50 deep boreholes from 29 m to 89 m in depth (GTN-P[6]) were available for model calibration of permafrost temperature profiles. For most of the borehole stations, the deviation between observed and measured mean annual ground temperatures (MAGTs) was less than 1^oC (Fig. 4.5). There were four stations at which the deviation was greater than 1^oC, three of which were located in the tussock area. The MAGTs for the tussock-like areas are usually sensitive to snow depth. If snow depth does not exceed the height of tussock, then cold air can penetrate deep into the ground; otherwise, when snow depth exceeds the height ofthe tussock, it isolates the ground from cold air. The permafrost observation station with the measured -3.81^oC and simulated -6.32^oC MAGTs at a depth of 20 m corresponds to the site in the continuous permafrost zone with MAATs around -10^oC. The fact that the measured MAGT was almost 3 degrees warmer might be due to the site's location, which was near small lakes. The convective heat transfer due to ground water movements or heat from the open water reservoirs might be an essential factor in producing warmer MAGTs.

In addition to deep borehole stations, we validated the MAGTs from the permafrost observation stations using data from the US Schools project[7] (Fig. 4.6). The measurements from these stations were taken at relatively shallow depths, ranging from 1 to 6 m. Most of the stations were located in close proximity to public schools, rivers or lakes. There were three stations where differences between measured and simulated temperatures were greater than 3^oC. One of them was located in the city, another close to the lake, and the third was close to one of the branches of the Yukon river. The first permafrost station experienced the influence of anthropogenic warming, and the other two may have experienced lateral heat exchange due to subsurface ground water movements.

Finally, we validated the simulated active layer thicknesses with observed ALTs from 43 CALM[8] observation stations in Alaska (Fig. 4.7). For the ALT comparison test we compared averaged active layer thicknesses over the available time periods with the cor-

[6]Global Terrestrial Network for Permafrost http://www.gtnp.org

[7]IPA-IPY Thermal State of Permafrost (TSP) Snapshot Borehole Inventory, Version 1.0 (http://nsidc.org/data/g02190.html)

[8]Circumpolar Active Layer Monitoring Network http://www.udel.edu/Geography/calm/

responding simulated ALTs. During ALT simulation, the soil moisture content was specified for each of the simulated stations and held constant throughout the entire simulation period. The major restriction of this approach reflects the limitation of available data on soil moisture content and its dynamics over time for each of the stations. There were two main uncertainties while comparing simulated and measured ALTs. First, there are several methods for measuring ALT, and all of them have their own limitations [Nelson and Hinkel, 2003]. Second, simulated AL depth was driven by monthly-averaged climate data and by the amount of prescribed soil moisture content. During model validation, the values for several observation stations were adjusted by assigning additional organic layers.

To evaluate overall model performance and model bias, we calculated the mean absolute error (MAE), root mean square error (RMSE), and mean bias error (MBE) according to the following series of equations [Willmott and Matsuura, 2005]:

$$MAE = \frac{1}{n}\sum_{k=1}^{n}|e_i|, \quad RMSE = \frac{1}{n}\sqrt{\sum_{k=1}^{n}e_i^2}, \quad MBE = \frac{1}{n}\sum_{k=1}^{n}e_i. \tag{4.10}$$

where e_i is a difference between simulated and observed MAGTs and ALTs and n is the number of stations.

The MAE shows an overall error for all compared stations, while the RMSE emphasizes an error variation within the individual stations and the MBE shows that the model underestimates or overestimates the observed data. The MBE in Table 4.1 shows that our simulations were mainly underestimates.

4.5 Optimization of ground thermal parameters

To ensure that the initial temperature conditions did not influence the results, we ran a spin-up with assigned initial ground temperature profiles (Fig. 4.1) corresponding to the middle of August 1980, until the soil temperature profile reached equilibrium with the upper and lower boundary conditions. The equilibrium temperature profile was determined when the maximum difference of soil temperatures at all levels between two successive annual cycles was less than 0.01°C. This was used as the initial condition.

After 30 years of simulations, the MAGTs at 1 m depth in the western and southwestern regions of Alaska were slightly warmer than the measured ground temperatures from

those areas (Fig. 4.8). These parts of Alaska correspond to subarctic oceanic and continental sub-arctic climates. During spring, when the Bering Sea is ice-free, the moderating influence of the open water helps to melt the snow early for some areas adjacent to the sea, when winter temperatures are more continental due to the presence of sea ice [Serreze and Barry, 2005]. The mean annual average air temperatures range from 1^oC to 2^oC from west to southwest Alaska. These regions correspond to ecosystem-protected permafrost zones that have formed under colder climate conditions and currently persist only in undisturbed late-successional ecosystems [Shur and Jorgenson, 2007]. The MAGTs for the areas with a sufficient amount of organic cover and soil moisture content usually experience gradual temperature increases even when MAATs are slightly higher than 0^oC [Jorgenson et al., 2010]. Therefore, an additional layer of organic matter might provide permafrost with necessary resilience. However, highly variable precipitation and thermal properties of mineral soils in the western and southwestern parts of the region makes the choice of an appropriate additional organic layer (AOL) non-trivial.

To address this issue, we developed an algorithm that assigns optimal additional organic layer(s) for every grid point based on the deviation coefficient between the modeled equilibrium temperature profile and the assigned initial ground temperatures. During model calibration we tested the effects of varying climatic and ecological conditions on ground temperatures, and developed nine classes of additional organic layers. The additional organic layer(s) varied from thinner to thicker, and had different amounts of soil moisture and slightly different thermal properties.

Our algorithm is based on the following principle. If the initial temperature profile represents the actual ground temperature distribution for the year 1980, then the equilibrated ground temperatures should not deviate significantly from the initial temperature distribution profile. Otherwise, we assign additional organic layer(s) in a successive manner. The layer(s) corresponding to the smallest deviation between equilibrated and initial ground temperature profiles are assigned as the final additional organic layer(s) at the corresponding location.

The obtained additional organic layer mask (Fig. 4.9) excludes lakes, rivers and mountain areas, and shows places where differences between initial temperature profiles and equilibrated temperatures vary significantly. These places required an additional organic

layer(s) located in areas where we do not have many observation stations, mostly in the discontinuous permafrost zone. The amount of AOL in the northwestern part is thin and not so extensive compared with the AOL in the southwestern territories. The thickness of the AOL is becoming more diverse in the south and southwestern parts of the region. The AOL mask indicates the places where the initial temperature profiles should be adjusted. As mentioned in the methods section, the initial temperature profiles were assigned according to the measured data, which were available for a limited number of places and do not cover the entire region.

The difference map between MAGTs at 1 m depth simulated with and without additional AOL (Fig. 5.1) showed colder annual ground temperatures in the western and southwestern parts of Alaska, which might more closely represent the current ground temperature distribution. This method does not necessary guarantee that assigned AOL is going to cool the 2010 MAGT after spin-up and 30 years of simulation. Nevertheless, we were able to cool the MAGT for 2010 in the south and southwestern areas (Fig. 5.1). This approach emphasized the importance of improved maps of soil organic layers and improved initial temperature profiles, and the necessity of further development of the permafrost temperature observation system, especially in the western and southwestern parts of Alaska.

4.6 Results

According to the decadal average of MAGTs over the twelve decades from 1980 to 2099, the overall area covered by MAGT less than 0^oC is projected to decrease. The model projects that the area of decadally-averaged MAGT warmer than 0^oC at 2, 5 and 20 m depths will increase at 3.7%, 3.5% and 2.4% per decade, respectively (Fig. 4.11).

The spatial snapshot of MAGTs at 2 m depth (Fig. 4.12) shows pronounced warming almost everywhere, including in the current continuous permafrost areas (e.g. Seward Peninsula and the south part of the Brooks Range). The amount of ground surface organic material may retard permafrost thaw in the discontinuous permafrost zone. This effect can be carried into the continuous permafrost zone via changes in vegetation. Therefore, discontinuous and sporadic permafrost areas with small or no organic layer and low soil moisture will be more vulnerable to rapid permafrost thaw. High altitude areas such as

the Chugach Mountains, the Wrangell Mountains, the Alaska Range and the Brooks Range maintain relatively stable MAGTs during first half of the 21st century due to cold annual air temperatures.

The MAAT dynamics for 120 years obtained from the downscaled GCM composite showed a larger positive temperature trend during the 21st century for the northern region. This high positive trend can be observed almost everywhere north of the Brooks Range. The simulated mean annual snow depth showed that the amount of annual snow fall decreases in the south and increases in the north, when the number of snow-free days increases in the whole region due to warmer MAATs. The increase of snow-free days combined with the increase of the thickness of snow greatly affects the mean annual surface temperatures in the northern part of Alaska. Eventually, this effect propagates further to the ground and transfers to the MAGTs. Fig. 4.13 illustrates the higher trend of the MAGT for the two northern sites in comparison with central and south-central locations.

4.7 Discussion

The GIPL2-MPI transient numerical model with proper input parameters is a valuable tool for mapping the thermal state of permafrost and its future dynamics with high spatial resolution. However, it is important to understand the limitations of the current model and the downscaled GCMs composite dataset.

The composite of five downscaled GCMs simulates well the seasonal cycle variations of near-surface temperature with a correlation between models and observations of 90% or higher (Figs. 4.2-4.4). However, the precipitation bias still remains high, and the correlation between GCMs and observations is 50% to 60% [Brown et al., 2008].

The stations where the GIPL2-MPI model showed high discrepancies with observed MAGTs (Fig. 4.6) were established recently (2005-2009) and do not have long-term data for more comprehensive analysis. A significant number of those stations are located along rivers and in populated areas. The strong differences between measured and simulated MAGT might be caused by changes in surficial geology due to flooding, ground water movement (convective heat transfer), or anthropogenic disturbances.

Besides the factors described above, forest fires are also an important factor affecting the permafrost ground temperature simulations. As a result of forest fires, the surface

albedo decreases and the soil thermal conductivity of the surface soil layer increases [Hinzman et al., 1991]. The areas where wildfires removed the upper organic layer are vulnerable to active layer thickening and warming of permafrost. If the burned area is ice-rich, then the thickening of the active layer might melt the buried ice, which would cause the soil to collapse and form thermokarst depressions [Yoshikawa et al., 2003]. In order to address the dynamics of mean annual ground temperatures in the burned area, it is important to include the development of the vegetation and soil organic layer after the fire event. At the current stage the model does not include the effect of forest fires.

The MAGTs in continuous permafrost zones are mostly climate-driven, as opposed to the discontinuous permafrost zone, where the effects of the ecosystem on the permafrost thermal state are more pronounced [Shur and Jorgenson, 2007]. With climate warming, present day continuous permafrost will turn discontinuous, and vegetation change can develop a thick enough organic layer to provide additional resilience to thaw. Therefore, the introduction of a dynamic vegetation layer might decrease current modeling bias. The impact of humans and wildfires will have to be taken into consideration where it is necessary. Further work is needed to improve the parameterization of soil properties for each type of surface and soil condition. Development of the spatial soil moisture map for Alaska will improve understanding of the soil moisture distribution and its dynamics as well as the results of permafrost modeling. Methods for calculating snow depth and snow thermal properties require further improvement. The 2 km distance between adjacent points is sufficient to neglect lateral heat transfer. However, for modeling watershed areas with grid resolution substantially finer than 1 km, the convective heat transfer by ground water movement likely needs to be taken into account. Therefore, coupling the current model with a hydrological model could be an important step towards better simulation of watershed and wetland areas.

4.8 Conclusion

The increase in mean annual air temperatures and the amount of precipitation for the northern part of the region, as predicted by the five-GCM composite with A1B emission scenario, could accelerate permafrost warming in the north (Fig. 4.13). The central part of the region is projected to experience permafrost degradation at different severity lev-

els depending on the ecosystem. The upper organic layer, soil water saturation and soil thermal properties play significant roles, providing necessary permafrost resilience even when MAATs are close to or slightly above $0^{o}C$. To provide an estimate of the permafrost degradation severity level for a specific geographic location, the effects of varying climatic and ecological conditions require more detailed investigation.

According to the model results, the average areal decadal permafrost degradation at 20 m depth will proceed at 2.4% per decade. Consequently, Alaska is projected to lose about 22% of its frozen ground over the next 90 years. Further analysis and development of the model is required to improve the MAGTs and ALTs simulations. In order to more accurately cover the entire region and to decrease uncertainty in the model predictions, more permafrost temperature observation stations are necessary. Increasing grid spatial resolution will require higher resolution maps of surficial geology, precipitation, vegetation, surface organic layer and soil moisture content.

4.9 Acknowledgements

We would like to thank the friendly personnel at ARSC Supercomputing Center. In particular, we thank Tom Logan and Don Bahl for their help with code parallelization and their constant assistance with model performance, and Kate Hedstrom and Patrick Webb for their help with visualization software. We extend a special thank you to Kenji Yoshikawa for the data from the high school project and to the anonymous reviewers for their valuable comments and suggestions to improve the quality of the paper. This work was supported by the State of Alaska and by the National Science Foundation under grants ARC-0520578, ARC-0632400, ARC-0856864, and ECO-MODI.

4.10 Tables

Table 4.1. The model error statistics obtained by comparing MAGTs and ALTs from 3 different datasets: 60 deep borehole stations compared for 2007-2009 years; 77 US School project stations from relatively shallow depths compared for 2009; 43 averaged active layer thicknesses from CALM stations compared over entire available time periods.

Names	n	RMSE	MAE	MBE
Deep borehole stations (^0C)	60	0.70	0.59	-0.20
US School project (^0C)	77	0.88	1.23	-0.17
ALT (m) (CALM)	43	0.10	0.08	-0.02

4.11 Figures

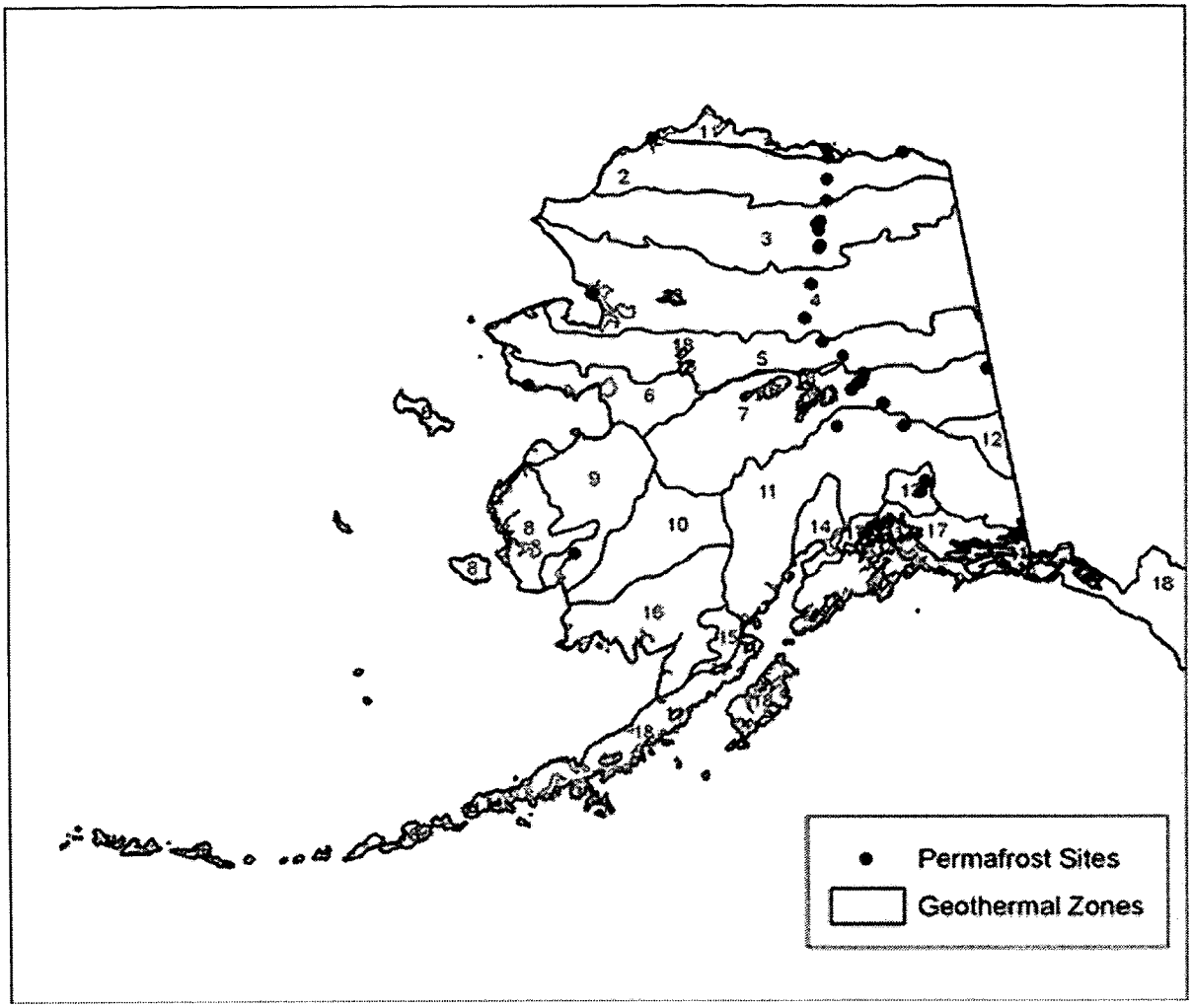

Figure 4.1. Permafrost observation station locations and 18 ground temperature zones. Each ground temperature zone corresponds to its own initial ground temperature distribution profile.

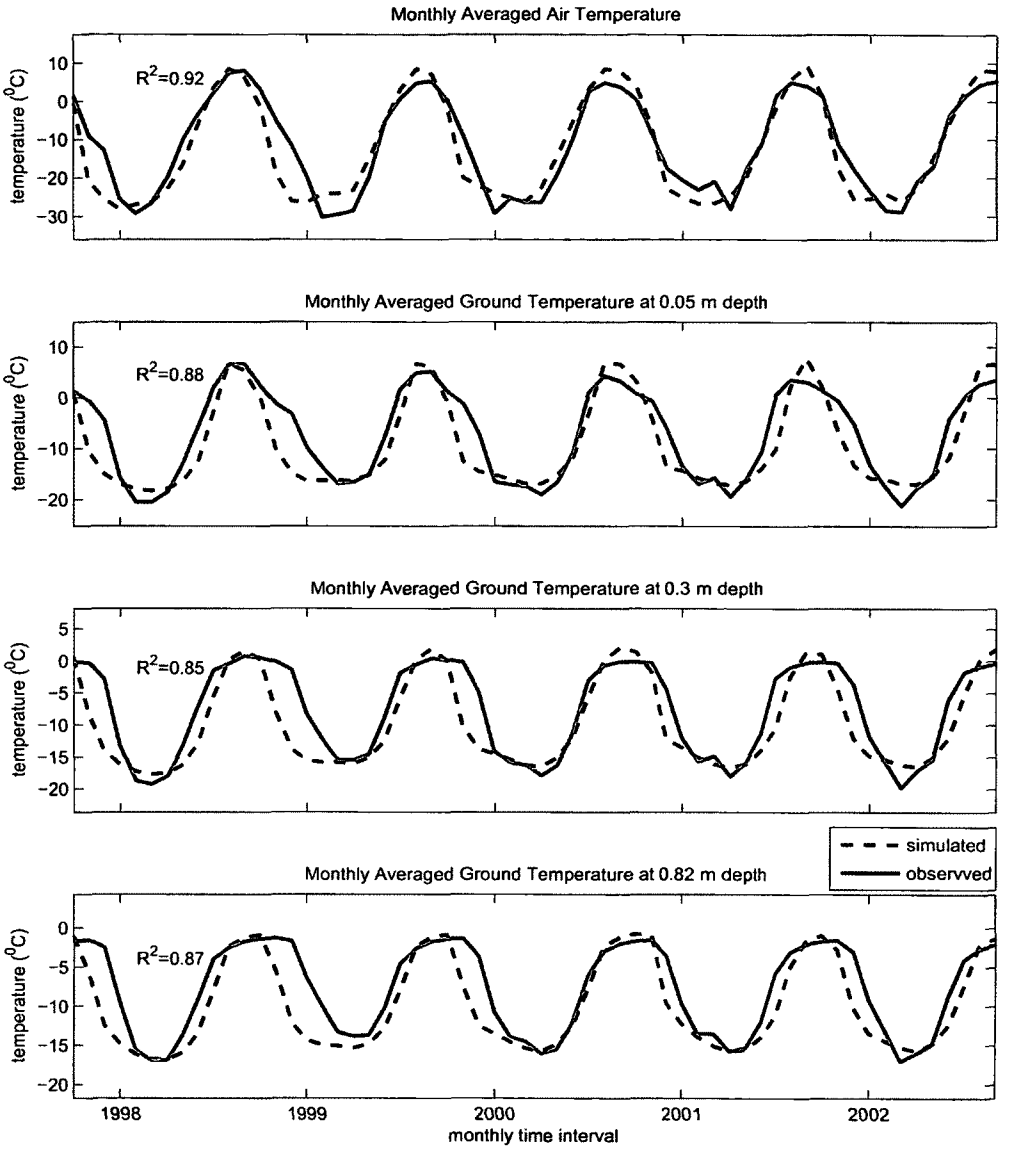

Figure 4.2. Measured (solid) and calculated (dashed) monthly averaged temperatures at 2 m above the ground and 0.05, 0.3 and 0.82 m depths for WestDock 70.37^o N, -148.55^o W permafrost observation stations.

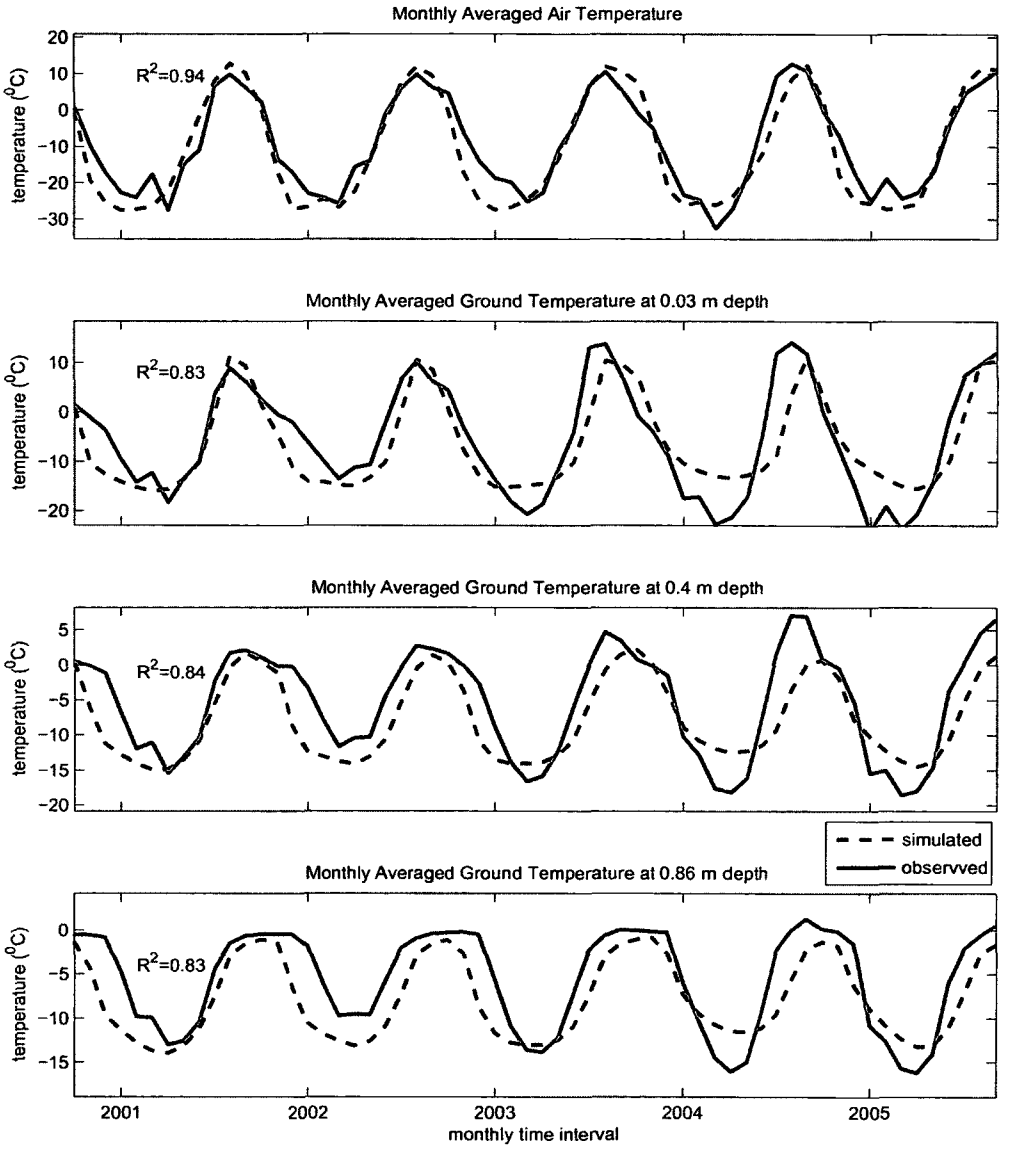

Figure 4.3. Measured (solid) and calculated (dashed) monthly averaged temperatures at 2 m above the ground and 0.03, 0.4 and 0.86 m depths for SagMat 69.43° N,−148.70° W permafrost observation stations.

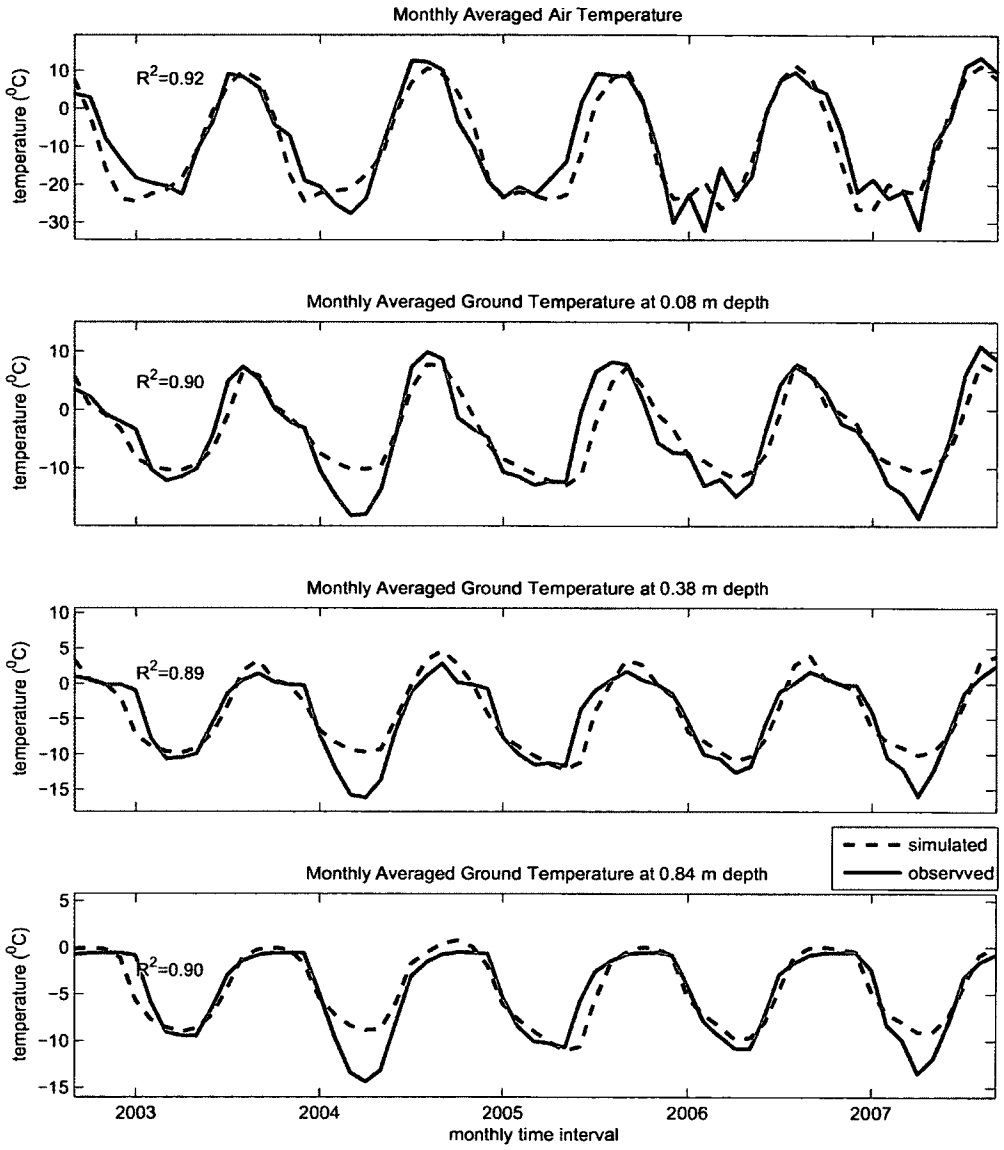

Figure 4.4. Measured (solid) and calculated (dashed) monthly averaged temperatures at 2 m above the ground and 0.08, 0.38 and 0.84 m depths for Galbraith Lake 68.48^o N, $-$149.50^o W permafrost observation stations.

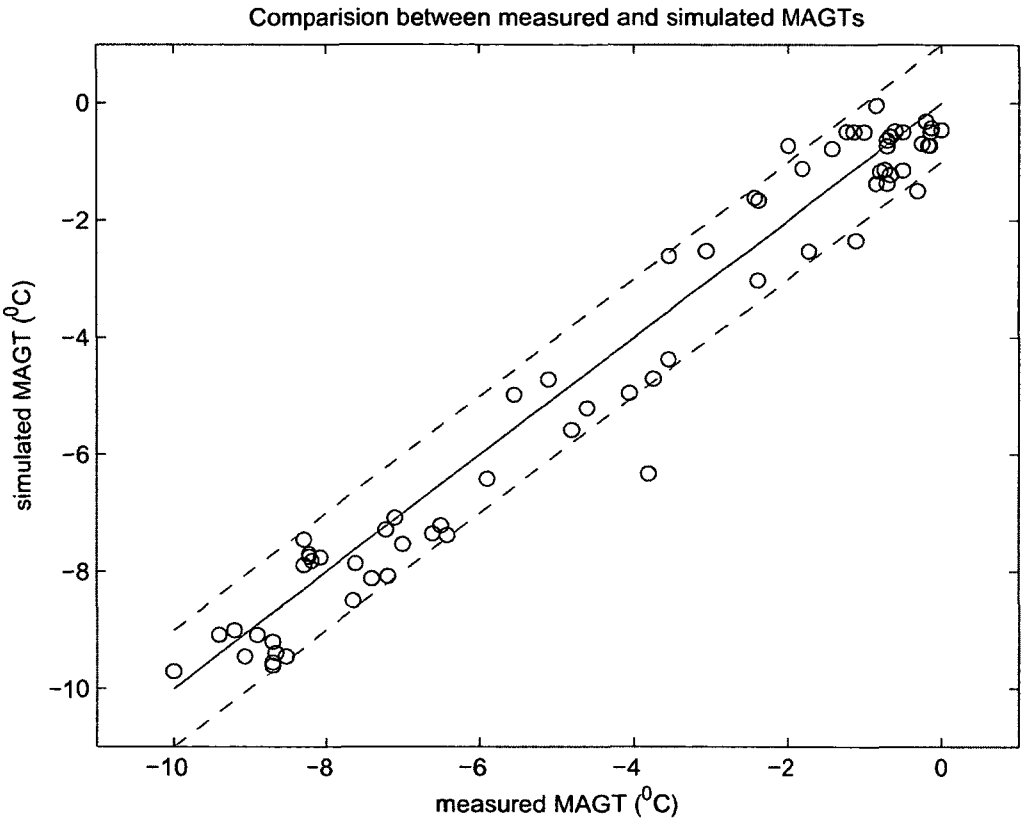

Figure 4.5. Simulated and measured MAGTs at different depths from 3 to 30 m during 2007-2009 IPY years.

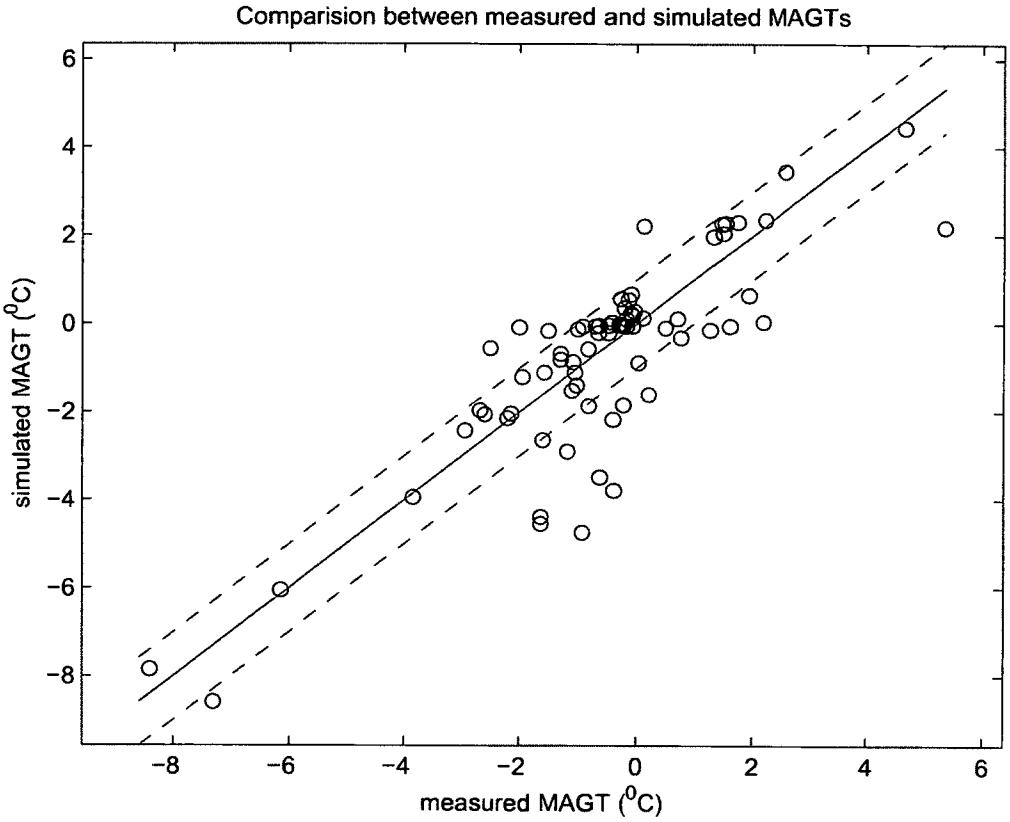

Figure 4.6. Simulated and measured MAGTs from 1 to 6 meters depths during 2009

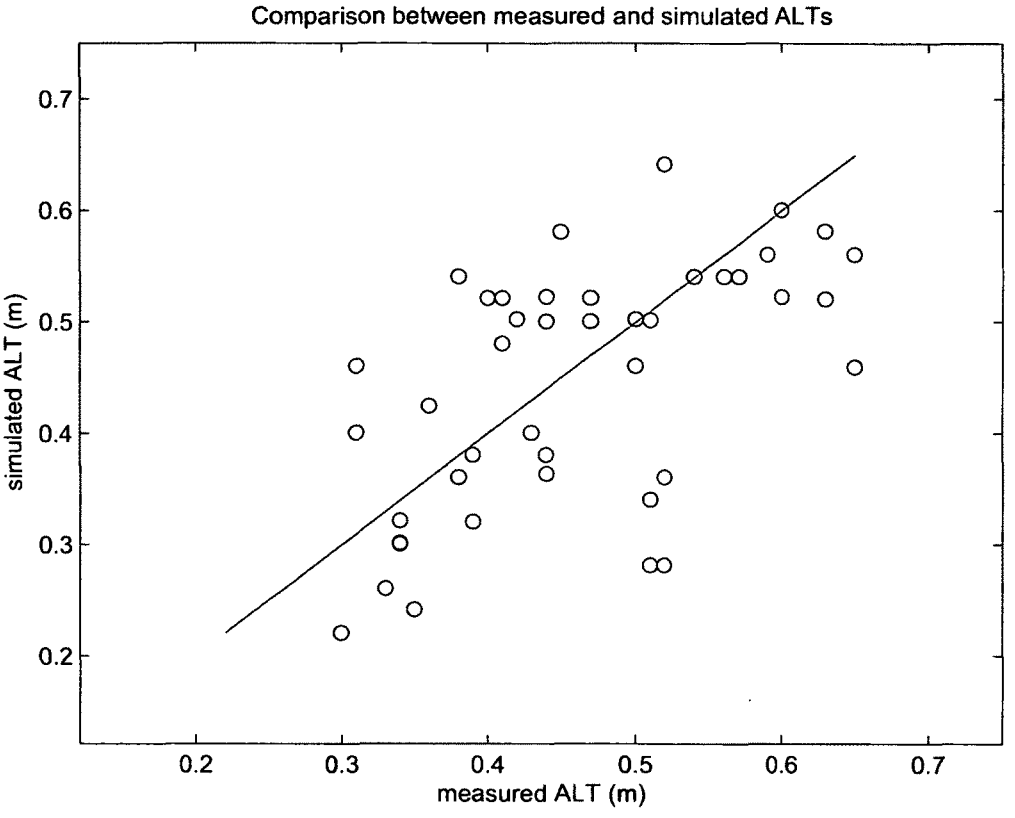

Figure 4.7. Comparision between simulated and observed ALTs from 43 CALM observation stations.

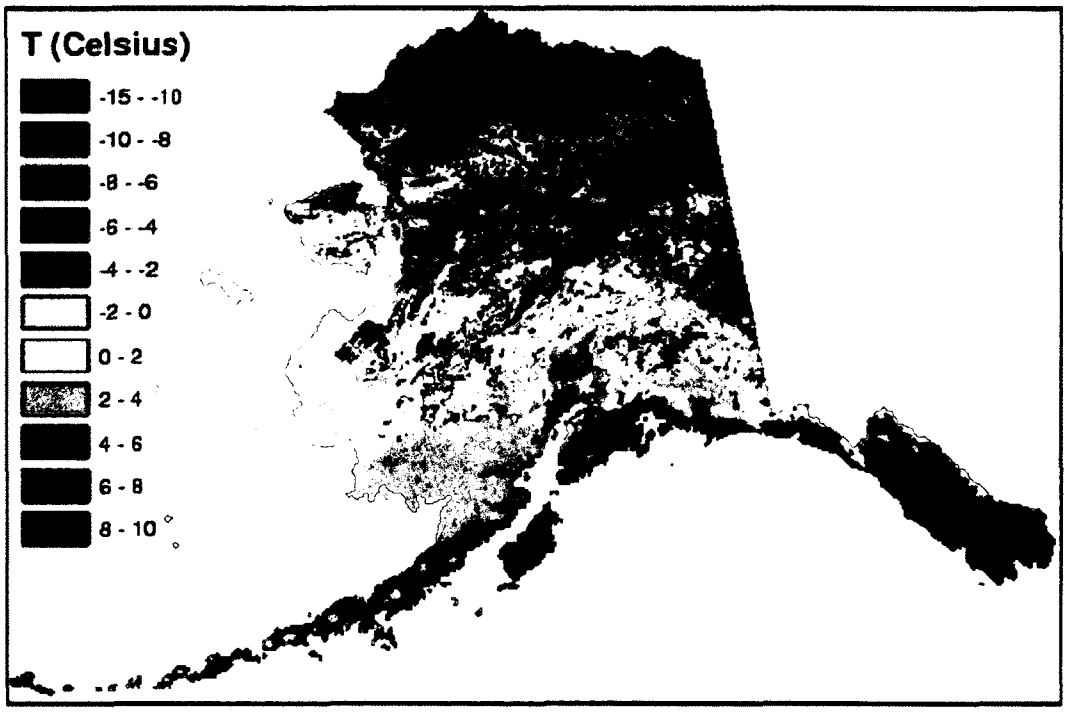

Figure 4.8. Simualted mean annual ground temperatures at 1 m depth for the year 2010.

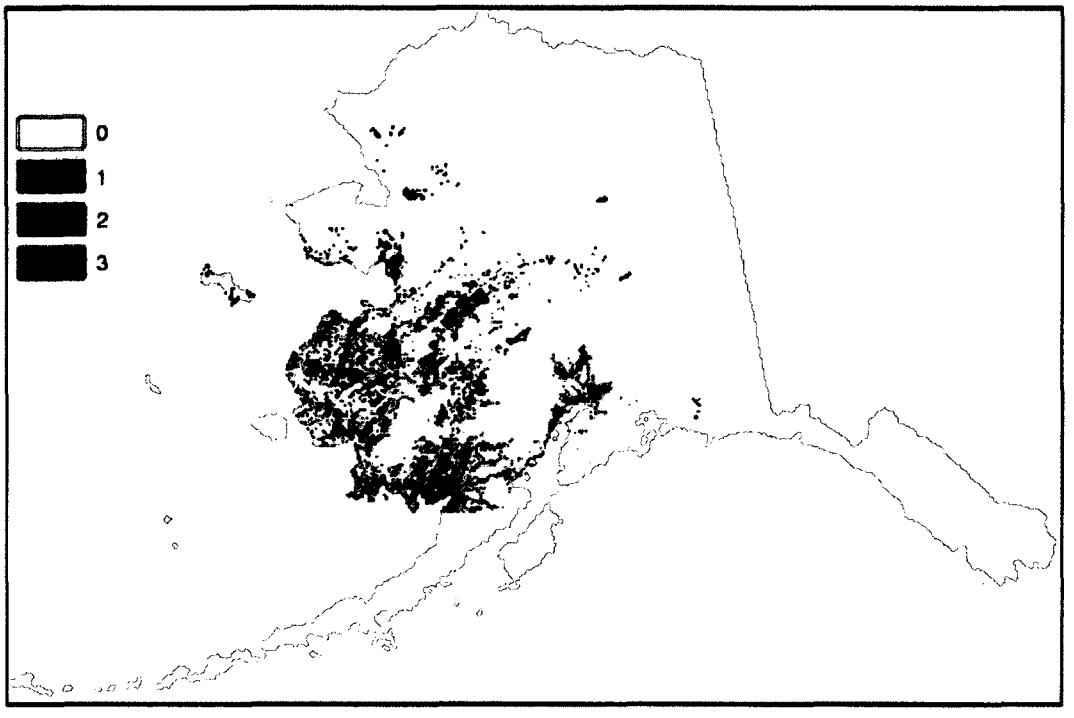

Figure 4.9. Additional organic layer map obtained after model tuning. 0-no additional organic; 1-one additional layer of organic matter (5cm); 2-two additional layers of organic matter (10cm); 3-three additional layers of organic matter (27cm).

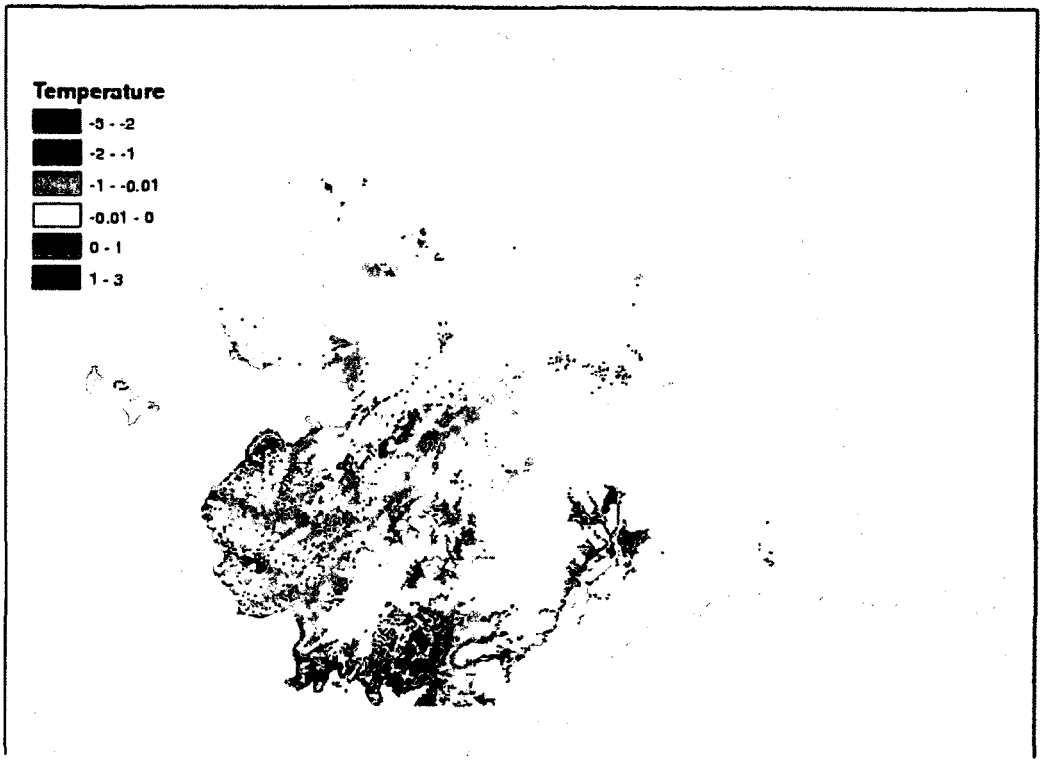

Figure 4.10. Projected differences between MAGTs simulated with and without additional organic layer(s) at 1 m depth for year 2010.

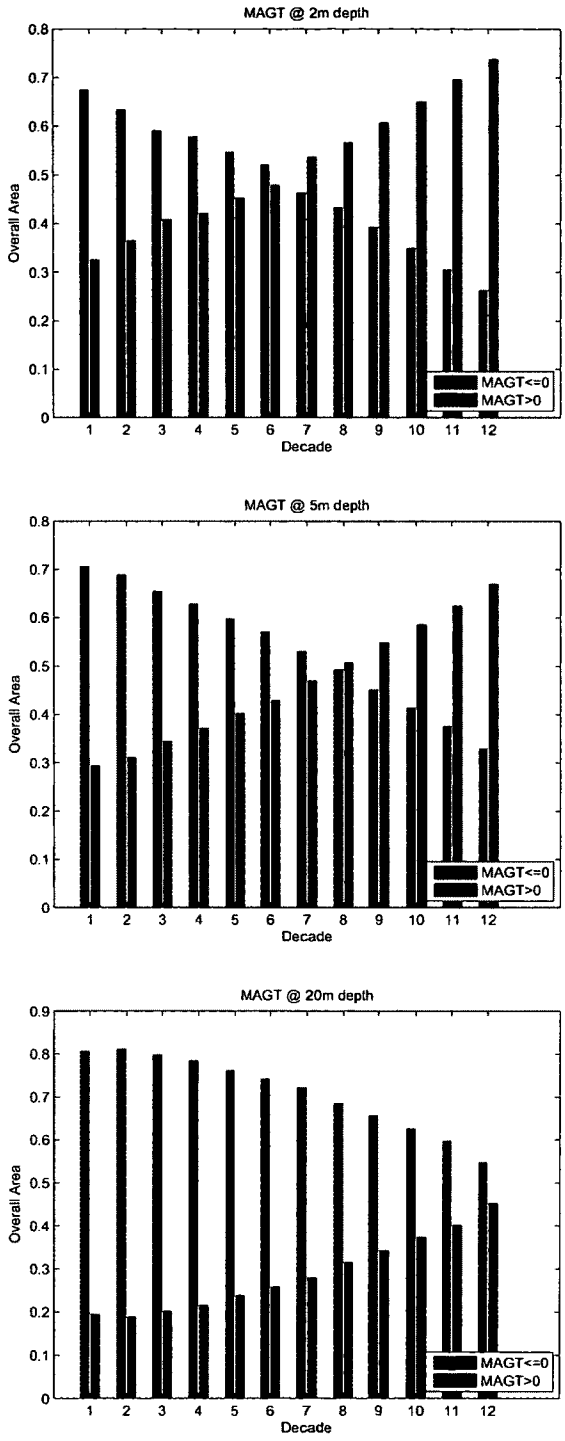

Figure 4.11. The amount of area over entire State of Alaska occupied by colder and warmer than 0°C MAGTs averaged over ten years time interval from 1980 to 2099 at different ground depths.

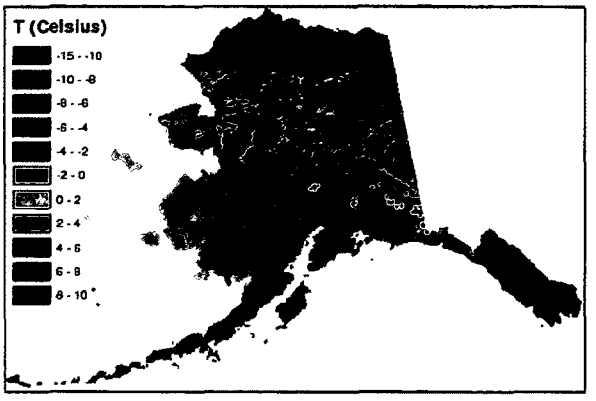

a)

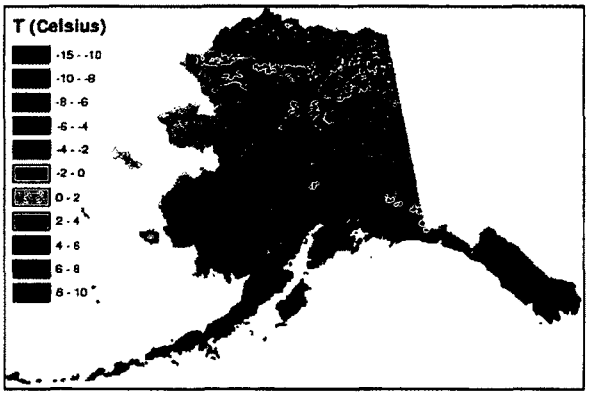

b)

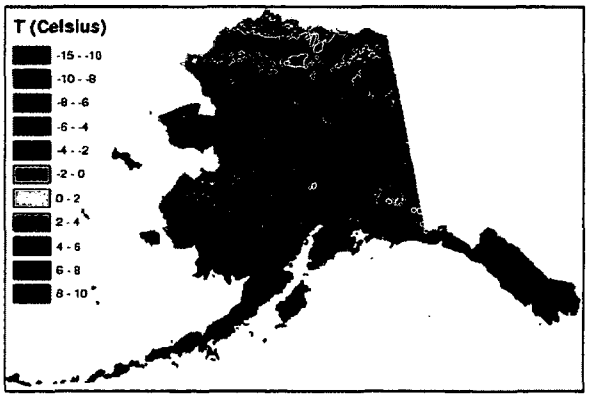

c)

Figure 4.12. Projected mean annual ground temperatures (MAGT) for the entire State of Alaska at 2 meter depth using downscaled to 2 by 2 km climate forcing from GCM composite output with A1B emission scenario for the 21st century for years (a) 2000, (b) 2050 and (c) 2099.

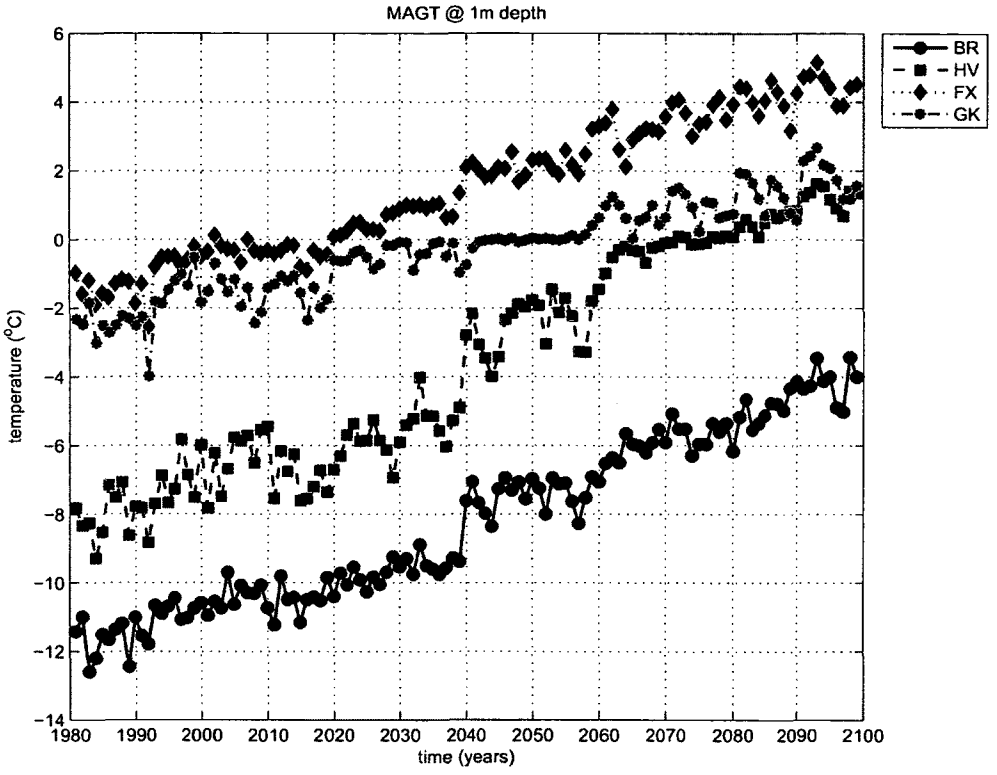

Figure 4.13. Projected MAGT at 1 m depth for four different locations (Barrow 71.32° N, 156.65° W, Happy Valley 70.38° N, 148.85° W, Fairbanks 64.95° N, 147.62° W, Gakona 62.41° N, 145.15° W). Forcing from the downscaled five composite GCMs with A1B emission scenario.

Bibliography

Brown, J., Smith, S. L., Romanovsky, V., Christiansen, H. H., Clow, G., and Nelson, F. E.: In Terrestrial Essential Climate Variables for Assessment, Mitigation and Adaptation, WMO Global Climate Observing System report GTOS-52, pp. 24–25, 2008.

Caldwell, J. and Chan, C. C.: Numerical solution of Stefan problems in annuli by enthalpy method and heat balance integral method, Numer. Methods Eng, 17, 395–405, 2001.

Etzelmuller, B., Schuler, T. V., Farbrot, H., and Gudmundsson, A.: Permafrost in Iceland – distribution, ground temperatures and climate change impact., In Proceedings of the Ninth International Conference on Permafrost, 29 June–3 July 2008, 2008.

Farbrot, H., Etzelmüller, B., Schuler, T. V., Gudmundsson, Á., Eiken, T., Humlum, O., and Björnsson, H.: Thermal characteristics and impact of climate change on mountain permafrost in Iceland, J. Geophys. Res., 112, doi:10.1029/2006JF000541, 2007.

Gruber, S., Hoelzle, M., and Haeberli, W.: Permafrost thaw and destabilization of Alpine rock walls in the hot summer of 2003., Geophysical Research Letters, 31, 4pp, doi: 10.1029/2006JF000547, 2004a.

Gruber, S., Hoelzle, M., and Haeberli, W.: Rock-wall temperatures in the alps: modeling their topographic distribution and regional differences., Permafrost Periglacial Processes, 15, 299–307, doi:10.1002/ppp.501, 2004b.

Hinzman, L. D., Kane, D. L., Gieck, R. E., and Everett, K. R.: Hydrologic and thermal properties of the active layer in the Alaskan Arctic, Cold Reg. Sci. Technol., 19, 95–110, 1991.

Jorgenson, M. T., Romanovsky, V., Harden, J., Shur, Y., O'Donnell, J., Schuur, E. A. G., Kanevskiy, M., and Marchenko, S.: Resilience and vulnerability of permafrost to climate change, Canadian Journal of Forest Research, 40, 1219–1236, doi:10.1139/X10-060, URL `http://dx.doi.org/10.1139/X10-060`, 2010.

Karlstrom, T. N. V. et al.: Surficial Geology of Alaska, U.S. Geol. Surv., Misc. Geol. Inv. Map I-357, scale 1:1,584,000, 1964.

Klene, A. E., Hinkel, K. M., and Nelson, F. E.: The Barrow Urban Heat Island Study: Soil temperatures and active-layer thickness, in: In Proceedings of the Eighth International Conference on Permafrost, edited by Balkema, L. A., vol. 1, pp. 555–560, Phillips M, Springman SM, and Arenson LU, 2003.

Kudryavtsev, V. A., Garagula, L. S., Kondratyeva, K. A., and Melamed, V. G.: Osnovy merzlotnogo prognoza (in Russian), MGU, p. 431pp, 1974.

Larsen, P. H., Goldsmith, S., Smith, O., Wilson, M. L., Strzepek, K., Chinowsky, P., and Saylor, B.: Estimating future costs for Alaska public infrastructure at risk from climate change, Global Environmental Change, 18, 442–457, 2008.

Lovell, C.: Temperature effects on phase composition and strength of partially frozen soil, Highway Research Board Bulletin, 168, 95, 1957.

Marchenko, S., Romanovsky, V., and Tipenko, G.: Numerical modeling of spatial permafrost dynamics in Alaska, in: In Proceedings of the Eighth International Conference on Permafrost, pp. 190–204, Willey, Institute of Northern Engineering, University of Alaska, Fairbanks, 2008.

Marchuk, G. I., Kuznetsov, Y. A., and Matsokin, A. M.: Fictitious domain and domain decomposition methods, Soviet J. Num. Anal. Math. Modelling, 1, 1–86, 1986.

Nelson, F. E.: Permafrost Distribution in Central Canada: Application of a Climate-Based Predictive Model, Annals of the Association of American Geographeers, 76, 550–569, 1986.

Nelson, F. E. and Hinkel, K. M.: Methods for measuring active-layer thickness, In: Humlum, O. and Matsuoka, N. (eds.) A Handbook on Periglacial Field Methods., 2003.

Nelson, F. E., Shiklomanov, N. I., Mueller, G. R., Hinkel, K. M., Walker, D. A., and Bockheim, J. G.: Estimating active layer thickness over a large region: Kuparuk River Basin, Alaska, USA, Arctic and Alpine Research, 19, 367–378 24, 1997.

Nicolsky, D. J., Romanovsky, V. E., and Tipenko, G. S.: Using in-situ temperature measurements to estimate saturated soil thermal properties by solving a sequence of optimization problems, The Cryosphere, 1, 41–58, 2007.

Osterkamp, T.: Freezing and Thawing of Soils and Permafrost Containing Unfrozen Water or Brine, Water Resources Research, 23, 2279–2285, 1987.

Osterkamp, T. and Romanovsky, V.: Evidence for Warming and Thawing of Discontinuous Permafrost in Alaska, Permafrost and Periglacial Processes, 10, 17–37, 1999.

Osterkamp, T. E.: Establishing Long-term Permafrost Observatories for Active-layer and Permafrost Investigations in Alaska: 1977–2002, Permafrost and Periglacial Processes, 14, 331–342, 2003.

Ping, C. L., Michaelson, G. J., Overduin, P. P., and Stiles, C. A.: Morphogenesis of frost boils in the Galbraith Lake area, Arctic Alaska, Proceedings of the Eighth International Conference on Permafrost, Zurich, Switzerland., 897–900, 2003.

Pollack, H. N., Hurter, S. J., and Johnson, J. R.: Heat Flow from the Earth's Interior: Analysis of the Global Data Set, Rev. Geophys., 31, 267–280, 1993.

Richter-Menge, J. and Jeffries, M.: The Arctic [in "State of the Climate in 2010"], Bull. Amer. Meteor. Soc., 92, S143–160, 2011.

Riseborough, D., Shiklomanov, N., Etzelmuller, B., Gruber, S., and Marchenko, S.: Recent advances in permafrost modeling, Permafrost and Periglacial Processes, 19, 137–156, URL `optional`, 2008.

Romanovsky, V. and Osterkamp, T.: Interannual variations of the thermal regime of the active layer and near-surface permafrost in Northern Alaska, Permafrost and Periglacial Processes, 6, 313–335, 1995.

Romanovsky, V. and Osterkamp, T.: Thawing of the active layer on the coastal plain of the alaskan arctic, Permafrost and Periglacial Processes, 8, 1–22, 1997.

Romanovsky, V. E., Smith, S. L., and Christiansen, H. H.: Permafrost thermal state in the polar Northern Hemisphere during the international polar year 2007–2009: a synthesis, Permafrost and Periglacial Processes, 21, 106–116, doi:10, 2010.

Sazonova, T. and Romanovsky, V.: A Model for Regional-Scale Estimation of Temporal and Spatial Variability of the Active Layer Thickness and Mean Annual Ground Temperatures, Permafrost and Periglacial Processes, 14, 125–139, 2003.

Sergueev, D., Tipenko, G., Romanovsky, V., and Romanovskii, N.: Mountain permafrost thickness evolution under the influence of long-term climate fluctuations (results from numerical simulation), in: In 8th International Conference on Permafrost, edited by Swets & Zeitlinger: Lisse, Z., pp. 1017–1021, Phillips M, Springman S, and Arenson L, 2003.

Serreze, M. C. and Barry, R. G.: The Arctic Climate System, Cambridge University Press, URL http://dx.doi.org/10.1017/CBO9780511535888, 2005.

Shiklomanov, N. and Nelson, F.: Active-layer mapping at regional scales: A 13-year spatial time series for the Kuparuk region, north-central Alaska, Permafrost and Periglacial Processes, 13, 219–230, doi:10.1002/ppp.425, 2002.

Shiklomanov, N., Nelson, F., Streletskiy, D., Hinkel, K., and Brown, J.: The Circumpolar Active Layer Monitoring (CALM) Program: Data collection, management, and dissemination strategies, in: In Proceedings of the Eighth International Conference on Permafrost, pp. 210–217, Willey, Institute of Northern Engineering, University of Alaska, Fairbanks, 2008.

Shiklomanov, N. I. and Nelson, F. E.: Analytic representation of the active layer thickness field, Kuparuk River Basin, Alaska, Ecological Modeling, 123, 105–125, doi: 10.1016/S0304-3800(99)00127-1, 1999.

Shur, Y. L. and Jorgenson, M. T.: Patterns of permafrost formation and degradation in relation to climate and ecosystems, Permafrost and Periglacial Processes, 18, 7–19, doi: 10.1002/ppp.582, URL http://dx.doi.org/10.1002/ppp.582, 2007.

Smith, S., Romanovsky, V., Lewkowicz, A., Burn, C., Allard, M., Clow, G., Yoshikawa, K., and Throop, J.: Thermal state of permafrost in North America: a contribution to the international polar year, Permafrost and Periglacial Processes, Fall Meet. Suppl., Abstract C12A-02, 21, 117–135, doi:10, 2010.

Sturm, M., Holmgren, J., and Liston, G. E.: A Seasonal Snow Cover Classification System for Local to Global Applications, J. Climate, 8, 1261–1283, 1995.

Sturm, M., Holmgren, J., Konig, M., and Morris, K.: The thermal conductivity of seasonal snow, Journal of Claciology, 43, 1997.

Tipenko, G., Marchenko, S., Romanovsky, V., Groshev, V., and Sazonova, T.: Spatially distributed model of permafrost dynamics in Alaska, EOS, Transactions of the AGU, 85(47), Fall Meet. Suppl., Abstract C12A-02, 2004.

Vasilios, A. and Solomon, A.: Mathematical Modeling of Melting and Freezing Processes, Hemisphere Publishing Corporation, 1993.

Verseghy, D. L.: ClassA Canadian land surface scheme for GCMS. I. Soil model, International Journal of Climatology, 11, 111–133, doi:10.1002/joc.3370110202, URL http://dx.doi.org/10.1002/joc.3370110202, 1991.

Walker, D. A., Epstein, H. E., Romanovsky, V., Ping, C. L., Michaelson, G. J., Daanen, R., Shur, Y., Peterson, R. A., Krantz, W. B., Raynolds, M. K., Gould, W. A., Gonzalez, G., Nicolsky, D. J., Vonlanthen, C. M., Kade, A. N., Kuss, P., Kelley, A. M., Munger, C. A., Tamocai, C. T., Matveyeva, N. V., and Daniels, F. J. A.: Arctic patterned-ground ecosystems: A synthesis of field studies and models along a North American Arctic Transect, Journal of Geophysical Research-Biogeosciences, 113, –, 2008.

Walsh, J. E., Chapman, W. L., Romanovsky, V., Christensen, H., and Stendel, M.: Global Climate Model Performance over Alaska and Greenland, J. Climate, 21, 6156–6174, 2008.

Williams, P. J. and Smith, M. W.: The Frozen Earth: Fundamentals of Geocryology, Cambridge University Press, 1989.

Willmott, C. J. and Matsuura, K.: Advantages of the mean absolute error (MAE) over the root mean square error (RMSE) in assessing average model performance, Climate Research, 30, 79–82, URL http://www.int-res.com/abstracts/cr/v30/n1/p79-82/, 2005.

Wright, J. F., Duchesne, C., and Cote, M. M.: Regional-scale permafrost mapping using the TTOP ground temperature model, in: In Proceedings of the Eighth International Conference on Permafrost, edited by Balkema, L. A., pp. 1241–1246, Phillips M, Springman SM, and Arenson LU, Zurich, Switzerland, 2003.

Yoshikawa, K., Bolton, W. R., Romanovsky, V. E., Fukuda, M., and Hinzman, L. D.: Impacts of wildfire on the permafrost in the boreal forests of Interior Alaska, J. Geophys. Res., 107, doi:10.1029/2001JD000438, 2003.

Zhang, T., Frauenfeld, O. W., Serreze, M. C., Etringer, A., Oelke, C., McCreight, J., Barry, R. G., Gilichinsky, D., Yang, D., Ye, H., , Ling, F., and Chudinova, S.: Spatial and temporal variability in active layer thickness over the Russian Arctic drainage basin, Journal of Geophysical Research-Atmospheres, doi:10.1029/2004JD005642, 2005.

Chapter 5
General Conclusions

Permafrost is not directly connected to the atmosphere; its thermal regime is mediated by topography, surface water, soil properties, vegetation, snow, and other environmental factors. The numerous interactions among these environmental components can lead to both positive and negative feedbacks on permafrost stability. The dependence of permafrost stability on air temperature and environmental factors greatly complicates the modeling of permafrost under changing climate conditions.

Snow is one factor that can affect heat exchange between the air and the ground. In Chapter 2, we estimated daily snow thermal conductivities using an inverse approach. The resulting time series provides insight into how snow thermal properties can change during a snow season. Next, we used the thermal conductivity time series to improve ground temperature simulations within the active layer and permafrost. The estimated snow thermal conductivities at different locations in Alaska will provide valuable information on snow density and conductivity distribution at each location, and under certain assumptions these values can be extrapolated to wider areas. This method illustrates how snow thermal parameterization can be improved without the implementation of more expensive snow heat exchange field measurements and models. An increase in the number of shallow borehole permafrost temperature observation stations is necessary to obtain better spatial coverage of snow thermal property estimates in the region. To better understand how local climate can affect the results of the inverse method, more stations should be evaluated in the future.

Forest fire is another factor that dramatically alters vegetation and soil physical properties. Fire changes permafrost thermal stability by burning the overlying soil organic layer. The amount of soil organic layer burned during the fire defines the "fire severity level." A high fire severity level corresponds to the burning of a significant amount of the organic layer, the removal of which can lead to an increase in active layer thickness combined with degradation of permafrost, which is irreversible in some cases. Sensitivity analysis applied to lowland and upland boreal forest permafrost environments showed that severe forest fire can accelerate permafrost degradation even under a stable climate. Irreversible permafrost degradation is especially impactful if the soil in the recently burned area is

ice-rich. Thawing of ice-rich soils causes the surface to subside and creates depressions in the ground surface. Thawing permafrost affects surface hydrology by impounding water in subsiding areas. In addition, the development of a thermokarst pond or lake could contribute to warmer ground surface temperatures. The consequences of changes in the states of ecosystems could range from micro-site changes in hydrology and vegetation to potentially global impacts from greenhouse gases released into the atmosphere.

Changes in the thermal state of permafrost affect its structure and stability. This in turn can affect boreal forest and tundra ecosystems, ground and surface hydrology, sequestration of soil carbon, and human facilities. Mapping of permafrost continues to remain a challenging problem, but an increase in the number of permafrost monitoring stations, advances in permafrost numerical modeling, and improvements to remote sensing techniques could significantly improve the quality of permafrost mapping and reduce uncertainties associated with its future dynamics in Alaska. In the current study, we map permafrost distribution based on available ground temperature datasets collected from deep and shallow boreholes in Alaska. We project future permafrost dynamics using outputs from a composite of five GCMs to calculate ground temperatures. Resulting ground temperatures reveal high-order heterogeneity, which is primarily due to high heterogeneity in soil texture and organic layer thickness. The highest warming trend was projected for the continuous permafrost zone north of the Brooks Range (Fig. 5.1). Uncertainties associated with the model are well-described in the discussion section of the corresponding chapter.

Projected future permafrost dynamics in Alaska are based on observed soil physics and provide a detailed picture of permafrost degradation in the region. Therefore, obtained permafrost projections can be used to better assess the effects of thawing permafrost on public infrastructure. However, care needs to be taken during downscaling of these results to specific geographic locations. In order to improve future permafrost modeling, it is necessary to further expand the permafrost observation network, apply recent permafrost remote sensing products, and better address snow and soil texture parameterizations. The work presented in this thesis highlights the steps that can be taken in order to improve permafrost spatial modeling. The inverse approach developed in Chapter 2 illustrates how improvements in snow thermal property parameterization could improve overall ground temperature modeling. In Chapter 3, we provide an overview of the factors that can in-

fluence permafrost degradation after severe forest fires. In Chapter 4, we implemented the Geographic Information System spatial mapping technique and used the power of the Arctic Regional Supercomputer Center to map the permafrost thermodynamics for the 21st century. Burning of the upper organic soil will accelerate permafrost thawing, however, the regional and global impact of fire on permafrost thermal dynamics has not been quantified yet. Simulating forest fire effects on permafrost requires coupling models of permafrost with models of forest fire generation. Changes in vegetation and organic soils due to fires or climate warming must be incorporated into permafrost models. Growing economic demands and increases in human activities in Alaska affect permafrost thermal stability, which must be considered as well. Finally, continued improvements to model computational performance are necessary in order to increase spatial resolution beyond the scale already achieved in this study.

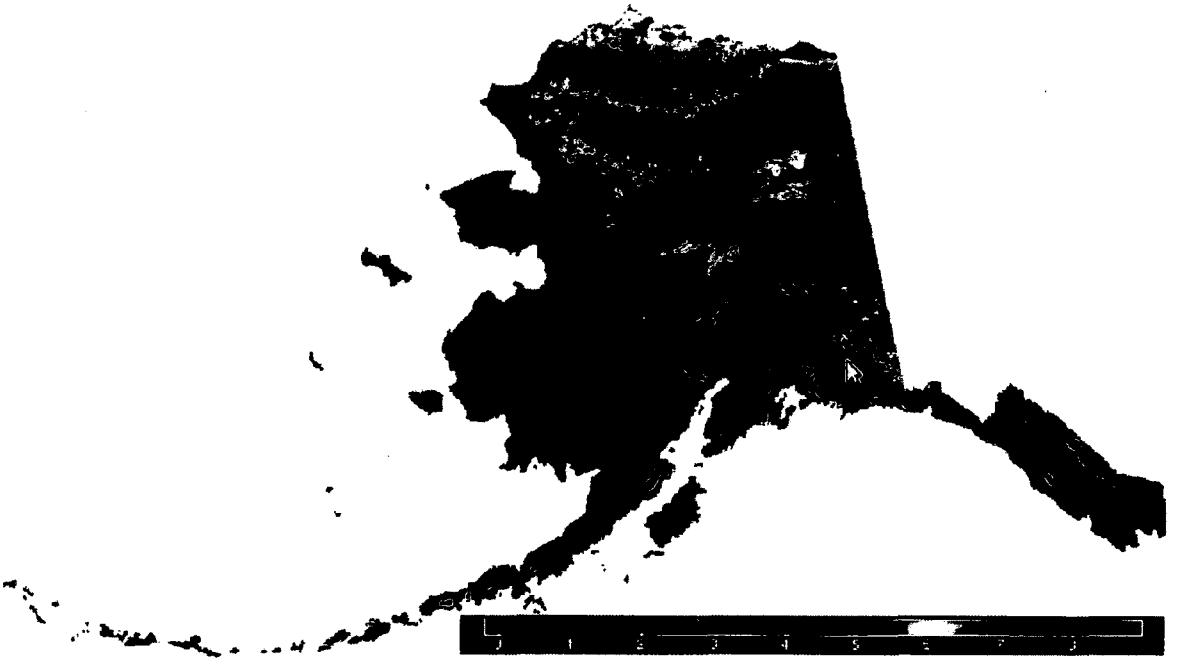

Figure 5.1. Projected warming at 1 meter ground depth. The plot illustrates the difference, in ^{o}C, between averaged mean annual temperatures for the first and last decades of the 1980-2099 time period.